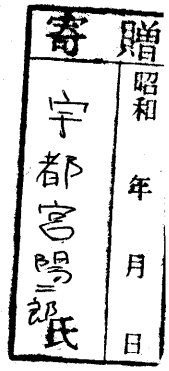

MODELING OF SOIL MOISTURE ESTIMATION AND ITS APPLICATION TO REMOTE SENSING AND MAPPING

YOJIRO UTSUNOMIYA

A DISSERTATION

SUBMITTED IN PARTIAL FULFILLMENT

OF THE REQUIREMENTS FOR

THE DEGREE OF DOCTOR OF

SCIENCE

at the

INSTITUTE OF GEOSCIENCE OF

THE UNIVERSITY OF TSUKUBA

1989

ABSTRACT

A thermal inertia model and some empirical models for determining soil moisture was established. These models were applied to airborne and spaceborne multispectral scanner (MSS) data to produce soil moisture maps and other thematic maps in various study areas. The results can be summarized as follows:

1. It was found that the spectral reflectance of soil surface varied inversely with soil moisture. However, at predawn the reflectance in the near IR wavelength region varied directly with soil moisture. The relationship resembled that obtained from the thermal IR spectral region.

2. A thermal inertia model based on the heat balance and one dimensional heat transfer of the earth's surface for the remote sensing was established by the analytic and mathematical solution techniques. This model was appropriately compared with that of previous thermal inertia models. The model for determining soil moisture was developed incorporating surface relative humidity and heat balance terms obtained at the observation field of the National Institute for Environmental Studies (NIES) and in the Kujukuri coastal plain. These models enabled estimation of the soil moisture for sparsely vegetated surface. The examination of the ratio of vegetation cover in the model needs further analysis.

The estimation error in the model was lesser than that of the other empirical models using visible and near IR data. Thus, the model can be applied to soil moisture estimation by remote sensing.

3. The soil moisture map using airborne MSS data obtained at noon shows the details of spatial variations in soil moisture distribution because of small instantaneous field of view and high irradiance from the earth's surface. On the other hand, maps derived from spaceborne observations can be useful for other thematic mapping such as geomorphological and potential wind erosion maps because of large coverage areas.

CONTENTS

Page

LIST OF FIGURES vii

LIST OF TABLES x

LIST OF PHOTOGRAPHS xii

LIST OF SYMBOLS xiv

1. Introduction 1

1.1 Purpose of this study 1

1.2 Review of previous studies 2

2. Methodology - Measurements and data processing 9

2.1 Study areas 9

2.2 Micro-meteorological observation 17

2.2.1 Soil moisture and meteorological measurements 17

2.2.2 Data processing 21

2.3 Spectral reflectance and moisture determination in the laboratory 22

2.4 Data acquisition in the Kujukuri coastal plain, Tsuchiura and the old Joban coal mining area 26

2.4.1 Airborne measurement and ground truth 26

2.4.2 Satellite measurement and ground truth 34

3. Modeling of soil moisture estimation 39

3.1 Modeling of soil moisture estimation with thermal IR data obtained by ground truth measurements 39

3.1.1 Variations in surface temperature and soil moisture. 39

3.1.2 Thermal model and soil physics 44

3.1.3 Thermal inertia model for estimating soil moisture

using micro-meteorological data obtained at the experimental field 51
3.2 Modeling with airborne MSS thermal IR data in the Kujukuri coastal plain 54
3.2.1 Thermal inertia model with airborne MSS data for soil moisture estimation 54
3.2.2 Moisture estimation with soil surface temperature... 60
3.2.3 Model for estimating soil moisture using the thermal parameter and thermal inertia 64
3.3 Estimation of soil moisture with visible and near IR data 69
3.3.1 Spectral reflectance of soil surface 69
3.3.2 Estimation of soil moisture with airborne MSS visible and near IR data 71
3.3.3 Estimation of soil moisture with Landsat MSS data... 76
3.3.4 Estimation of soil moisture with Landsat TM data.... 79
4. Soil moisture map and its application 83
4.1 Soil moisture distribution mapping 83
4.1.1 Data analysis for computer mapping 83
4.1.2 Kujukuri coastal plain 87
4.1.3 Tsuchiura and its vicinity 98
4.1.4 Old Joban coal mining area 100
4.2 Application of the soil moisture map to the geomorphological mapping and potential wind erosion mapping 102
4.2.1 Significance of automatic geomorphological mapping 102

4.2.2 Automatic geomorphological classification 105

4.2.3 Automatic mapping of potential wind erosion 114

5. Discussion 117

6. Conclusion 136

ACKNOWLEDGMENTS 139

REFERENCES 140

LIST OF FIGURES

Figure		Page
1	Index map of study areas.	10
2	Southern Kujukuri coastal plain.	13
3	Tsuchiura city and its vicinity.	14
4	Old Joban coal mining area.	16
5	Schematic profile of paddy soils in the containers and measurement system in the field of the Air monitoring station(AMS).	18
6	Ground truth points and flight path in the southern Kujukuri coastal plain (Jan. 23, 1981).	25
7	Relation between net radiation and global solar radiation observed at the field from August 6 to 27, 1986.	30
8	Regression of albedo and amount of CCT count of airborne MSS data (Channel 1-10).	33
9	Locations of sampling points in the Kujukuri coastal plain (Jan. 17-20, 1980).	37
10	Variations in surface temperature of paddy soil in 1980.	40
11	Daily and day-to-day variations in soil moisture at depths of 5 and 10 cm obtained from the experiment at the Air monitoring station in 1980.	41
12	Day-to-day variations in soil moisture (mass wetness)	

of Kanto loamy soil obtained from the experiment at the field from May 1 to September 30, 1986. 42

13 Regression of thermal inertia and total water storage of Kanto loamy soil obtained from the experiment at the field. 52

14 Relationships between albedo, estimated relative humidity of soil surface and total water storage obtained from the field and in the Kujukuri coastal plain. 58

15 Relationship between total water storage and surface temperature of soil obtained from the experiment in the Kujukuri coastal plain on Jan. 23, 1981. 61

16 Total water storage versus thermal parameter(dS/dTs) obtained from the experiment in the Kujukuri coastal plain on Jan. 23, 1981. 65

17 Regression of thermal inertia and total water storage of sandy soil obtained from the experiment in the Kujukuri coastal plain. 67

18 Spectral reflectance of sand obtained from the Kujukuri coastal plain. 70

19 Airborne MSS CCT count versus total water storage in the Kujukuri coastal plain on Jan. 23, 1981. 72

20 Landsat MSS CCT count versus total water storage in the Kujukuri coastal plain. 77

21 Landsat TM CCT count versus total water storage in the Kujukuri coastal plain. 80

22 Flow chart of soil moisture and other thematic

mapping. 85

23 Land subsidence in the Kujukuri coastal plain measured by Environmental Department of Chiba Prefecture. 93

24 Geomorphological classification map in the Kujukuri coastal plain. 106

25 CCT count of each topographical category. 110

LIST OF TABLES

Table		Page
1	Particle size of the paddy soil obtained from Obusa, western Ibaraki Prefecture.	17
2	Particle size of the sandy soil obtained from the Kujukuri coastal plain	23
3	Spectral wavelengths in each band of airborne MSS data.	27
4	Meteorological data in the airborne MSS measurements.	28
5	Spectral wavelengths of Landsat data.	35
6	Thermal properties of soil	50
7	Regression results of total water storage and surface temperature in the Kujukuri coastal plain.	62
8	Regression results of total water storage and the thermal parameter (dS/dTs) obtained from the experiment in the Kujukuri coastal plain.	66
9	Regression results of total water storage and airborne MSS visible and near IR data for bare soil 74	
10	Regression results of total water storage and airborne MSS visible and near IR data for mixed surfaces.....	75
11	Regression results of total water storage and Landsat MSS visible and near IR data in the Kujukuri coastal plain.	78
12	Regression results of total water storage and Landsat TM visible and near IR data in the Kujukuri coastal	

plain. 81

13 Averaged spectral reflectance of each topographical category. 111

LIST OF PHOTOGRAPHS

Photograph		Page
1	Experimental equipments in the field and the Air monitoring station at the National Institute for Environmental Studies.	11
2	Observation system at the experimental field.	11
3	Measurement of instrument error.	19
4	Measurement system of surface reflectance of sandy soil.	19
5	Distribution of total water storage in the Kujukuri coastal plain (Jan. 23, 1981).	88
6	Distribution of total water storage in and around Iyobo village in the Kujukuri coastal plain(Nov. 15, 1985).	90
7	Land cover in the Kujukuri coastal plain (Jan. 19, 1980).	92
8	Distribution of total water storage in the Kujukuri coastal plain (Jan. 19, 1980).	92
9	Land cover in the Kujukuri coastal plain (Feb. 14, 1987).	95
10	Distribution of total water storage in the Kujukuri coastal plain (Feb. 14, 1987).	96
11	Land cover at Tsuchiura and its vicinity (Jan. 19, 1980).	99

12 Distribution of total water storage at Tsuchiura and its vicinity (Jan. 19, 1980). 99

13 Land cover in the old Joban coal mining area (Jan. 19, 1980). 101

14 Distribution of total water storage in the old Joban coal mining area (Jan. 19, 1980). 101

15 Geomorphological map in the southern Kujukuri coastal plain. 112

16 Potential wind erosion map in and around Iyobo village in the the Kujukuri coastal plain (Nov. 15, 1985). 115

LIST OF SYMBOLS

a : thermal diffusivity of soil (cm^2/sec)

B :soil heat flux (heat flow beneath surface) (cal/cm^2 min)

Band 5,6,7 : band of Landsat CCT video data

c : specific heat of soil

Cp : specific heat of air at constant pressure (cal/g $^{\bullet}$C)

Cv : volumetric heat capacity (cal/cm^3 $^{\bullet}$C)

D : diffusion velocity (cm/sec)

D^2 : Mahalanobis's D statistic

Dg : weight of dry soil(g)

dS : daily range in net radiation (cal/cm^2 min)

dTs : daily range in surface temperature ($^{\bullet}$C)

e : water vapor pressure (mmHg)

E : evaporation

F : effective radiation (cal/cm^2 min)

h : height(cm)

H : sensible heat flux (cal/cm^2 min)

K : diffusion coefficient (cm^2/sec)

K1 : molecular diffusion coefficient for water vapor

K2 : thermal conductivity of air

ka : thermal diffusivity of air

kw : coefficient of kinematic viscosity of air

L : downward longwave radiation from the sky (cal/cm^2 min)

ℓ : 580 cal/g

ℓE : latent heat flux (cal/cm^2 min)

n : number of sample

P : air pressure (mmHg)

q : specific humidity (g H_2O/g air)

r : correlation coefficient

r : specific gravity of soil

S : net radiation (cal/cm^2 min)

SD : standard deviation

SM : soil moisture

R : solar radiation (cal/cm^2 min)

SV : mass wetness (water content by weight(g/g))

SW : total water storage (mm/cm)

SW COM : total water storage of mixed surface (mm)

SW EXP : total water storage of bare soil(mm)

T : air temperature ($^{\circ}$C)

t : time

Ts : soil surface temperature ($^{\circ}$C)

U : upward longwave radiation from the surface (cal/cm^2 min)

Wg : weight of wet soil (g)

WV : volume wetness (g/cc, %)

z : depth (cm)

α : albedo (0.0 - 1.0)

α' : estimated albedo (0.0 - 1.0)

λ : thermal conductivity of soil layer (cal/cm sec^{-2} $^{\circ}C$)

$\sqrt{\lambda c\rho}$: heat conductance capacity or thermal inertia (cal/cm^2 sec $^{\circ}C$)

μ : relative humidity of soil surface (0.0 - 1.0, absolute number)

μ' : estimated relative humidity of soil surface (0.0-1.0)

τ : time

τ_o : periodic time

σ : Stefan-Boltzmann constant

δ : emissivity of soil surface

ρv : bulk density (g/cm^3)

ω : angular velocity

*,**,*** : level of significance at 5%, 1 % and 0.1%, respectively

1. INTRODUCTION

1.1 Purpose of this study

Remote sensing with spaceborne and airborne sensors can observe wide areas of the earth's surface and get information with homogeneous quality from a distance in a short period of time. Therefore, the technology has been applied to examine environmental pollution and the evaluation of land use and natural resources (i.e. crop production and desertification). Soil moisture is important for agricultural production and other environmental factors such as air temperature, evaporation and albedo.

Since the 1970's, remote sensing technology has been applied to estimate soil moisture. Many models estimating soil moisture were proposed using visible, near IR and thermal IR data, and these models still have some ambiguities. Soil moisture maps were not produced very much in the previous studies by overlay operation and computer mapping techniques. Furthermore, automatic thematic mapping based on the soil moisture maps obtained from remote sensing data were only developed a little. Therefore, the purpose of this study is to firstly establish analytically a thermal inertia model for determination of soil moisture based on thermal models on the earth's surface; secondly examine the relationships between thermal inertia, visible/thermal IR data and soil moisture; thirdly apply these established models to remote

sensing data for mapping of soil moisture; fourthly produce thematic maps such as geomorphological maps and potential wind erosion maps by using soil moisture maps and land cover maps, and applying Strendansky model.

1.2 Review of previous studies

Review of previous studies are arranged in order of studies on i) soil moisture estimation, ii) geomorphological classification and iii) wind erosion.

i) Basic interpretations in many fields such as optical science, thermodynamics, meteorology, soil physics and electromagnetism have been applied to remote sensing. Since 1970, various computer techniques and algorithms for processing of remote sensing data have been developed. The evaluation of soil moisture based on airborne and spaceborne visible, thermal and microwave data has been empirically developed. Some empirical equations for soil moisture estimation were developed using parameters such as weather elements, visible, near and thermal IR data and brightness temperature or backscatter of microwaves. Yamanaka (1949) and Yamamoto (1962) proposed an equation based on weather data from clear days for estimating soil moisture. Relationships between soil moisture and spectral reflectance have been investigated. (Bowers and Hanks, 1965, Maruyama, 1967; Condit, 1970; Fukuhara, 1974; Idso et al., 1974, 1975a; Jackson and Idso, 1975; Curran, 1978, 1979; Darch, 1979; Imamura et al., 1980; Utsunomiya, 1981).

Maruyama (1967) determined an exponential relationship between soil moisture and albedo of soil surface. Bowers and Hanks (1965) and Condit (1970) made laboratory experiments for examination of relationships between soil moisture and spectral reflectance of soil. They found that the intensity of reflectance increased with decrease of soil moisture (SM).

Soil moisture has been evaluated using thermal parameters such as surface temperature, soil-air temperature difference, rising rate of surface temperature (Ts) and thermal inertia (Umetani, 1951, Myers and Heilman, 1969; Pohn et al.,1974; Rosema, 1975; Nappo, 1975; Idso et al., 1975b,1976; Reginato et al., 1976; Heilman et al., 1977, 1982; Price, 1977, 1980, 1982, 1985; Gillespie and Kahle, 1977; Schmugge et al., 1978; Huntley, 1978; Pratt and Ellyett, 1978, 1979; Viellefosse and Favard, 1979; Zhang, 1980; Soer, 1980; Carlson et al., 1981; McCumber et al., 1981; Watson, 1971, 1975, 1982; Jackson, S. D., 1982; Vlcek and King, 1983; Kahle, 1977; Kahle et al., 1976, 1984, 1985; Abdellaoui et al., 1986; Utsunomiya and Yamaguchi, 1986, 1987; Utsunomiya, 1980, 1982, 1984, 1988, Flores et al., 1987; Wetzel and Woodward, 1984, 1987; Ho, 1987; Matthias et al., 1987).

Some investigators examined the relationships between parameters such as surface temperature(Ts), daily difference between air temperature and Ts and soil moisture. In the early stages of the examination, these relationships were evaluated by using advantageous data i.e., high temperature data with low SM and low temperature data with high SM in order to try to obtain good correlation.

Prediction models for determining soil moisture based on climatological and water balance theory have been proposed to obtain the geographical distribution and seasonal change of soil moisture. Nevertheless, these approaches neglected the influence of micro-topography on the soil moisture regime in cultivated fields.

Estimation parameters such as Ts and diurnal amplitude of Ts have been examined. However, the soil temperature immediately below the soil surface instead of real surface temperature was used as a parameter in the previous studies, because there were no thermal IR radiometers before the 1970's.

The difference between Ts and air temperature has also been used to estimate soil moisture (Idso et al., 1975b; Reginato et al., 1976). Zhang(1980) obtained soil moisture by subtracting the minimum values (Tsmin) from the maximum values (Tsmax) of the surface temperature (Ts) and dividing the result by the summation of Tsmin and Tsmax. This overall result was then multiplied by a weighting function of soil moisture estimation which can be adjusted seasonally. Soil moisture and evapotranspiration have also been investigated using both visible and thermal IR data (Kanemasu et al., 1977; Heilman et al., 1977). These parameters change with time and seasons, therefore, these models are less applicable. The inadequate parts of these models have been improved by introducing parameters such as the rising rate of Ts normalized by net radiation (Utsunomiya, 1982). The model is still influenced by seasonal changes.

In these circumstances, a parameter such as thermal inertia that isn't seasonally influenced, has been examined for determining soil moisture and evapotranspiration (Watson, 1971, 1975, 1982; Pohn et al., 1974; Rosema, 1975; Idso et al., 1976; Gillespie and Kahle, 1977; Huntley, 1978; Pratt and Ellyett, 1978,1979; Price, 1980,1982; Carlson et al., 1981; Utsunomiya and Yamaguchi, 1986, 1987; Utsunomiya, 1988).

Concerning thermal inertia (TI), there have been two different approaches in acquiring the data. One is the iterative calculation method by Rosema and his coworker (Rosema, 1975; Price, 1980, 1982, Dajaces et al., 1979). The other an analytical approach by Watson and his coworker (Watson, 1975, 1982, Huntley, 1978; Pohn, 1974, Pratt and Ellyett, 1979). In the iterative calculation of the simulation methods, heat balance and heat transfer equations were solved repeatedly for various sets of albedo, surface roughness, surface humidity, thermal conductivity, and surface temperature. Furthermore, the surface relative humidity is sometimes assumed to be saturated. Watson(1971, 1975, 1982) tried to theoretically evaluate thermal inertia based on a one-dimensional heat transfer model. Nevertheless, his procedure still included some iterative solution methods for the determination of some parameters. In some approaches based on a heat balance model, some heat balance terms were excluded. For example, the latent heat flux was assumed to be zero because of no latent heat flux in an arid and semi-arid area (Kahle et al., 1984). Price's model excluded soil heat flux, because of no net

heating or cooling of the earth over a 24-hour period by time averaging (Price, 1980).

Even in 1985, Price evaluated apparent thermal inertia (ATI) assuming the ATI as a function of other variables such as net radiation, surface temperature, solar constant, atmospheric transmittance and ground heat flux. His evaluation of ATI was not based on a physical and mathematical solution, but on a iteration method.

Recently, Ho(1987) proposed a soil thermal model relating to soil heat flux. However, heat balance terms were obtained from regression analyses.

As above, in previous models based on both of the iterative calculation and analytical approaches, regression analyses were sometimes applied to evaluate the value of latent heat flux or sensible heat flux (Price, 1977, 1980, 1982; Watson,1975, 1982; Ho, 1987). Therefore, previous investigators have not successfully obtained a mathematical solution for the evaluation of thermal inertia based on one-dimensional heat transfer and heat balance models on the earth's surface. Furthermore, previous research simultaneously used thermal inertia (TI) and albedo (Pratt et al., 1978; Pratt and Ellyett, 1979).

The previous investigators included too many complicated input parameters for the atmospheric correction and other subjective parameters and excluded essential parameters of heat balance in their models. The relative humidity of soil surface in the thermal inertia model has been ignored or insufficiently adopted (Kahle, 1977). Sometimes, it was assumed to be saturated

and constant. This assumption overestimates the volume of the evaporation from soil surface.

Relationships between SM and the brightness temperature/ coefficient of backscatter of microwaves were evaluated (Schmugge et al., 1974; Ulaby et al., 1974, 1978, 1979, 1982, 1983a,b,; Eagleman and Lin, 1976; Njoku et al., 1977, 1982; Estes et al.,1977; Hirosawa et al., 1978; Chang et al., 1980; Newton et al., 1982; Wang, 1983, 1985, 1987; Wang et al., 1980,a, b, c; 1981, 1982, 1983; Burke et al., 1982; Dobson et al., 1981, 1985, 1986a, 1986b; Jackson, 1986, Jackson et al., 1981, 1982, 1984, 1986, 1987a,b; Bernard et al., 1982, 1986; O'Neill et al., 1984; Theis et al., 1984; Fung et al., 1985; Hallikainen et al., 1985; Camillo, et al., 1986; Rao et al., 1986; Schmugge et al., 1986; Stroosnijder et al, 1986; Bruckler et al., 1988; Musick and Polletier, 1988; Owe et al., 1988).

In these approaches, appropriate parameters (wave bands) and measurement systems for soil moisture were examined. Backscatter radiation from vegetated fields , the effects of surface roughness and soil texture were also examined to detect the energy below these canopies for the soil moisture estimation. In passive microwaves, brightness temperature was examined for SM estimation. Recently, the concept of a thermal model was introduced into the consideration of these passive microwaves (Camillo et al., 1986).

ii) As for landform classification, landform divisions have traditionally been attempted from map reading, morphometry and geological structure (Fenneman, 1914, 1928; Shimomura, 1926; Shimomura et al., 1934; Hall and Watanabe, 1932; Mino, 1935;

Watanabe, 1940, 1952). Recently, geomorphological mapping has progressed using the photogrammetrical method and photo-interpretation (Linton, 1951; Asami, 1951; Nakano, 1952; Nakano et al., 1968; Parry and Beswick, 1973; Verstappen, 1977; Stancioff and Hill, 1979; Oya et al., 1987). In order to avoid individual differences of methodology for geomorphological classifications, the quantitative analysis has been applied to the terrain classification (Okabe, 1968; Tarnocai and Kristof, 1976; Connors et al.; 1987; Franklin, 1987).

iii) As for wind erosion, the mechanism of sand drift and micro-topography of sand dunes have been studied by wind tunnel experiments. In these experiments, relationships between threshold velocity of wind speed and roughness, particle size and cohesion of soil were examined (Chepil and Milne, 1941; Chepil, 1945, 1946, 1950; Tanaka et al., 1954, 1959; Shiyatyy et al., 1972; Wilson and Cooke, 1980). The relationship between soil moisture and volume of soil erosion has not yet been discussed in detail. Strendansky(1981) obtained regression equations between wind speed and soil erosion as influenced by soil moisture on the basis of wind tunnel experiments.

Wind erosion in the Tokachi (Hokkaido) and Kanto Districts in Japan was studied by the field observation in relation to precipitation and soil moisture (Tanaka et. al., 1959; Kusakabe, 1964). Recently, a hazard map such as the erodibility map was constructed by a computer mapping procedure (Madsen et al., 1986). However, this map did not show actual soil erosion but soil properties affecting its erodibility.

2. Methodology - Measurements and data processing

2.1 Study Areas

Surface temperatures and soil moisture were measured at an air monitoring station (AMS). The soil moisture and meteorological elements were obtained at the experimental field (referred to as the field) of the National Institute for Environmental Studies (NIES). The reflectance of soil surface was measured in the laboratory of the NIES. Airborne and spaceborne multispectral scanner (MSS) and ground truth data were obtained in the Kujukuri coastal plain, Tsuchiura and old Joban coal mining areas. Figure 1 shows sites of these study areas. The overview of these areas can be summarized as follows.

(1) Air monitoring station

An air monitoring station (AMS) is located at 36°2'42"N, 140°7'21"E, in western Ibaraki Prefecture in central Japan. Since April 1978, air pollution and meteorological elements have been continually observed. Since 1980, surface temperature (Ts) and soil moisture have been also observed in the measurement system at the AMS. Photograph 1 shows soil containers at the left side of the tower. The instrument monitoring building of the AMS is behind the tower.

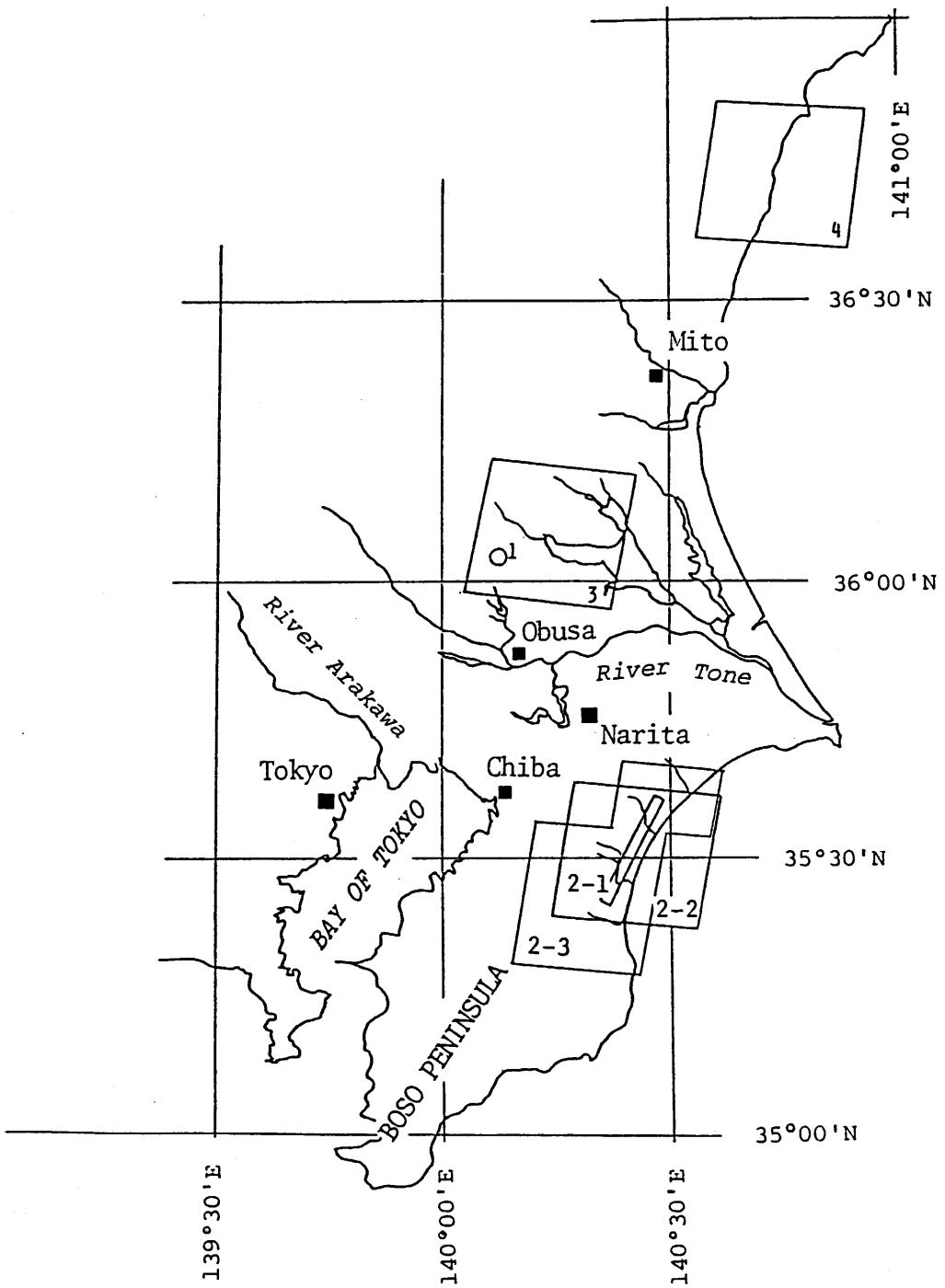

Figure 1 Index map of study areas.

1: Air monitoring station and experimental field at the National Institute for Environmental Studies, 2: Southern Kujukuri coastal plain (2-1: area of airborne MSS experiment, 2-2: area of Landsat TM experiment, 2-3: area of Landsat TM experiment), 3: Tsuchiura and its vicinity, 4: Old Joban coal mining area.

Photograph 1

Experimental equipments in the field and the Air monitoring station at the National Institute for Environmental Studies.

Photograph 2

Observation system at the experimental field.

(2) Experimental field

The experimental field is located at 36°00'35"N, 140°4' 50"E. Since 1985, heat balance terms have been observed to develop the thermal inertia model for determining soil moisture. Photograph 2 shows the experimental system of the field.

(3) Kujukuri coastal plain

Micro-reliefs such as beach ridges, elevated bars, sandspits and dunes with heights of several meters are arranged in parallel to the shoreline in the Kujukuri coastal plain. At least ten elevated sandspits or bars are observed in this area. The most inland part of this plain is covered by very moist and peaty soil. Elevated sand spits and bars are covered by sandy soil, having back marshes with peaty soil. The cities of Mobara, Togane and Naruto and towns of Shirako, Kujukuri and Hasunuma are formed on large elevated sandspits and bars. The southern part of this plain (Fig. 2), particularly Shirako and Kujukuri, have been damaged by severe land subsidence due to natural-gas mining. Land subsidence has resulted in submergence of paddy fields, the contamination of well water by sea water, and the inundation of inner parts of the plain by sea water.

(4) Tsuchiura and its vicinity

The lowland area with 2 - 10 m elevation in the lower basin of the Sakura river near Tsuchiura is surrounded by the Tsukuba-Inashiki upland area, the Nihari-Dejima upland area and Lake Kasumigaura (see Fig. 3). Micro-topographies such as natural

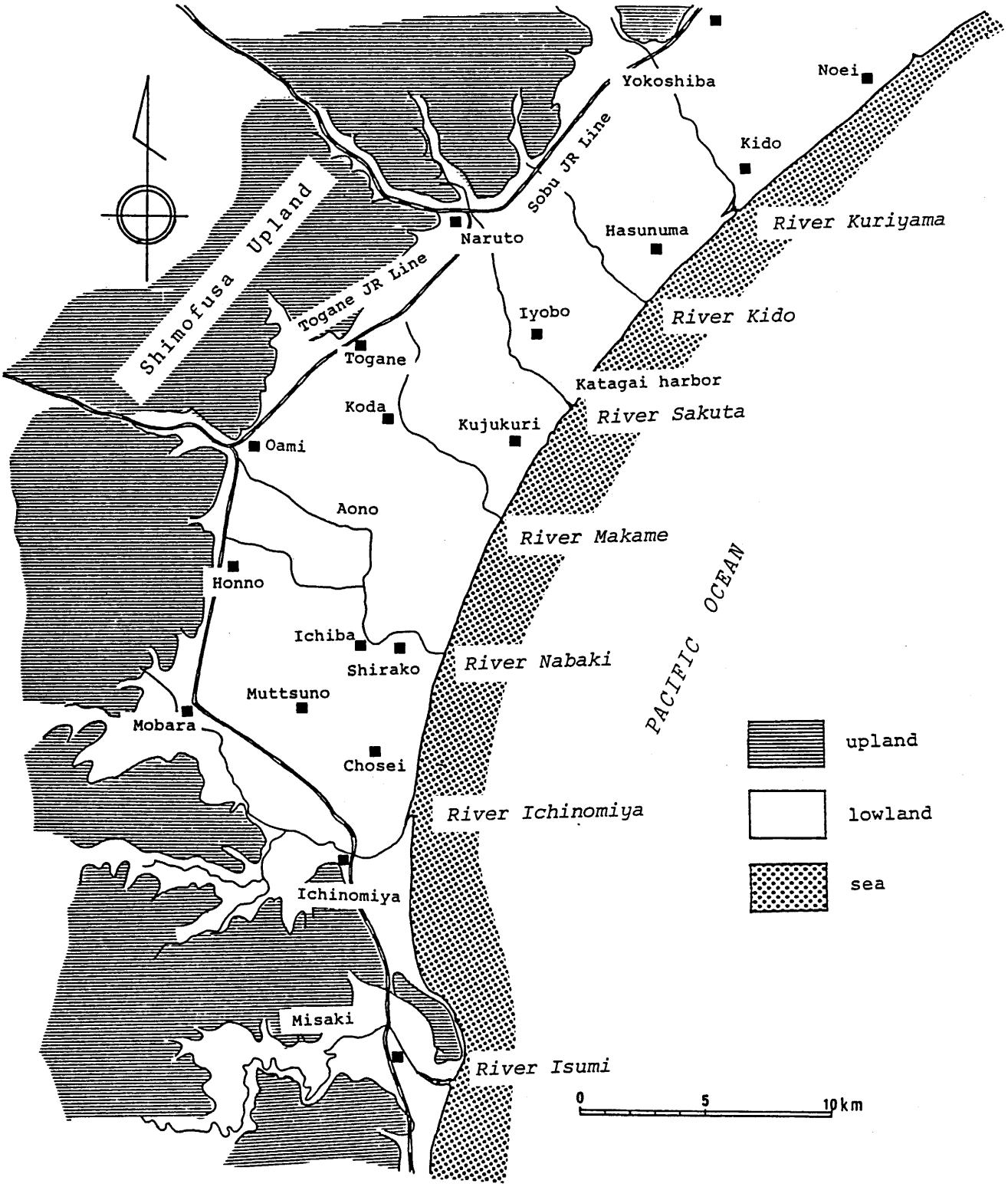

Figure 2 Southern Kujukuri coastal plain.

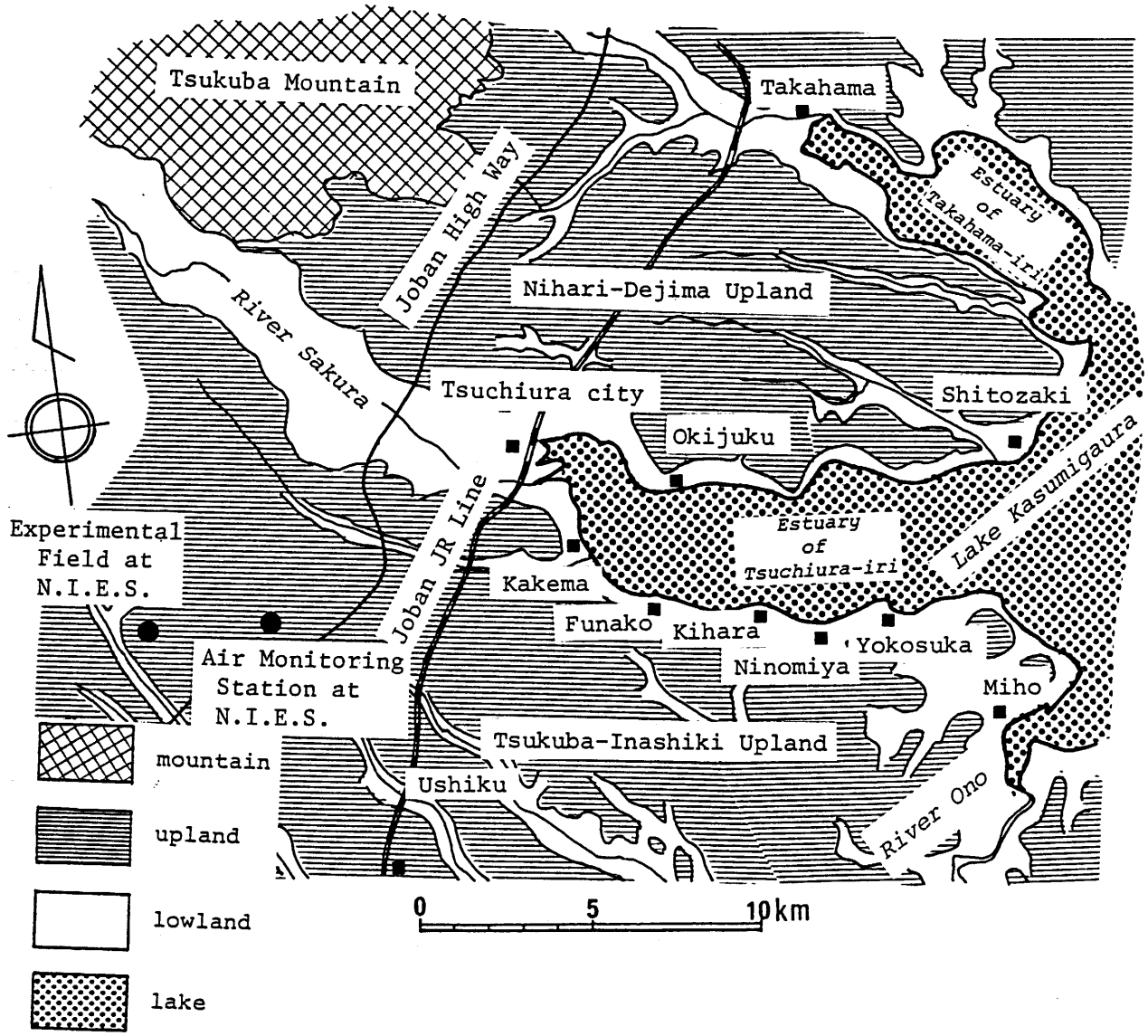

Figure 3 Tsuchiura city and its vicinity.

levees, elevated sand-spits and alluvial terraces were observed in the alluvial plain.

The relief between swells and the lowland plain is about 1 to 2 m. The water flow is very slow. The city of Tsuchiura has developed on elevated bars or spits in this plain. The hinterland of the city has remained swampy lowland.

In the lowland around Lake Kasumigaura, lotus plants have been cultivated. Lotus fields are also found in Ninomiya and Yokosuka areas towards the east, and Kakema and Funako areas towards the south. These fields are observed as flooded and swampy areas in winter.

(5) Old Joban coal mining area

The old Joban coal mining area is a general name of the region, which consists of Taga, Iwaki and Futaba coal mining areas in the northern part of the Ibaraki Prefecture (Marui, 1961). The town of Isohara is located in the Taga mining area. The alluvial lowland at Isohara and its vicinity consists of coastal and deltaic plains with elevations of about 1 to 10 m above sea level (Fig. 4).

Emerged sand bars, spits and beach ridges near the coastline are parallel to the shoreline. Depressions and submergence of lowland fields were caused by no gobbing in the levels and shafts after the mining. These phenomena were observed around the village of Waku and the western part of Isohara (Yamazaki, 1963). Intensive land reclamation work has been done in this severe land

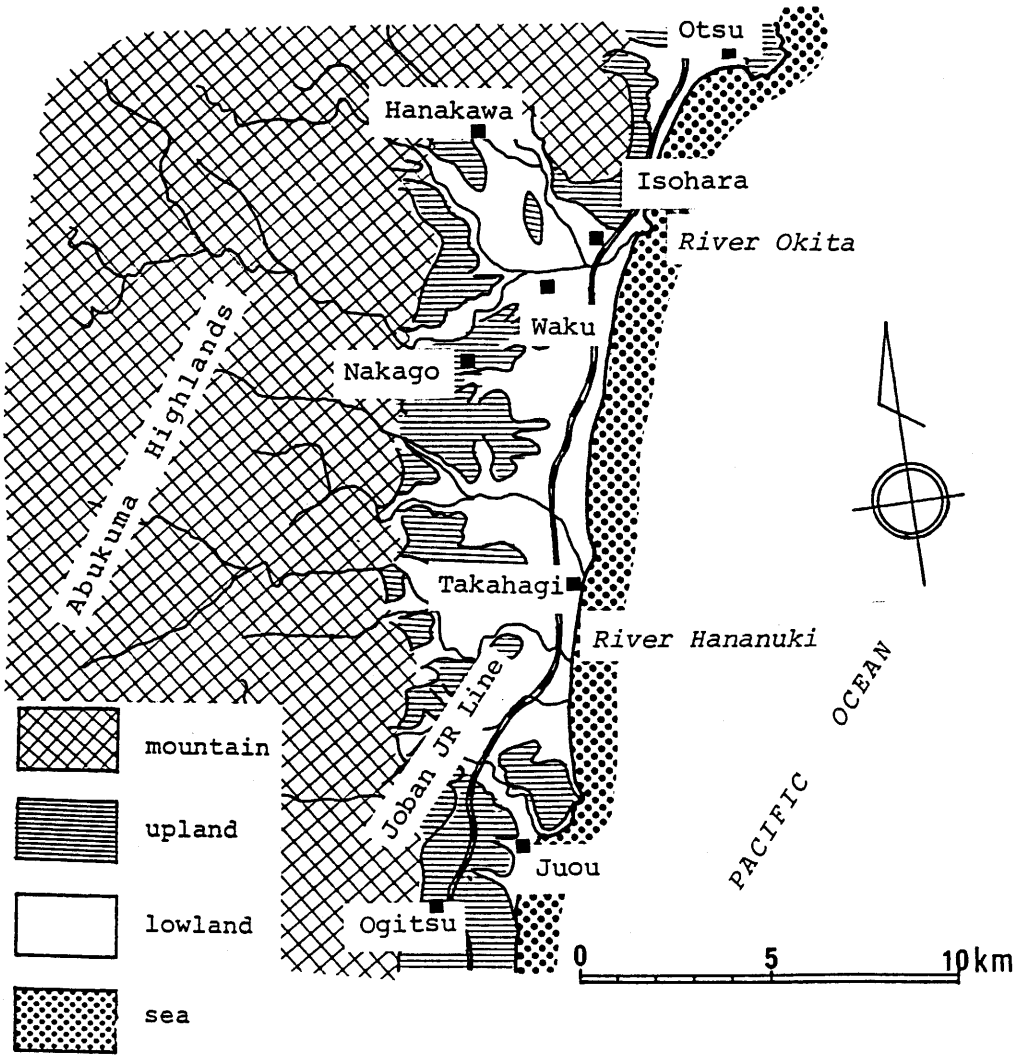

Figure 4 Old Joban coal mining area.

subsidence area near Waku. The ground in that area is used as lowland fields and farmers' residential areas.

2.2 Micro-meteorological observation

2.2.1 Soil moisture and meteorological measurements

(1) Meteorological measurements at Air monitoring station.

Figure 5 shows Kanto loamy soil and soil taken from paddy fields. These soils were observed by a thermal IR radiometer (Toshiba ER2006-IR radiometer). Figure 5 (A) shows a cross section of the paddy soil in containers and the equipment arrangement. These containers were wrapped up in polystyrene foam to avoid lateral heat flow.

Paddy soil was sampled from 0 to 60 cm in depth of lowland field at Obusa in western Ibaraki Prefecture. Size distribution of the soil is shown in Table 1.

Table 1 Particle size of the paddy soil obtained from Obusa, western Ibaraki Prefecture. (According to the Wentworth grade scale)

particle size	distribution ratio	
> 0.25 mm	7.8 %	(coarse/medium sand)
0.25 - 0.0625	13.6 %	(fine/very fine sand)
< 0.0625mm	78.6 %	(silt/clay)

One of the potted paddy soils was kept under natural conditions. Another soil container was supplied water through a

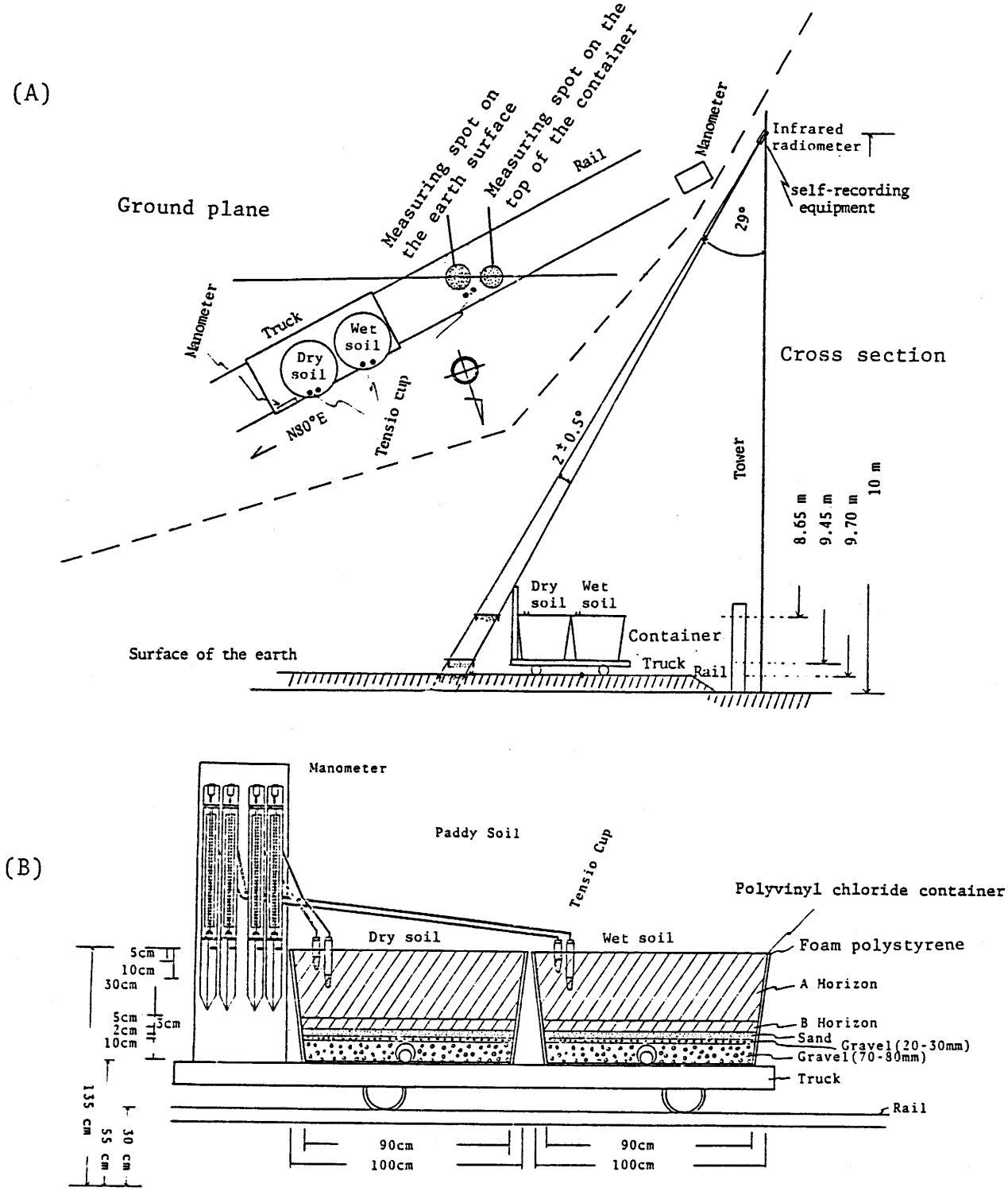

Figure 5 Schematic profile of paddy soils in the containers and measurement system in the field of the Air monitoring station(AMS)

(A): Measurement system in the field, (B): Profiles of paddy soils in the containers and tensiometers

Photograph 3

Measurement of instrument error.

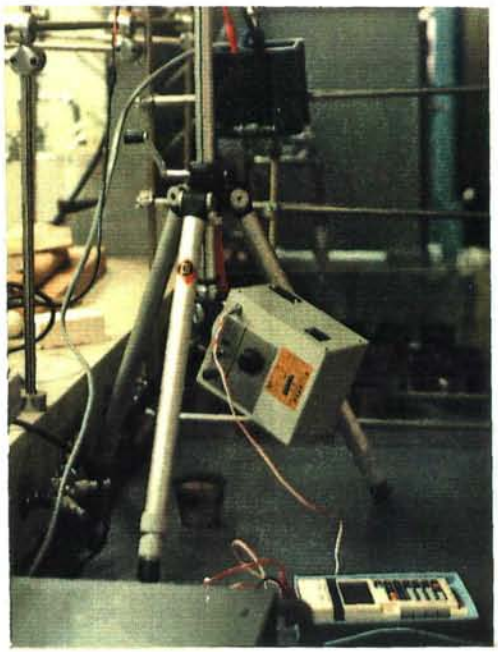

Photograph 4

Measurement system of surface reflectance of sandy soil.

siphon connected with a water tank. Six porous cups were set at 5 and 10 cm depths in each soil pot. The surface temperature and soil moisture of each pot were measured every hour. From August 1980 to September 1981 surface soil moisture and meteorological elements were observed at the AMS to evaluate the relationships between moisture and surface temperature of soil.

(2) Meteorological observations at the observation field.

The validity of the study's thermal model for soil moisture estimation was examined by measuring micro-meteorological elements on the surface of Kanto loamy soil from December 1986 to July 1987. Photograph 2 shows the arrangement of the micro-meteorological observation system at the field. Electrodes were set at 1, 5, 10 and 20 cm depths for the soil moisture measurements by the electrical conductivity method. In addition, one tensio cup (Kiya-type porous cup) was set at 5 cm depth to measure soil moisture. An Eiko CN-9 type heat flux plate was set at 0.5 cm depth for the heat flux measurement of the soil.

Net radiation was observed using an Eiko CN-11 type net radiometer at 1.3 m above the ground. The surface temperature was measured by a National ER-2007 SAI type IR radiometer set at a height of 1.5 m. Global solar and reflected solar radiation were observed by Eiko MR-21 type solarimeters. Dry and wet bulb thermocouple thermometers were set at 0.1 and 1.1 m above the ground.

The soil temperature was measured with thermocouple thermometers with electric terminals at the depths of 0.5, 1.0, 2.0, 5.0, 10.0, 20.0, 40.0, 60.0, 80.0 and 100.0 cm. Air pressure and wind speed were observed using an Uizin-type pressure gauge and Ota P-type wind vane/anemometers respectively.

These meteorological elements were measured at one minute intervals. Row data of one minutes intervals and values averaged over 30 minutes were processed by micro-computer (NEC PC9801-Vm2 / EPSON HC-20) and fed to floppy disks every 30 minutes.

2.2.2 Data processing

Relationships between the surface temperature and the soil moisture were depicted in the first step. In the second step, daily variations in the soil moisture at 5 and 10 cm depths were depicted graphically. These data were processed by regression analyses in the third step. Before these analyses, the soil moisture data were averaged. Diurnal ranges in Ts and meteorological elements were obtained by subtracting minimum data from maximum data. Each of the heat balance terms was calculated by the heat balance method. These thermal inertia of soil were calculated by these heat balance terms for the evaluation of the thermal inertia model.

2.3 Spectral reflectance and moisture determination in the laboratory

Ground truth for a remote sensing experiment may contain errors. To reduce these errors, sensors were corrected by the measurement of instrument error. Photograph 3 shows the calibration of thermal IR radiometers which is one of the instruments for the field measurement. In the laboratory, the calibration was carried out using a standard thermometer before the field observation. Also spectral reflectance of soil was measured and soil moisture was determined in the laboratory.

(1) Spectral reflectance of soil.

The spectral reflectance of soil was determined using a hand-carried photometer (Abe Sekkei type 2703). Relationships between spectral reflectance and soil moisture were examined using these data.

Reflected radiation intensity was measured at 19 wavelengths (0.4, 0.425, 0.450, 0.475, 0.500, 0.525, 0.550, 0.575, 0.600, 0.625, 0.650, 0.675, 0.700, 0.750, 0.850, 0.950, 1.050, 1.150 and 1.250 μm.

A soil sample with particle sizes of smaller than 2 mm was prepared by sieving coarse sand from the original soil sample. Size distribution of soil is shown in Table 2.

Table 2 Particle size of the sandy soil obtained from the Kujukuri coastal plain. (According to the Wentworth grade scale)

particle size	distribution ratio	
> 0.25 mm	2.1 %	(coarse/medium sand)
0.25 - 0.125 mm	36.4 %	(fine sand)
0.125 - 0.0625mm	60.3 %	(very fine sand)
< 0.0625mm	1.2 %	(silt/clay)

Observation systems used in this experiment are shown in Photo. 4. The soil sample was set in a small metal cup. Its inside wall was painted black. It was illuminated by a standard tungsten halogen lamp (Ushikata Electric Company, JPD 100-500CS) with an incident angle of 30 degrees.

The light beam reflected from the soil surface was detected by the photometer. The soil surface and a standard white plate were alternately measured. The white plate was painted with white color-Kodak reflectance coating (CAT. No. 6080).

For accuracy in measurement, the lamp was calibrated using the standard lamp of the Japan Electric Meters Inspection Cooperation. The electric current from the sensor was fed into a digital voltmeter in front of the hand-carried photometer.

(2) Soil moisture determination.

The moisture in soil samples was determined by weighing before and after oven-drying at a constant temperature (110°C) for

48 hours. Mass wetness (SV) and total water storage (SW) were calculated from:

$$SV = (Wg - Dg) / Dg \times 100$$

and

$$SW = SV \times \text{dry bulk density} \times \text{depth} \times 0.1$$

where SV is mass wetness (%), SW, total water storage (mm), Dg, dry weight of soil, and Wg, wet weight of soil. The error associated with this procedure is minimal and less than one percent of the dry weight.

The dry bulk density of the soil was also calculated from:

$$\text{Dry bulk density} = Dg / \text{total volume (solids and pores)}$$

Though a soil sample at a depth from 0 to 10 cm is used in the determination of total water storage, soil sampled from a depth of 0 to 5 cm was used for efficient sampling of soil in field surveys in this study.

The bulk density varied from 0.4 to 1.1 in the Kujukuri coastal plain. The wettest soil (peaty soil) in the trough-like lowland showed the minimum of bulk density. The value obtained from the loamy soil at the field of NIES was averaged as 0.64.

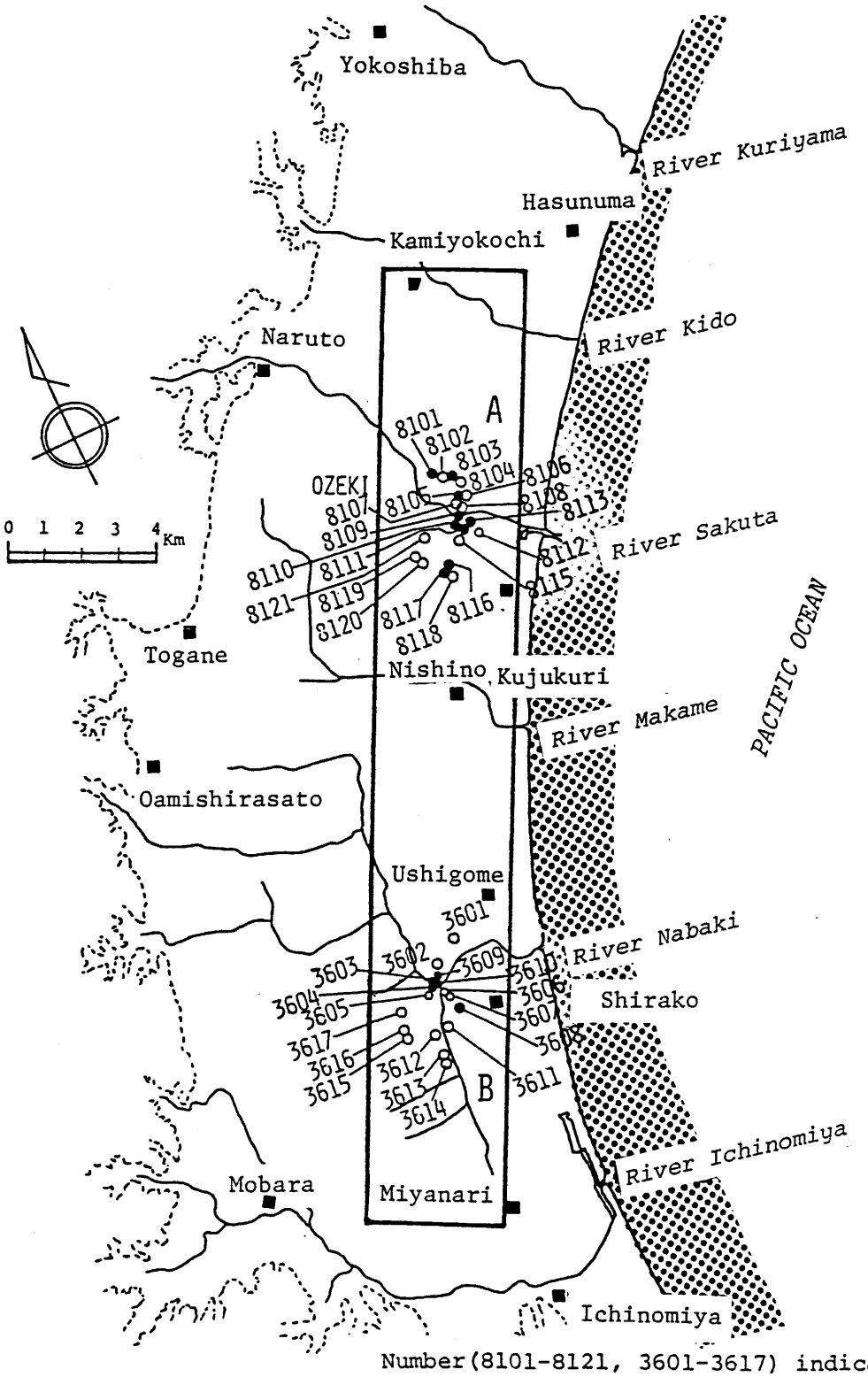

Number(8101-8121, 3601-3617) indicates soil sampling and surface temperature measurement point. Locality of 8101 is ground truth center.

Figure 6 Ground truth points and flight path in the southern Kujukuri coastal plain (Jan. 23, 1981)

2.4 Data acquisition in the Kujukuri coastal plain, Tsuchiura and the old Joban coal mining area

2.4.1 Airborne measurement and ground truth

(1) Airborne MSS measurement

An area of about 25 km length was observed by two airborne MSS (MSS-BG-1A and Bendix M^2S). These measurements were carried out three times, at 7:05, 9:35 and 12:05 on January 23, 1981. These measurements were also carried out at 6:18, 9:15 and 12:59 on November 15, 1985. The spectral wavelengths utilized on each date are showed in Table 3.

The sensor can detect radiation in 13 wavelength bands; however, Channels 12 and 13 were out of order for the measurement in 1981. Spectral reflectances in 11 channels as shown in Table 3 were recorded into the onboard data recorder. The ground resolution was about 4.8 to 4.9 m/pixel and the swath width was about 3000 m.

The flight days were fairly clear and free from haze. Objects and aircraft several kilometers distant from the observer were clearly distinguished, thus the visibility was good for the experiments.

(2) Ground truth

Figure 6 shows the ground truth areas. The temperature and other weather elements are shown in Table 4. Land use surveys and soil sampling were carried out in the ground truth areas (Areas A

Table 3 Spectral wavelengths in each band of airborne MSS data.

MSS-BG-1A Jan. 23, 1981			Bendix M^2S Nov. 15, 1985		
Channel No.	Wavelength	Data analyzed	Channel No.	Wavelength	Data analyzed
0	0.30-0.35 μm				
1	0.35-0.40		1	0.38-0.44 μm	o
2A	0.43-0.45				
3A	0.47-0.49	o	2	0.44-0.49	o
4A	0.51-0.53		3	0.49-0.54	o
5A	0.54-0.56	o	4	0.54-0.58	o
6	0.60-0.65	o	5	0.58-0.62	o
7A	0.66-0.68	o	6	0.62-0.66	o
			7	0.66-0.77	o
9	0.80-0.90	o	8	0.70-0.74	o
			9	0.77-0.86	o
			10	0.97-1.06	o
11	10.5 -12.5	o	11	8.0-13.0	o
12	4.3 - 5.5	N.A.			
13	4.5 - 4.9	N.A.			

symbol(o) : used in this study, N.A. : not available

Table 4 Meteorological data in the airborne MSS measurements.

Jan. 23, 1981					Nov. 15, 1985				
Flight time	Air temperature	Humidity	Wind dir.	speed	Flight time	Air temperature	Humidity	Wind dir.	speed
7:01 -7:07	-4.7 °C	56%	N	0.3m/S	6:15 -6:22	0.8 °C	96%	SSW	0.3m/s
9:31 -9:37	3.1	44	NW	3.5	9:13 -9:19	12.7	58	N	2.3
12:04 -12:10	7.3	39	N	3.8	12:58 -13:00	15.0	51	E	0.8

and B) in the Kujukuri coastal plain. In general, soil moisture in Area B was considerably higher than that in Area A.

1) Soil surface temperature.

Soil surface temperatures used to correct airborne thermal IR data were measured with hand-carried IR radiometers. Thermal IR radiometers with view angles of 2° were set at 1.5 m above the surface. Thus, the ground resolution of the IR radiometer was about 5 cm x 5 cm, and that of the airborne MSS was about 5 m x 5 m. Therefore, to reduce the gap in sizes of target areas, surface temperatures were measured three times in each corner and the center of the square target (5 m x 5 m) site. Therefore, fifteen data points were averaged for each ground truth site.

2) Meteorological observation.

Meteorological elements were obtained from the ground truth center (No. 8101 in Fig. 6). Data on air temperature, relative humidity, wind direction and wind speed 1.5 m above the soil surface at the ground truth center are shown in Table 4.

Micro-meteorological elements such as net radiation, albedo, air pressure, surface temperature, heat flow in soil, reflected radiation from the earth surface, global solar radiation and air temperature were observed at the ground truth center on November 15, 1985. However, the net radiation at the ground truth center was estimated using relationships between net radiation and global solar radiation obtained from the experiments at the field (Fig. 7), and the albedo was estimated from empirical relationships

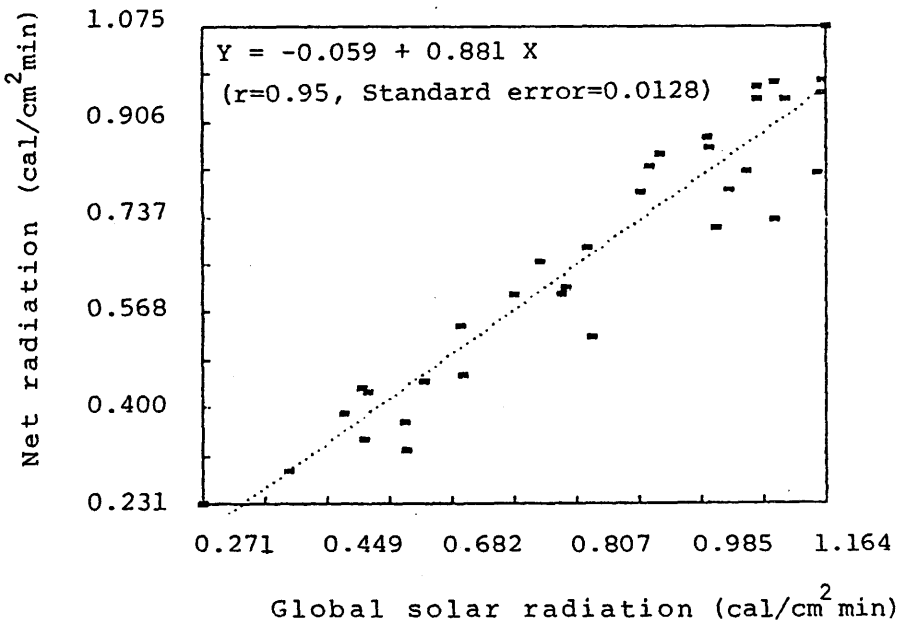

Figure 7 Relation between net radiation and global solar radiation observed at the field from August 6 to 27, 1986.

Dotted line indicates the regression line.

between albedo and spectral reflectance in the airborne experiment in 1981.

3) Soil sampling.

Soil samples of 100 cm^3 were collected from twenty sites using soil samplers. Soil from 0 to 5 cm depth was sampled after the measurement of surface temperature. Soils were sampled at 20 ground truth sites in the center of each site. About 60 minutes were needed to obtain soil samples from these sampling points.

4) Land cover observations.

After the meteorological measurements and soil sampling, 29 land cover types were observed over a 4 days period. The land cover types are as follows:

1),2) paddy fields, 3) green pasture, 4) barley, 5) radish, 6) cabbages, 7) welsh onion, 8) young welsh onion, 9) grass sprout, 10) bare soil with buried straw, 11) pasture, 12) sparse weed, 13) lawn, 14) dense weeds, 15) pine grove, 16) Japanese cedar forests, 17) mixed forests, 18) wet sand, 19), 20), 21) dry sand, 22) silt, 23) water, 24) concrete, 25) asphalt, 26) straw-thatched roofs, 27) tiled roofs, 28) slated roofs, and 29) greenhouse.

(3) Data processing

Original data in the high density digital tapes (HDDT) were converted to computer compatible tapes (CCT). The total number of

scan lines in the high density digital tape (HDDT) data was 21880. Every scan line consisted of 802 pixels in the CCT obtained at 12:05 on Jan. 23, 1981. They were reduced to 5470 lines for the CCT by sampling every four lines.

Geometric distortion due to pitching, yawing and rolling of the platform was mechanically corrected using onboard systems. The data obtained in the first flight at 7:05 on Jan. 23, 1981 was not used for mapping of soil moisture, because the gyro-compass unit was not in operation.

For the analysis, two data sets (imageries), each consisting of 768 (pixel) x 768 (lines), were extracted from the CCT data having 802 (pixel) x 5470 (lines). While locating ground truth sites and ground control points for geometric rectification of MSS images, several conspicuous targets were picked up on the 1:5000 air photo maps. These points showed land marks such as crossroads, corner of plowland and paddy fields, buildings, forests, rivers, and bridges. These points were plotted on digital maps derived from MSS data. The control points were used for the reference for geometric rectification and registration of the two MSS images. The registration of two images was carried out by computer programming based on a projective transformation method. Two images obtained on the first (6:15-6:22) and third flights (12:58-13:00) on Nov. 15, 1985 were geometrically rectified. Later, sample data for the statistical processing were extracted from each CCT.

Figure 8 shows the relationships between CCT data and albedo. The albedo was measured in and around the ground truth center (No.

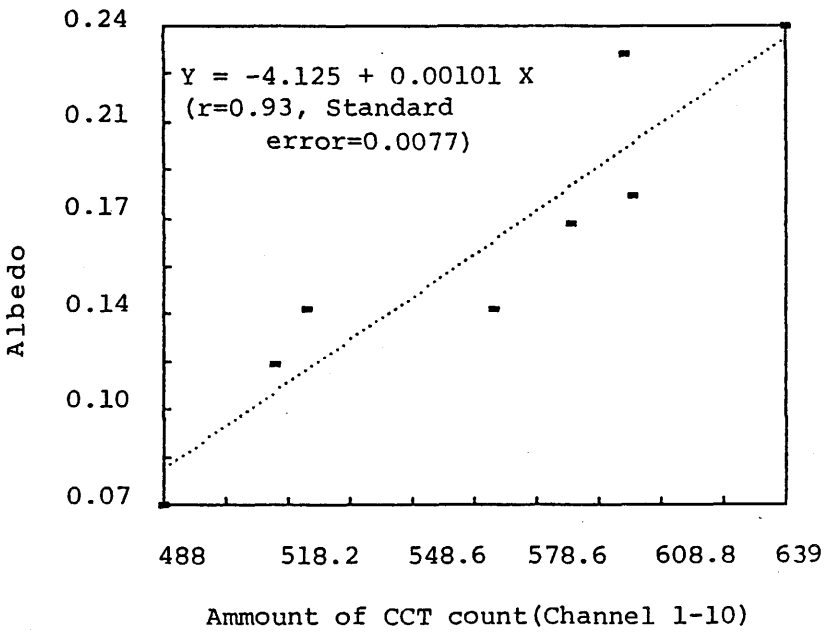

Figure 8 Regression of albedo and amount of CCT count of airborne MSS data (Channel 1-10)

Dotted line indicates the regression line.

8101 in Fig. 6). Since the CCT count in the visible and near IR spectral region was strongly correlated with albedo, a linear regression line was fitted to pixel data of the imagery for estimating albedo (α'). At the ground truth center, downward longwave radiation (L) and diffusion velocity (D) were calculated. This analysis based on the heat balance method will be discussed fully in Chapter 3.2.1. Surface temperature (Ts), albedo and downward longwave radiation so estimated, were fed onto another magnetic tape. Later, MSS data were processed with discriminant and regression analyses and computer mapping techniques.

2.4.2 Satellite measurement and ground truth

(1) Satellite MSS and TM measurements

The swath width of the scanner of Landsat is 185 km, and a full scene covers an area of 185 km x 170 km. The ground resolution of one pixel of Landsat-3 MSS data is 57 m x 57 m and that of Landsat-5 Thematic Mapper (TM) CCT data of Band 1, 2, 3, 4, 5, and 7 is about 28.5 m x 28.5 m. The pixel size of band 6 of TM data is 114 m x 114 m.

The Landsat data were obtained from the Earth Observation Center, National Space Development Agency (NASDA), Saitama Prefecture in Japan. The dimensions of the imagery selected from Landsat MSS scenes (Path 115 Row 34, 35, Fukushima and Tokyo, Path 117 Row 25, Tokyo) are 512 (pixel) x 512 (lines). The Landsat-3 MSS data obtained at 9:33 on January 19, 1980, consists of bands 4, 5, 6 and 7. The Thematic mapper (TM) imagery at about

Table 5 Spectral wavelengths of Landsat data.

Landsat-3 MSS(Jan. 19, 1980)			Landsat-5 TM(Feb. 14, 1987)		
Band No.	Wavelength μm	Data analyzed	Band No.	Wavelength μm	Data analyzed
4	0.50-0.60	o	1	0.45-0.52	o
5	0.60-0.70	o	2	0.52-0.60	o
6	0.70-0.80	o	3	0.63-0.69	o
7	0.80-1.10	o	4	0.75-0.90	o
			5	1.55-1.75	o
			6	10.4-12.5	
			7	2.08-2.35	o

symbol(o) : used in this study

9:30 on February 14, 1987, consists of seven bands. These bands are listed in Table 5.

(2) Ground truth

Ground truth was carried out twice, each time for four days (January 17 to 20, 1980 and February 14 to 17, 1987) in the Kujukuri coastal plain (see Fig. 9). Field work was carried out to observe the land use in and around Tsuchiura and Tsukuba for application to photo-interpretation.

1) Land cover observation.

For the discrimination of land cover by the remote sensing data, many land covers were observed by photo-interpretation and field works in the Tsuchiura and Kujukuri area. These sampled data for the discrimination of land cover are as follows:

1) bare soil, 2) bare soil (with straw of one meter spacing), 3) bare soil after radish harvest, 4) swampy bare soil after harvesting of lotus root, 5) paddy fields (with stubble), 6) frozen paddy fields, 7) frost covered paddy fields, 8) partly flooded paddy fields, 9) mossy paddy fields, 10) truck farm, 11) welsh onion, 17) barley (sprouting), 13) weeds, 14) lawn, 15) reeds, 16) evergreen forests, 17) farm houses, 18) dry sand, 19) blackish gray sand, 20) sea water,21) flooded fields, 22) flooded paddy fields, 23) inland water, 24) concrete building, and 25) slate-roofed houses.

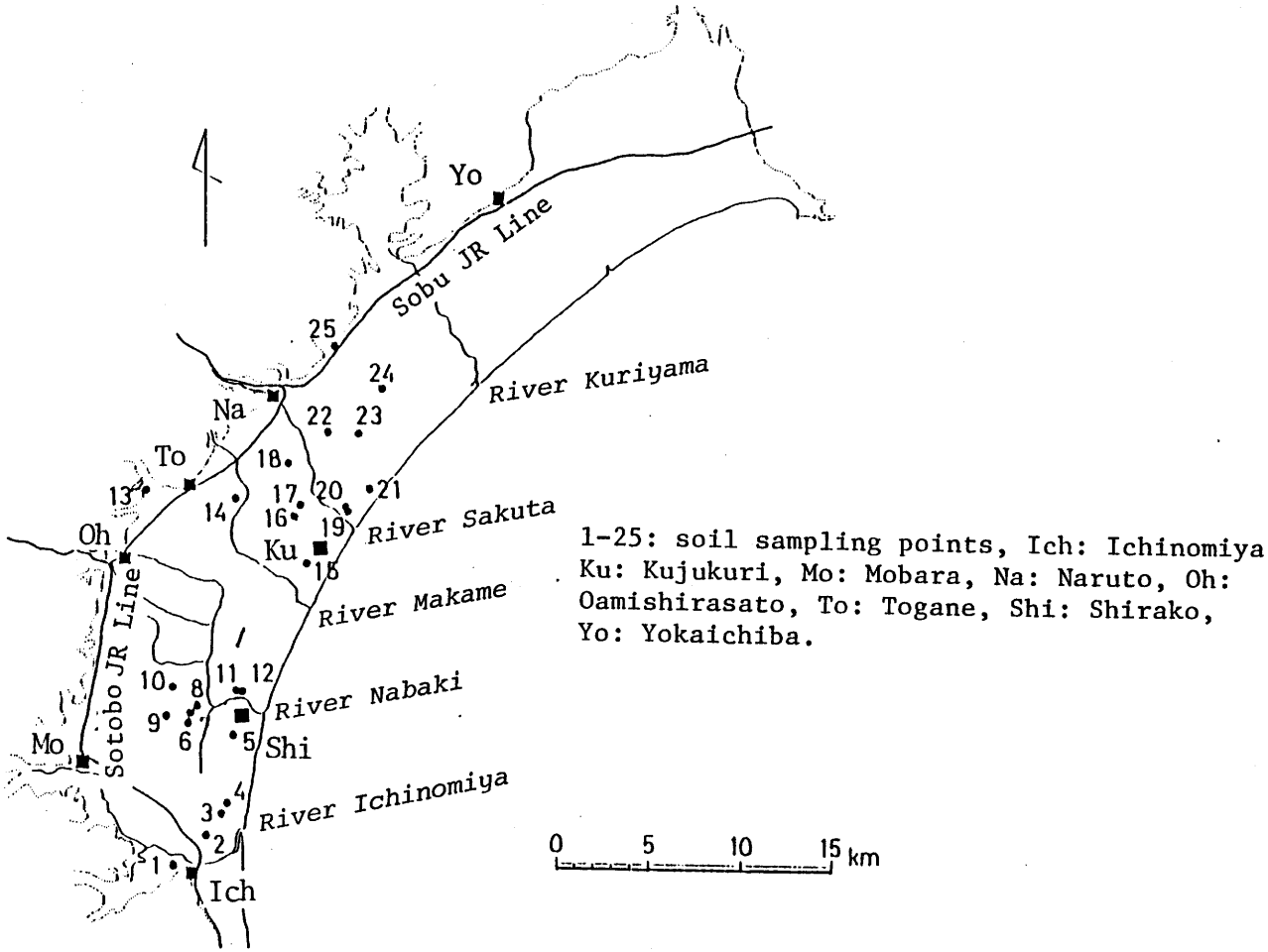

Figure 9 Locations of sampling points in the Kujukuri coastal plain (Jan. 17-20, 1980).

2) Soil sampling.

The procedures of soil sampling and determining soil moisture were the same as those used in the airborne MSS measurements. Two soil samples were obtained in each target area from January 17 to 20, and five samples were obtained from February 14 to 17. Then, the soil moistures were averaged. In both sampling for MSS and TM measurement, soil was very dry because of no precipitation for a week preceding this measurement.

(3) Data processing

The spaceborne MSS and TM data were processed with the same procedure (discriminant and regression analyses, and computer mapping techniques) as the experiments with the airborne MSS data.

3. Modeling of soil moisture estimation

First, the daily variations of surface temperature and soil moisture are examined, and a thermal inertia model is established in this chapter. Secondly, models for estimating soil moisture are developed using data obtained from the field of the National Institute for Environmental Studies (NIES) and the Kujukuri coastal plain.

The models for SM estimation are also developed empirically using visible reflectances from soil surfaces. These models will be applied to MSS and TM data to illustrate the geographical distribution of soil moisture in Chapter 4.

3.1 Modeling of soil moisture estimation with thermal IR data obtained by ground truth measurements

3.1.1 Variations in surface temperature and soil moisture

(1) Variations in surface temperature

Relationships between surface temperature (Ts) and soil moisture (SM) were examined using the data obtained from the potted soils at the air monitoring station (AMS). Figure 10 shows that the surface temperature in the daytime was higher for the dry soil than for the wet soil. This was caused by the higher evaporative cooling in the wet soil.

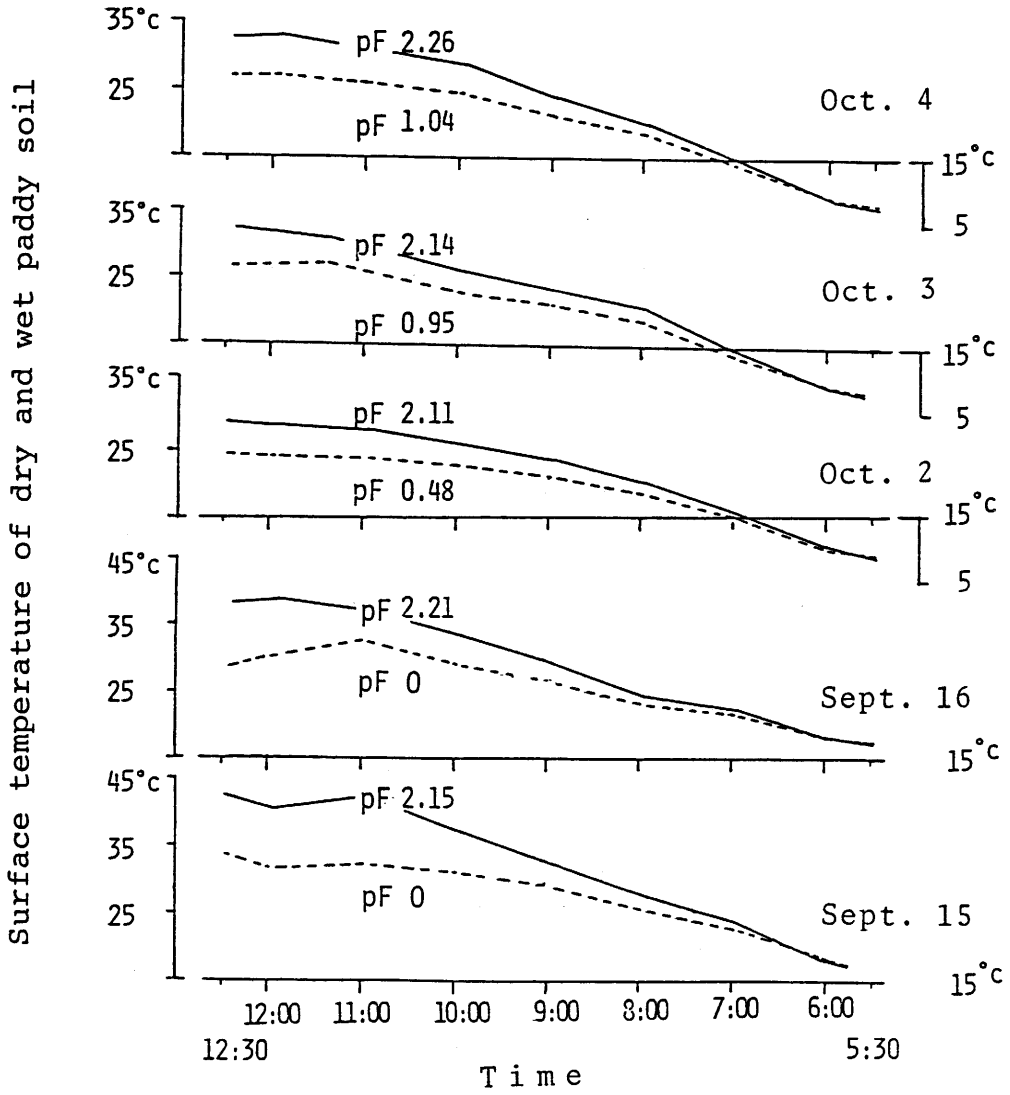

Figure 10 Variations in surface temperature of paddy soil in 1980.

The value of the line shows pF value of paddy soil. Solid line: dry paddy soil, dashed line: wet paddy soil.

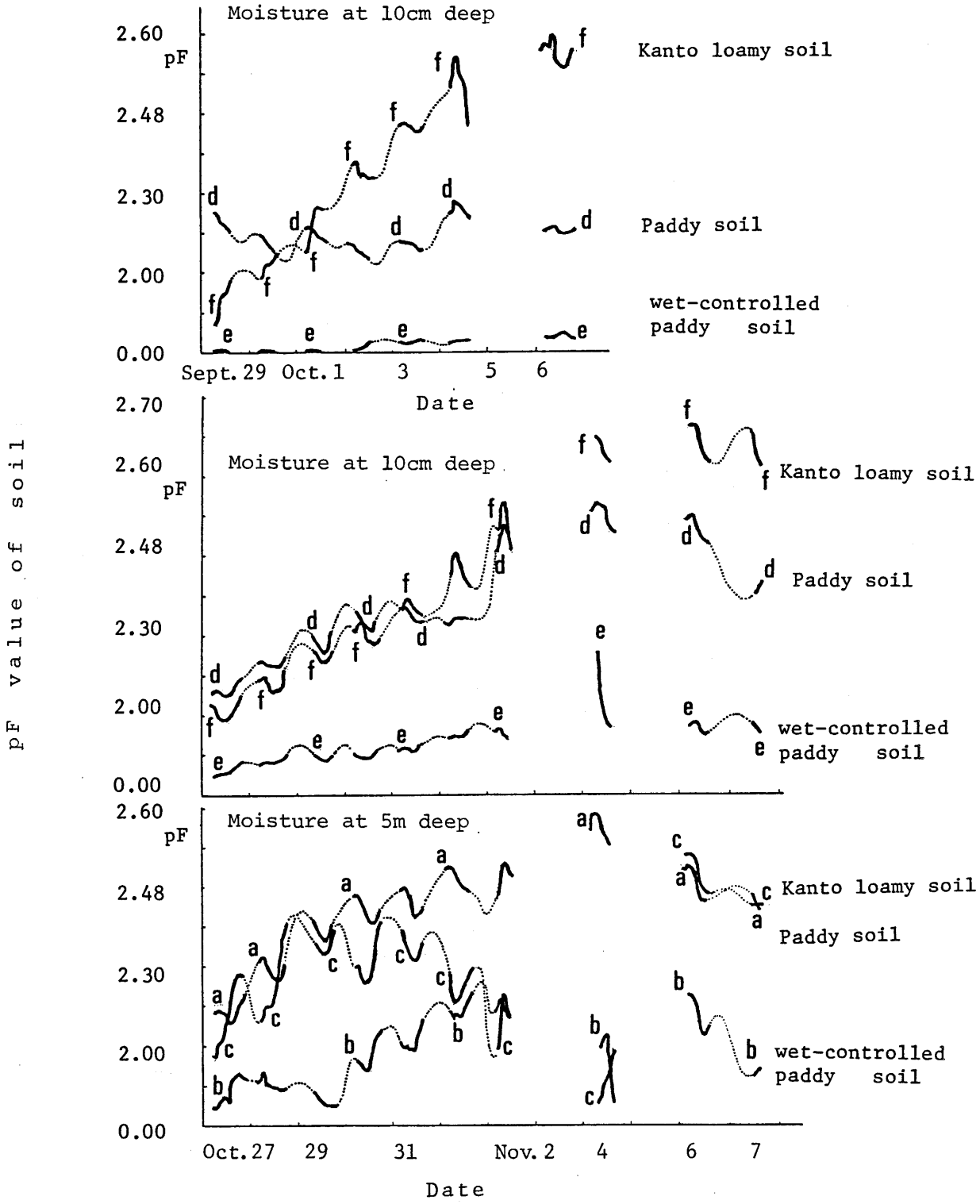

Figure 11 Daily and day-to-day variations in soil moisture at depths of 5 and 10 cm obtained from the experiment at the Air monitoring station in 1980.

Dotted line shows the extrapolation of the variations in the soil moisture. Superscribed letters a-c indicate paddy soil, wet controlled paddy soil and Kanto loamy soil at 5 cm depth, respectively. Letters d-f indicate paddy soil, wet controlled paddy soil and Kanto loamy soil at 10 cm depth, respectively.

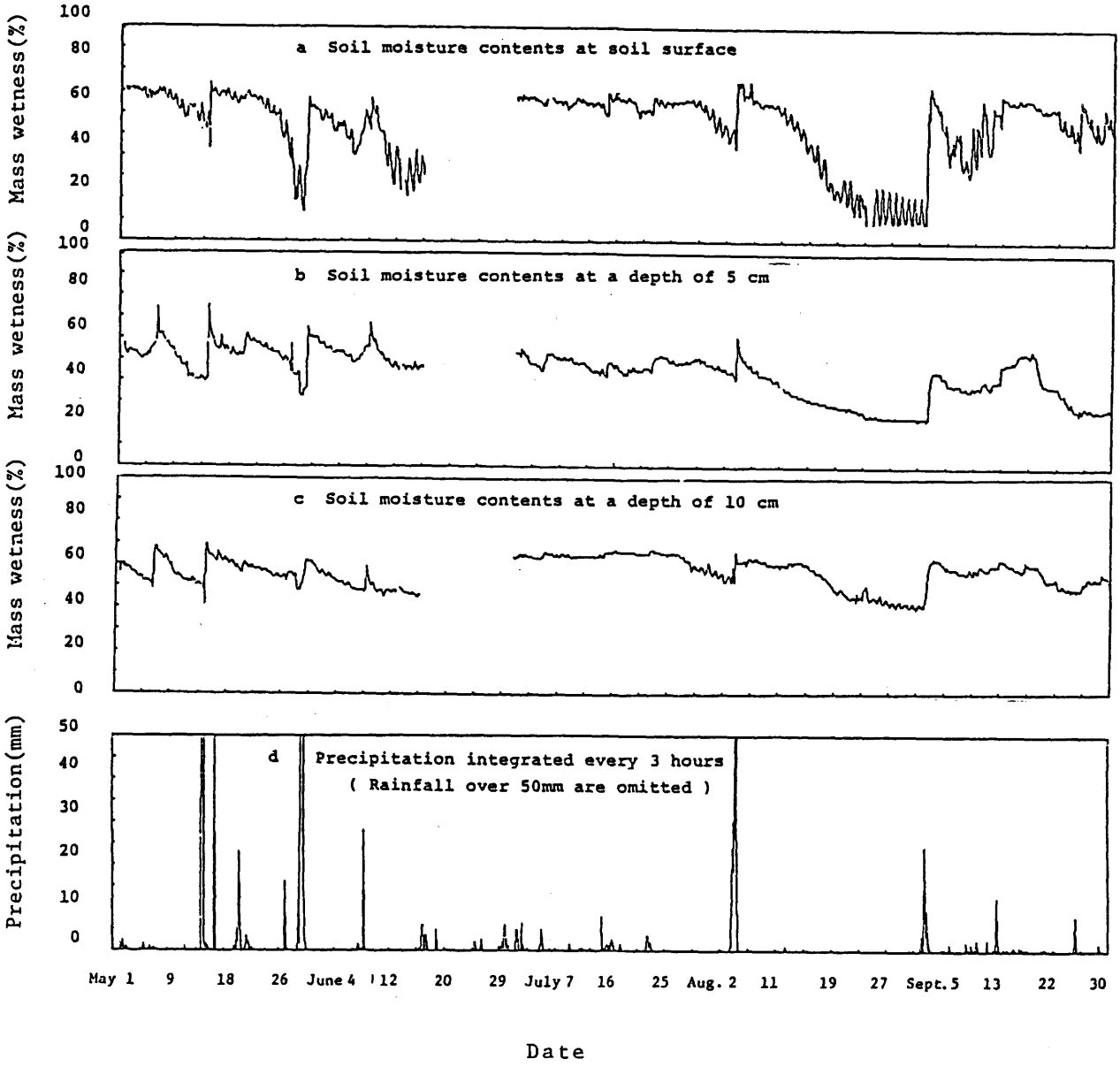

Figure 12 Day-to-day variations in soil moisture (mass wetness) of Kanto loamy soil obtained from the experiment at the field from May 1 to September 30, 1986.

(2) Variations in soil moisture

Figure 11 shows daily variations in pF value of soils at depths of 5 and 10 cm obtained from the AMS. The moisture of the surface soil exposed to sun light in the morning was rapidly lost due to intensive evaporation. The pF value of soils at depths of 5 and 10 cm increased with time from 5:00 to 8:00 and afterwards it decreased. The values went up again during the period from 15:00 to 21:00.

In the drying process, the pF value of soil layers increased curvilinearly with diurnal fluctuations. The diurnal range in pF values at a depth of 10 cm was lower than that at a depth of 5 cm. The pF value of Kanto loamy soil was higher than that of the paddy soil.

Figure 12(a), (b) and (c) show daily variations in soil moisture obtained at depths of 0, 5 and 10 cm by the electrical conductivity method. In a long range record of soil moisture variations obtained from the field, these daily variations were obvious. According to the meteorological data taken from May to October 1986, no rainfall was recorded from the 11 th to the 29 th of August.

The soil moisture was determined using the degree of electrical conductivity of the soil sample. Moisture determined by the electrical conductivity method was used in the following examination because of good reliability.

3.1.2 Thermal model and soil physics

(1) Thermal model

As previously described by Budyko (1956), the energy balance of the earth's surface is essentially formulated as follows:

$$S = \ell E + H + B \quad \text{.....(1)}$$

where S is net radiation flux, ℓE, latent heat flux, H, sensible heat flux, and B, soil heat flux.

According to a one-dimensional heat transfer, ℓE, H and B are given by Eqs. (2), (3) and (4), respectively (Oga, 1931; Laiktman, 1961; Uchijima, 1964; Monteith, 1973).

$$\ell E = -K1 \left.\frac{dTs}{dh}\right|_{h=0} \quad \text{.....(2)}$$

$$H = -K2 \left.\frac{dTs}{dh}\right|_{h=0} \quad \text{.....(3)}$$

$$B = -\lambda \left.\frac{dTs}{dz}\right|_{z=0} \quad \text{.....(4)}$$

where K1 is the molecular diffusion coefficient for water vapor, K2, thermal conductivity of air, λ, thermal conductivity of soil, q, specific humidity, Ts, surface temperature, q and Ts denote deviation from daily mean, h, height, z, depth, and p, air pressure. Boundary condition of height (h) and depth(z) are zero.

Substituting Eqs. (2), (3) and (4) into Eq. 1, we get the following results:

$$-K1\frac{dq}{dh} - K2\frac{dTs}{dh} - \lambda\frac{dTs}{dz} = S'\cos\omega t \quad .....(5)$$

$$-kw\ell\rho\frac{dq}{dh} - kaCp\rho\frac{dTs}{dh} - \lambda\frac{dTs}{dz} = S'\cos\omega t \quad .....(5')$$

where K1 is the molecular diffusion coefficient for water vapor, K2, thermal conductivity of air, kw, the coefficient of kinematic viscosity of air (kw = K1 /$\rho\ell$), ka, thermal diffusivity of air (ka = K2 /ρCp), ρ, air density, Cp, specific heat of air, a, thermal diffusivity of soil (a = λ/cr), c, specific heat of soil, r, specific gravity of soil, ℓ, latent heat of vaporization, S', amplitude of net variation, and ω, angular velocity, t, time.

The specific humidity (q) at the earth's surface can be approximated by saturated specific humidity of the soil surface at a surface temperature, Ts. (Laiktman, 1961; Uchijima, 1964):

$$q\Big|_{h=0} \simeq \mu\, q(Ts)\Big|_{h=0} \quad .....(6)$$

where μ is relative humidity of the earth's surface. q, specific humidity, and q(Ts) is a saturated specific humidity at a surface temperature, Ts.

In spite of decreased evaporation from dry soil, the evaporation rate is overestimated without this parameter (μ). Therefore, the evaporation from dry soil can be estimated more precisely by introducing the relative humidity of soil surface.

This was described by Laiktman (1961) as "g" and lately defined by Uchijima (1964) as "μ, (es/e(Ts))".

where μ is relative humidity of the earth's surface, es, water vapor pressure of the atmosphere, e(Ts), saturation vapor pressure at soil surface, and Ts, surface temperature.

μ is defined as :

$$\mu = (\ell E / \rho \ell D + e(T)) / e(Ts) \quad \text{.....(7)}$$

because

$$\ell E = \rho \ell D (\mu e(Ts) + e(T)) \quad \text{.....(7')}$$

where D is diffusion velocity, T, air temperature, and e, water vapor pressure.

The value of the parameter (μ) varies from 0.0 to 1.0. When the soil moisture exceeds 60 % of field capacity, the value of the parameter (μ) is approximately 1.0 (Uchijima, 1964).

To simplify the analysis, the value of the coefficient of kinematic viscosity (kw) will be assumed as equal to that of the thermal diffusivity of air (ka). Therefore, both of them can be expressed as k. Rearrangement of Eq.(5') and substitution of Eq.(6) into Eq. (5') result in:

$$-K\rho Cp \left(1 + \frac{\ell \mu q}{Cp} \right) \frac{dTs}{dh} - \lambda \frac{dTs}{dz} = S' \cos \omega t \quad \text{.....(8)}$$

One-dimensional heat transfer into air and soil layer under periodic heating are written in the following form:

$$Ts = \theta m^{e\,-h\sqrt{\frac{\pi}{K\tau_o}}} \cos\left(h\sqrt{\frac{\pi}{K\tau_o}} - 2\pi\frac{\tau}{\tau_o}\right) \quad \text{.....(9)}$$

$$Ts = \theta m^{e\,-z\sqrt{\frac{\pi}{a\tau_o}}} \cos\left(h\sqrt{\frac{\pi}{a\tau_o}} - 2\pi\frac{\tau}{\tau_o}\right) \quad \text{.....(9')}$$

After the differentiation of Eqs.(9) and (9'), substitution of the result into Eq.(8) was done. Then, the first and second terms of Eq.(8) give the following equations:

$$-K\rho Cp\left(1+\frac{\ell\mu q}{Cp}\right)\frac{dTs}{dh} = -\sqrt{K}\rho Cp\left(1+\frac{\ell\mu q}{Cp}\right)\theta m\sqrt{\frac{2\pi}{\tau_o}}\cos\left(2\pi\frac{\tau}{\tau_o}+\frac{\pi}{4}\right)d\tau \quad \text{...(10)}$$

$$-\lambda\frac{dTs}{dz} = -\sqrt{\lambda cr}\,\theta m\sqrt{\frac{2\pi}{\tau_o}}\cos\left(2\pi\frac{\tau}{\tau_o}+\frac{\pi}{4}\right)d\tau \quad \text{.....(11)}$$

where Θm is temperature amplitude and τ_o is periodic time. Daily range dQH and dQZ can be written as:

$$dQH = -\sqrt{K}\,\rho Cp\left(1+\frac{\ell\mu q}{Cp}\right)\theta m\sqrt{\frac{2}{\pi}}\sqrt{\tau_o} \quad \text{.....(12)}$$

and

$$dQZ = -\sqrt{\lambda cr}\,\theta m\sqrt{\frac{2}{\pi}}\sqrt{\tau_o} \quad \text{.....(13)}$$

Daily range of net radiation is dQH+dQZ, so

$$-\sqrt{K}\,\rho Cp\left(1+\frac{\ell\mu q}{Cp}\right)-\sqrt{\lambda cr}\,\theta m\sqrt{\frac{2}{\pi}}\,\sqrt{\tau_o}=dS \quad \text{.....(14)}$$

We can rewrite the Eq.(14) as follows:

$$\sqrt{\lambda cr}=\frac{dS}{\theta m\sqrt{\frac{2}{\pi}}\sqrt{\tau_o}}-\sqrt{K}\,\rho Cp\left(1+\frac{\ell\mu q}{Cp}\right) \quad \text{.....(15)}$$

The parameter $\sqrt{\lambda cr}$ is heat conductance capacity (Oga, 1931). It was recently named as thermal inertia(Rosema,1975; Idso et al., 1976; Pratt and Ellyette, 1979; Price, 1980, etc.). Thermal inertia ($\sqrt{\lambda cr}$) controls heat diffusion in the soil. The value of thermal inertia is largely affected by the first term on the right side of the equation. In the precise definition of thermal inertia, the second term on the right side cannot be neglected.

(2) Soil physics

In soil, λ is a function of soil moisture and expressed as λ = f(WV). Multiplying c by density (r) gives Cv. Cv is also well known as a function of volume wetness (WV). It is expressed in the following Eqs.(16) and (16′):

$$Cv = 0.46\ fm + 0.60\ fo + fw \qquad \text{(de Vries, 1963).....(16)}$$

$$Cv = 0.2\ \rho v + WV / 100 \quad \text{(Chudnovsky, 1959).....(16')}$$

where Cv is volumetric heat capacity (cal/cm^3 $^\circ$C), ρv, bulk density (g/cm^3), fm, fo, fw, soil's solid phase such as mineral, organic matter and water. WV is volume wetness.
Therefore, the parameter($\sqrt{\lambda cr}$) is a function of volume wetness (WV) and expressed as $\sqrt{\lambda cr} = f(WV)$. Soil moisture can be estimated from Eq. (17).

$$WV = f^{-1}(\sqrt{\lambda cr}) \quad .....(17)$$

In general, soil moisture influences properties of soil physics such as thermal conductivity, thermal diffusivity, specific heat and heat capacity of soil. A linear relationship exists between evaporation (E) and soil moisture below a critical value which is about 60% of the field capacity (Uchijima, 1964).

As described by Fujiwara and Oneda (1959), Kasubuchi (1978), Monteith (1973) and Oke (1978), the increase in heat loss due to evaporation causes proportional decrease in heat conducted and stored into soil layers. Heat capacity and porosity of soil also have effects on the heat budget at the soil surface. Conversely, an increase in soil moisture brings about a distinct increase of heat capacity and heat conductivity of soil. Heat conductivity of

Table 6 Thermal properties of soil (Oke, 1978).

Thermal properties	Kind of soil					
	Sandy soil		Clay soil		Peat soil	
	dry	wet	dry	wet	dry	wet
Density	1.60	2.00	1.60	2.00	0.30	1.10
Specific heat	0.80	1.48	0.89	1.55	1.92	3.65
Heat capacity	1.28	2.96	1.42	3.10	0.58	4.02
Thermal conductivity	0.30	2.20	0.25	1.58	0.06	0.50
Thermal diffusivity	0.24	0.74	0.18	0.51	0.10	0.12

(Unit: Density, $Kg^{-3} \times 10^{3}$; Specific heat, $JKg^{-1}K^{-1} \times 10^{3}$
Heat capacity, $Jm^{-3}K^{-1} \times 10^{6}$; Thermal conductivity, $Wm^{-1}K^{-1}$;
Thermal diffusivity, $m^{2}s^{-1} \times 10^{-6}$)

water is twenty-three times as large as that of air. When water fills pore space in soil, it connects soil particles closely with each other. Then, the heat capacity and the heat flux in soil layers both increase (Editorial committee for handbook of soil physics measurement, 1980; Kasubuchi, 1973; Shinjo, 1977; Maruyama, 1957; Fujiwara and Oneda, 1959). As a result, daily range of Ts of a wet soil is lower compared with that of a dry soil. Therefore, the energy balance theory at the soil surface can be used to estimate soil moisture. Table 6 summarizes physical properties of soil in relation to soil moisture.

3.1.3 Thermal inertia model for estimating soil using micro-meteorological data obtained at the experimental field

Soil moisture is physically and closely correlated with thermal inertia ($\sqrt{\lambda cr}$) as described above. The diffusion coefficient (K) and relative humidity (μ) of soil surfaces were calculated using heat balance terms obtained at the field. The diffusion velocity is an adequate parameter for determining sensible and latent heat flux (Uchijima, 1974). Thus, diffusion velocity (D) between two heights of 10 and 110 cm above the ground was used in place of the diffusion coefficient(K). The parameter (D) is calculated by the following well-known heat balance method.

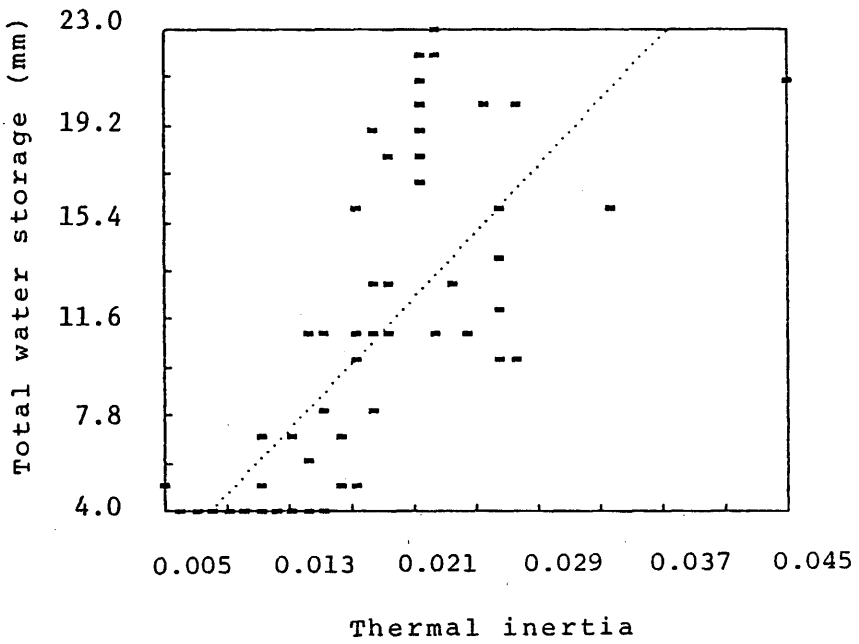

Figure 13 Regression of thermal inertia and total water storage of Kanto loamy soil obtained from the experiment at the field.

$$D_{10-110\,cm} = \ell E / ((0.622\,\ell\rho\,(e_{10} - e_{110})/p) \quad \text{.....(18)}$$

$$D_{10-110\,cm} = H / (Cp\,\rho\,(T_{10} - T_{110})) \quad \text{.....(18')}$$

Therefore, all of the heat balance terms such as dS, Θm, D, and μ were obtained. Then, thermal inertia was determined using Eq.15 and heat balance terms obtained at the field.

Total water storage (SW) and thermal inertia were plotted in the scatter diagram (Fig. 13). The values of thermal inertia obtained from 11:30 to 12:00 on fair days during the period, from December 1986 to July 1987, vary from 0.006 to 0.045. Soil moisture (total water storage) was adequately correlated to thermal inertia, with a correlation coefficient of approximately 0.72. The model for estimating total water storage (SW) obtained at the field is as follows:

$$SW = -1.88 + 662.89\ \sqrt{\lambda cr} \quad \text{.....(19)}$$

($R^2 = 0.57$, standard error of the residuals = 4.04)

where SW is total water storage (mm), and $\sqrt{\lambda cr}$, thermal inertia.

3.2 Modeling with airborne MSS thermal IR data in the Kujukuri coastal plain

3.2.1 Thermal inertia model with airborne MSS data for soil moisture estimation

(1) Determination of energy balance term

The energy balance of earth's surface is also expressed as components of short and long wavelengths:

$$(1 - \alpha) R + L = U + \ell E + H + B \quad \text{.....(20)}$$

Substituting of Eq.(1) into Eq.(20) yields the following Eq.(21):

$$L = U + S - (1 - \alpha) R \quad \text{.....(21)}$$

where S is net radiation, R global solar radiation, L downward longwave radiation from the sky, U upward longwave radiation from the soil surface, and α albedo of the soil surface.

Meteorological elements were observed in and around the ground truth center. These were heat balance terms such as air temperature, relative humidity, wind direction, wind speed at the level of 0.5 and 1.5 m above the ground, global solar radiation, net radiation, albedo, air pressure at the level of 1.5 m above the ground, surface temperature, and heat flow from a depth of 0.5 to 1.0 cm.

Longwave radiation from the earth's surface (U) is calculated from Eq.(22).

$$U = \delta\sigma(Ts + 273.15)^4 + (1 - \delta) L \quad \text{.....(22)}$$

where Ts is surface temperature obtained by a hand-carried thermal IR radiometer and MSS, δ, emissivity of soil surface and σ, Stefan-Boltzmann constant. In this study, emissivity (δ) is assumed to be 0.961. The second term on the right hand side of Eq.(22) can be disregarded because this second term is negligibly small when the emissivity (δ) is larger than 0.95 (Uchijima, 1974). Therefore, the downward longwave radiation (L) at the ground truth center is obtained by Eq.(21). Then, the parameter U and L can be easily calculated for the ground truth center. Effective radiation (F) is calculated by Eq.(23).

$$F = L - U \quad \text{.....(23)}$$

The airborne sensor (MSS) enables measurement of reflected spectral energy within a narrow wavelength and thermal IR radiation in each pixel. As described above, R and L are obtained using data from the ground truth center. Strictly speaking, the downward long wave radiation (L) varies with location (pixel). This is due to the change of air temperature. Downward longwave radiation (L), thus obtained in a short time during the MSS measurement, was substituted into Eq.(23). Albedo in each pixel of the MSS is estimated from:

$$\alpha' = f\left(\sum_{i=1}^{10} \lambda i\right) \quad \text{.....(24)}$$

where α' is the estimated albedo, and λi, reflectance of the visible wavelength band. Function f(x) is obtained by a regression analysis using albedo and CCT count of airborne MSS data. Albedo is observed in and around the ground truth center.

Net radiation (S) in each pixel of MSS data can be calculated from Eq.(25) by substituting the heat balance terms.

$$S = (1 - \alpha') R - F \quad \text{.....(25)}$$

dS and dTs are estimated from Eqs.(26) and (27), respectively:

$$dS = S_{max} - S_{min} \quad \text{.....(26)}$$

$$dTs = Ts_{max} - Ts_{min} \quad \text{.....(27)}$$

where dS and dTs are daily range of net radiation and surface temperature, respectively. Each subscripted max and min indicates the maximum and minimum of S and Ts. The minimum value was obtained on the first flight (6:15 - 6:22) and the maximum value was obtained on the third flight (12:58 - 13:00) on November 15, 1985.

(2) Normalized albedo

Albedo is defined as the ratio between reflected energy shorter than 3μm and global solar radiation. Albedo was observed both at the field and on the Kujukuri coastal plain. Albedo is an important heat balance term, and it is also used to estimate relative humidity of the soil surface. Figure 14 shows the relationship between albedo and total water storage. These data were obtained from the field and in the Kujukuri plain. The incident angle at noon during August in 1986 varied from 22 to 19 degrees. The angle at noon was 56 degrees on November 15, 1985.

It is well known that the albedo varies with time and season and with different incident angles of solar radiation. Therefore, the influence of season is unavoidable, but the albedo was sampled at noon to avoid variations of time. It is also well known that albedo increases exponentially with the decrease of soil moisture (Maruyama, 1967). Excluding the part of the curve from high soil moisture, the curve in Figure 14 also agrees with the result of Maruyama's experiment.

In airborne remote sensing, relative humidity (μ) at the soil surface cannot be calculated by the heat balance method because latent heat flux (ℓE) in Eq.(7) is an unknown quantity. Therefore, such parameter as surface relative humidity (μ) was substituted by an estimated relative humidity (μ').

High soil moisture for example, 31.8 mm was observed at a location in the Kujukuri coastal plain. Up to this time, maximum values of sample data over 37.5 mm were rarely observed in this plain. According to observations at the field, saturation of the

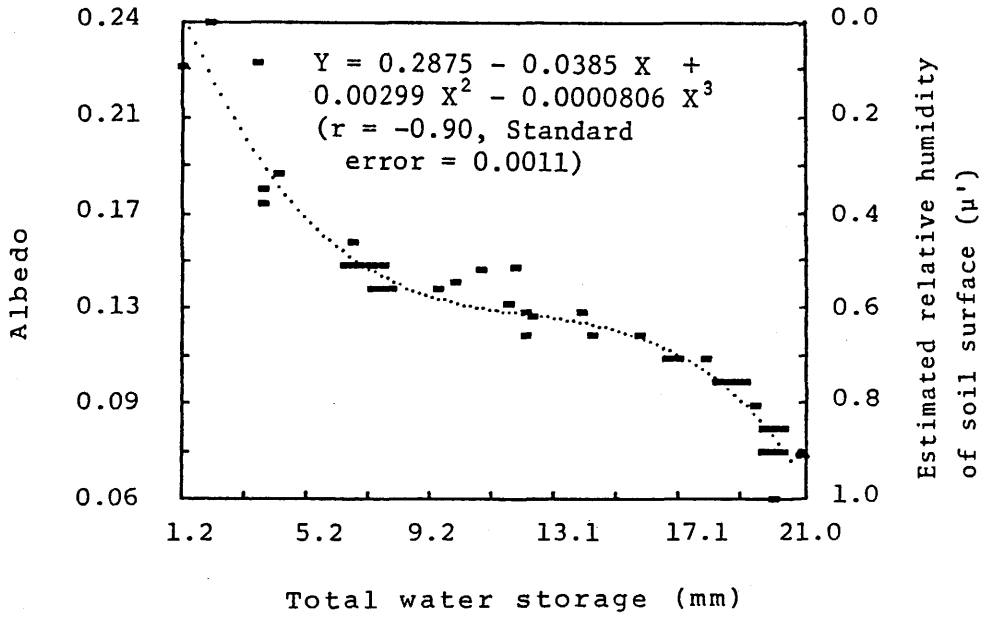

Figure 14 Relationships between albedo, estimated relative humidity of soil surface and total water storage obtained from the field and Kujukuri coastal plain.

soil took only 24 hours of rainfall and was about 21.0 mm in total water storage. Thus, soil moisture at field capacity for loamy soil is assumed to be over 21.0 mm.

Minimum albedo of the wettest soil, which is 21.0 mm at field capacity was about 6 %. Conversely, maximum albedo was approximately 24 % in dry conditions, which is 1.2 mm of total water storage. The albedo was well correlated with soil moisture as shown in Fig. 14. The estimated albedo (α') using airborne MSS data is assumed to vary between the maximum and minimum values of albedo. The albedo (α') minus the value of minimum albedo (0.06) was divided by the value of total variation or range of albedo (0.18). Thus, the normalized albedo of soil surface varies from 0.0 to 1.0. Then, the albedo (α') was evaluated by regression analysis based on relationships between albedo and total water storage as given in Fig. 14. The normalized albedo can be substituted for relative humidity of soil surface in the airborne MSS measurement. Therefore, the relative humidity of soil surface is estimated by Eq.(28).

$$\mu' = 1 - \frac{\alpha' - \alpha min}{\alpha max - \alpha min} \quad \text{.....(28)}$$

where μ' is estimated relative humidity of soil surface, α', an estimated albedo, αmin, the minimum albedo of the wettest soil, and αmax, the maximum albedo of the driest soil.

Thus, the estimated relative humidity (μ') of soil surface varies from 0.0 for the driest soil conditions to 1.0 for the wettest soil conditions. The estimated relative humidity (μ') of soil surface can be used in place of the relative humidity (μ) based on the heat balance method in the airborne MSS measurements.

As mentioned above, heat balance terms such as dS, dTs, D (in place of K), L, U, F, μ' and q were obtained from the airborne MSS and ground truth measurements. Therefore, such terms as ds, dTs, μ' and q in each pixel can be easily substituted into Eq.(15). These terms enable evaluation of thermal inertia for each pixel of the MSS data.

3.2.2 Moisture estimation with soil surface temperature

Total water storage (SW) and surface temperature (Ts) were observed at 7:05, 9:35 and 12:05 on Jan. 23, 1981. Figure 15 shows relationships between SW and Ts. This figure includes two cases, bare soil plot (A) and mixed plot (B). A mixed plot (B) consists of bare soil with sparse grass and paddy fields after harvest.

Except the relationship obtained at 7:05, total water storage (SW) increases exponentially with the decrease of surface temperature (Ts) as shown in Fig. 15. Results of regression analyses are shown in Table 7. The correlation coefficients for bare soil obtained at 7:05, 9:35 and 12:05 were 0.94, -0.88, and -0.92, respectively. For the mixed surface, the correlation

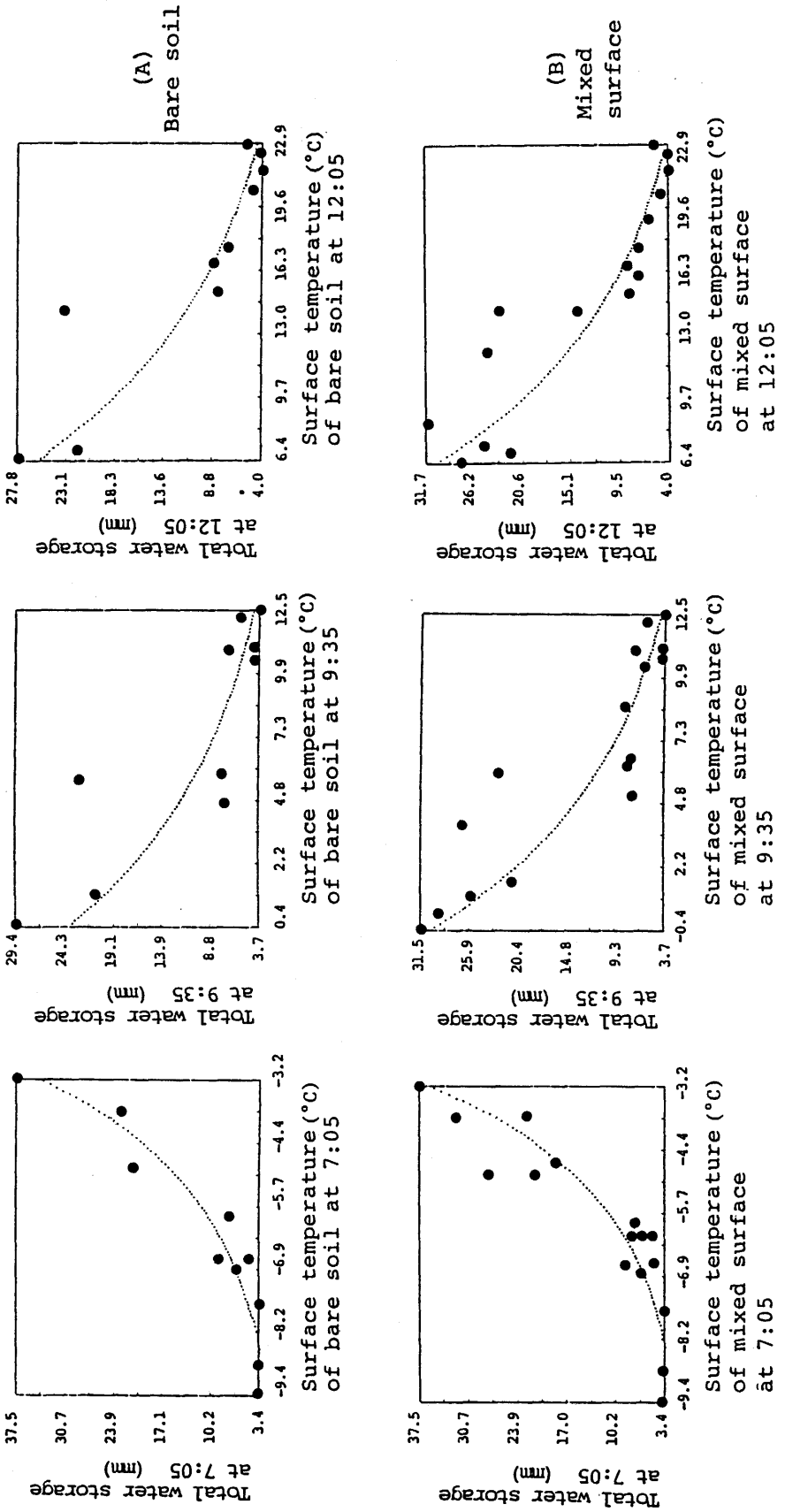

Figure 15 Relationship between total water storage and surface temperature of soil obtained from the experiment in the Kujukuri coastal plain on Jan. 23, 1981.

Table 7 Regression results of total water storage and surface temperature in the Kujukuri coastal plain.

Equation					r	R^2	Standard error of residuals
Equation of bare surface (n=10)							
LnSW7 =	4.705	+ 0.404***	x	Ts 7	0.936	88%	0.322
LnSW9 =	3.308	- 0.153***	x	Ts 9	-0.879	77	0.390
LnSW12=	4.069	- 0.115***	x	Ts12	-0.922	85	0.303
Equation of mixed surface (n=16)							
LnSW7 =	4.903	+ 0.439***	x	Ts 7	0.909	83	0.364
LnSW9 =	3.396	- 0.160***	x	Ts 9	-0.907	82	0.340
LnSW12=	4.267	- 0.124***	x	Ts12	-0.928	86	0.288

SW 7, 9, 12 is total water storage(mm) at 7, 9:35, 12:05, Ts7, Ts9, Ts12, surface temperature(°C) at 7:05, 9:35, 12:05, ***, significance of t-value at 0.001 level. n is number of samples. Mixed surface consists of bare and sparsely vegetated surfaces. Ln, log transformation(natural)

coefficient obtained at 7:05, 9:35, 12:05 were 0.91, -0.91 and -0.93, respectively.

According to Table 7, SW is directly or inversely proportional to Ts. During the early morning (7:05), the value of SW varied directly with Ts. At other times (9:35 and 12:05) with more intensive radiation, SW varied inversely with Ts. Therefore, the correlation coefficient between them varies from -0.93 to +0.94.

The correlation coefficient between Ts and SW was higher for the bare soil plot than for the mixed plot. This is mainly because the mixed plot consists of three surfaces with different physical properties affecting thermal conditions of the soil layer. The better line fitness was recognized in the processing using logarithmic transformed values excluding Ts-data obtained at 7:05.

The level of significance for t-values and correlation coefficients in these equations is 0.001. While the coefficient and constant terms of these equations vary with diurnal variation of Ts, regression coefficient for bare soil is higher than that of the mixed surface. The following equations were derived from the lowest estimation error and significance of t-value:

$$\text{LnSW EXP} = 4.069 - 0.115 \times \text{Ts12} \quad \ldots\ldots\ldots\ldots\ldots (29)$$

($R^2 = 0.85$, standard error of the residuals = 0.303)

$$\text{LnSW COM} = 4.267 - 0.124 \times \text{Ts12} \quad \ldots\ldots\ldots\ldots\ldots (30)$$

($R^2 = 0.86$, standard error of the residuals = 0.288)

where SW is total water storage (mm), EXP, bare soil, COM, mixed surface, and Ts12, surface temperature obtained at 12:05.

3.2.3 Model for estimating soil moisture using the thermal parameter and thermal inertia

(1) Model for estimating soil moisture with the thermal parameter

Figure 16 shows relationship between the thermal parameter (dS/dTs) and SW of two data sets. One is bare soil and the other is mixed surface. Table 8 shows results of regression analyses between them. As shown in this table, correlation coefficients for bare soil were 0.94, 0.79, and 0.93 during the periods from 7:05 to 12:05, 9:35 to 12:05, and 7:05 to 9:35, respectively. For mixed surface, they were 0.94, 0.70, and 0.93 during the periods from 7:05 to 12:05, 9:35 to 12:05, and 7:05 to 9:35, respectively.

Correlation coefficients between soil moisture at 12:05 and the thermal parameter (dS/dTs) for the period from 9:35 to 12:05 was usually lower than that for the other period in the morning, and the value for bare soil was higher than that of the mixed surface. Since soil moisture is closely related to the parameter (dS/ dTs) except for the period from 9:35 to 12:05, the soil moisture can be estimated quantitatively. The following equations were derived from the lowest estimation error and significance of t-value:

$$\text{LnSW EXP} = 6.880 + 1.216 \times \text{LndS/dTs31} \quad \ldots\ldots (31)$$

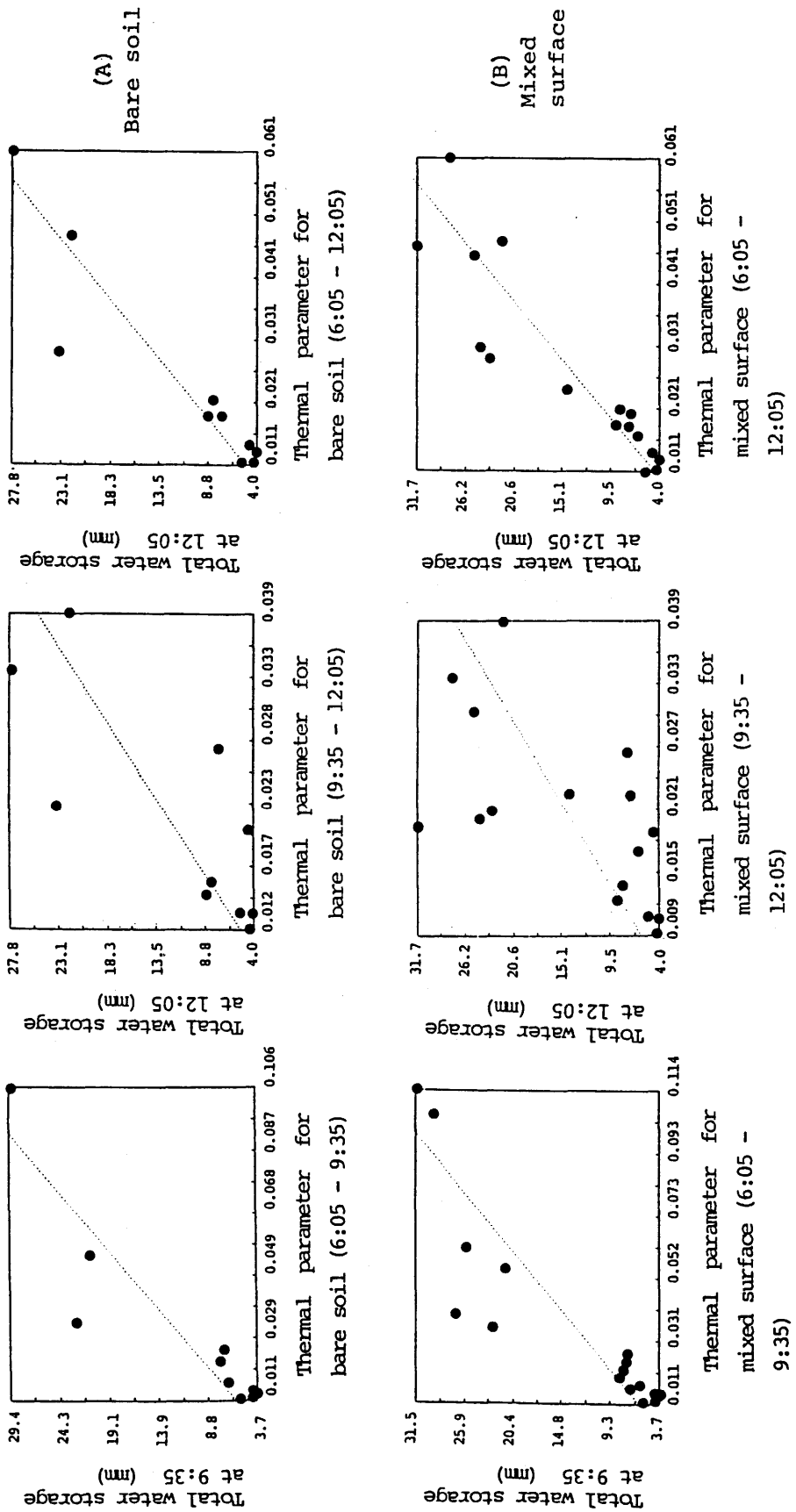

Figure 16 Total water storage versus thermal parameter (dS/dTs) obtained from the experiment in the Kujukuri coastal plain on Jan. 23, 1981.

Table 8 Regression results of total water storage and the thermal parameter (dS/dTs) obtained from the experiment in the Kujukuri coastal plain.

Equation	r	R^2	Standard error of residuals
A) Equation for bare soil (n=10)			
LnSW12= 6.880 + 1.216 *** x LndS/dTs31	0.944	89%	0.258
LnSW12= 7.600 + 1.373 ** x LndS/dTs32	0.786	62	0.485
LnSW9 = 5.726 + 0.952 *** x LndS/dTs21	0.931	87	0.298
B) Equation for mixed surface (n=16)			
LnSW12= 7.358 + 1.327 *** x LndS/dTs31	0.941	89%	0.261
LnSW12= 8.167 + 1.490 ** x LndS/dTs32	0.704	50	0.548
LnSW9 = 5.783 + 0.959 *** x LndS/dTs21	0.931	87	0.295

SW9, SW12 is total water storage (mm) at 9:35, 12:05, dS, dTs, difference of net radiation and that of surface temperature, subscript 21, 32, 31, range in the period from 7:05 to 9:35, 9:35 to 12:05, 7:05 to 12:05, and symbol *** , **, significance of t-value at 0.001, 0.01 level, respectively. n, number of samples, Ln, log transformation (natural). Mixed surface consists of bare and sparsely vegetated surfaces.

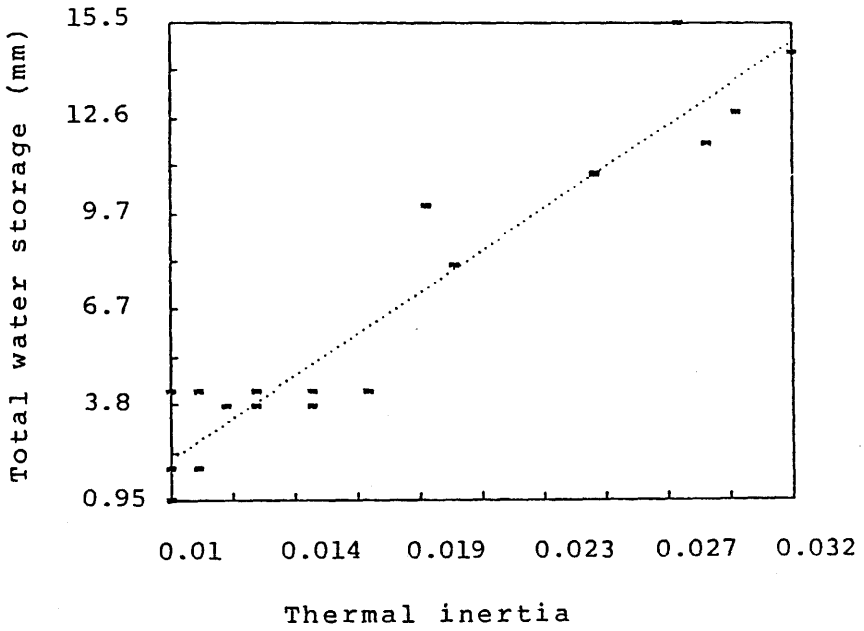

Figure 17 Regression of thermal inertia and total water storage of sandy soil obtained from the experiment in the Kujukuri coastal plain.

(R^2 = 0.89, standard error of the residuals = 0.258)

LnSW COM = 7.358 + 1.327 x LndS/dTs31 .....(32)

(R^2 = 0.89, standard error of the residuals = 0.261)

where SW is total water storage (mm), EXP, bare soil, COM, mixed surface, and dS/dTs, daily range of net radiation divided by daily range of surface temperature.

(2) Thermal inertia model for estimating soil moisture

The thermal inertia can be calculated using the heat balance terms at the ground truth center and from the airborne MSS data as mentioned in Chapter 3.2.1. Figure 17 and Eq.(33) obtained from airborne MSS and ground truth measurements in the Kujukuri coastal plain show linear relationships similar to those obtained from the experiments at the field. Significant correlation exists between soil moisture (SW) and thermal inertia. Values of coefficients and constant terms of the equation are not equal to those derived from the experiment at the field, because of the difference in porosity and mineral components of soil between these two areas. The thermal inertia model for estimating soil moisture from airborne MSS measurements is as follows:

$$\text{Soil moisture (mm)} = -3.621 + 581.13\ \sqrt{\lambda cr} \quad ....(33)$$

(R^2 : 0.92, standard error of the residuals: 1.37)

where soil moisture is expressed by total water storage (mm), and $\sqrt{\lambda cr}$, thermal inertia.

3.3 Estimation of soil moisture with visible and near IR data

3.3.1 Spectral reflectance of soil surface

The surface reflectance varies with SM. Therefore, examination of spectral reflectance of soil surface was done to develop the empirical models for estimating SM.

In the laboratory experiments, samples were reconstructed by mixing individual components obtained by sorting sandy soil from the Kujukuri plain.

The percent reflectance and moisture of tested soil samples were plotted using an XY plotter. The results are shown in Fig. 18. The upper limit of total water storage of wet soil was about 16.5 mm. In spectral regions over 0.75 μm, the reflectance of soil surface approximated the respective upper limit of soil moisture and peaked at 1.15 μm.

The spectral reflectance curve gives strong support for the relationship between spectral reflectance of soil and moisture to evaluate soil moisture.

No change in spectral reflectance curves was observed for soil samples with moisture higher than about 16.5 mm, because the soil was so saturated that the soil surface was covered by a thin water layer. In this case, the spectral reflectance is mainly determined by optical properties of the water layer.

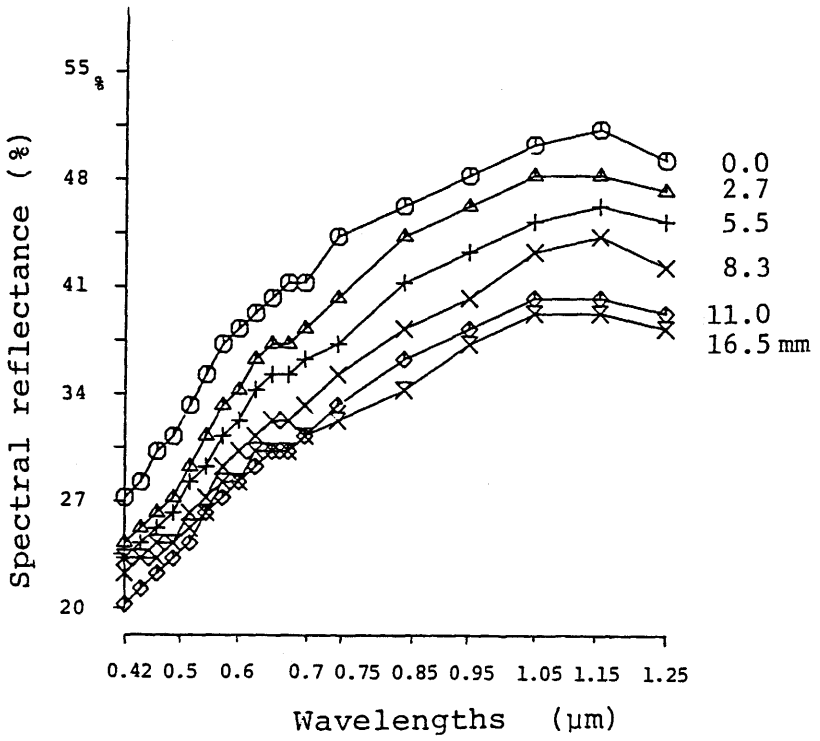

Figure 18 Spectral reflectance of sand obtained from the Kujukuri coastal plain.

Adscripts of lines 0 - 16.5 mm indicate total water storage of wet controlled sand in the laboratory.

3.3.2 Estimation of soil moisture with airborne MSS visible and near IR data

Relationships between total water storage and CCT counts of airborne MSS data are shown in Fig. 19. This figure consists of two data sets. One is bare soil (Fig. 19, A1-3) and the other is mixed surface, which is bare ground with sparse vegetation and paddy fields after harvest (Fig. 19, B1-3).

Figure 19 (A1 and B1) obtained on the first flight (7:01 - 7:07) shows that the MSS data, excluding Channel 9 (0.8 - 0.9 μm), vary inversely with soil moisture. The reflectance of Channel 9 obtained in the condition of so weak solar radiation on the first flight (7:05) shows the positive relationships between them. This relationship in the near IR spectral region (Channel 9) is similar to that of thermal IR data of Channel 11 on the early morning flight.

Tables 9 and 10 show regression results for reflectance and total water storage (SW). As shown in these tables, correlation coefficients between reflectance and total water storage (SW) for bare soil obtained at 7:05, 9:35 and 12:05 were -0.28 to +0.49, -0.71 to -0.92 and -0.71 to -0.95, respectively. For mixed surface, correlation coefficients obtained at 7:05, 9:35 and 12:05 were -0.06 to +0.28, -0.57 to -0.90 and -0.61 to -0.96, respectively. These tables show that relationships between reflectance of bare soil and total water storage is similar to that for the mixed surface. At noon, the correlation coefficient between them varied from -0.71 to -0.95, and that of the first

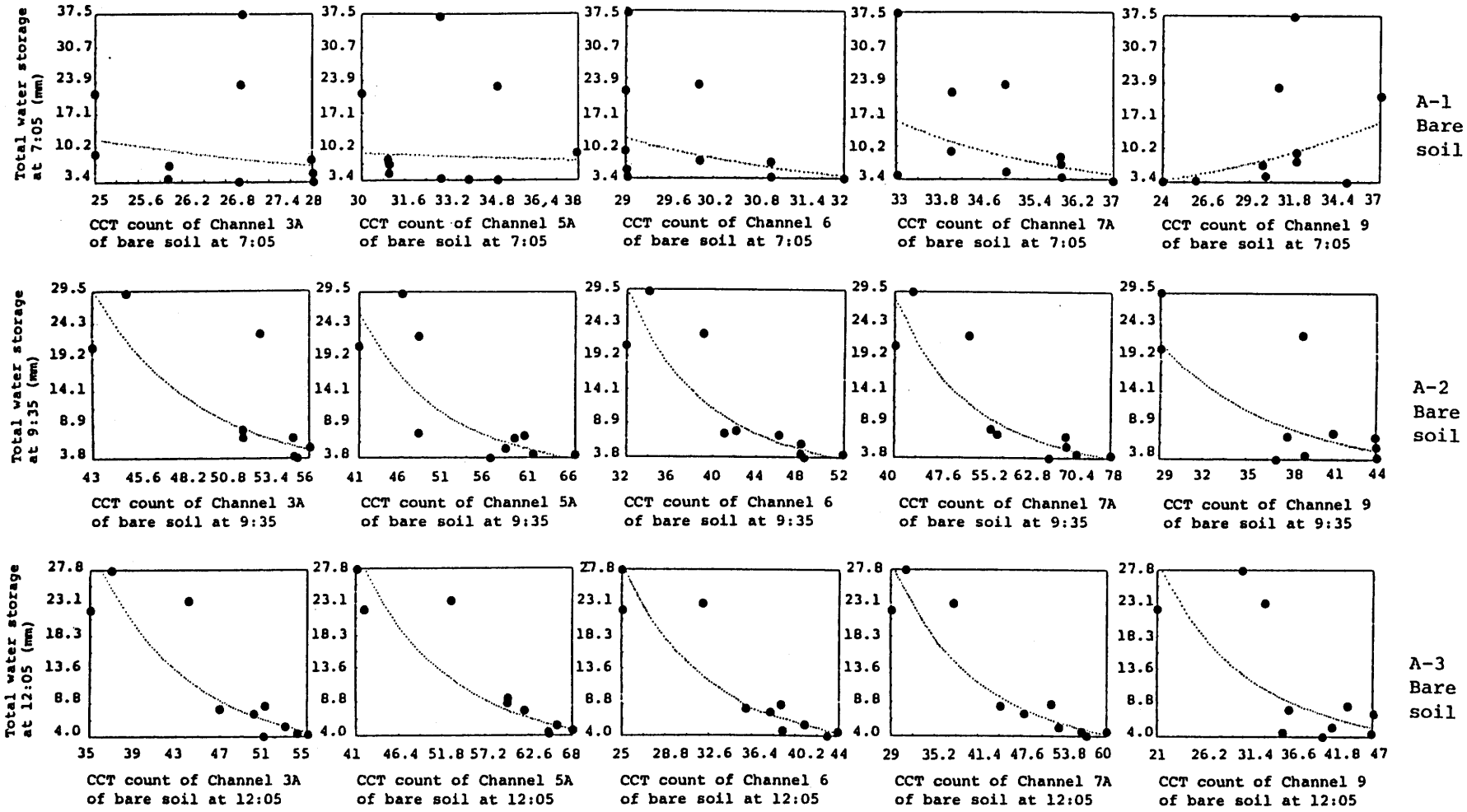

Figure 19 Airborne MSS CCT count versus total water storage in the Kujukuri coastal plain on Jan. 23, 1981.

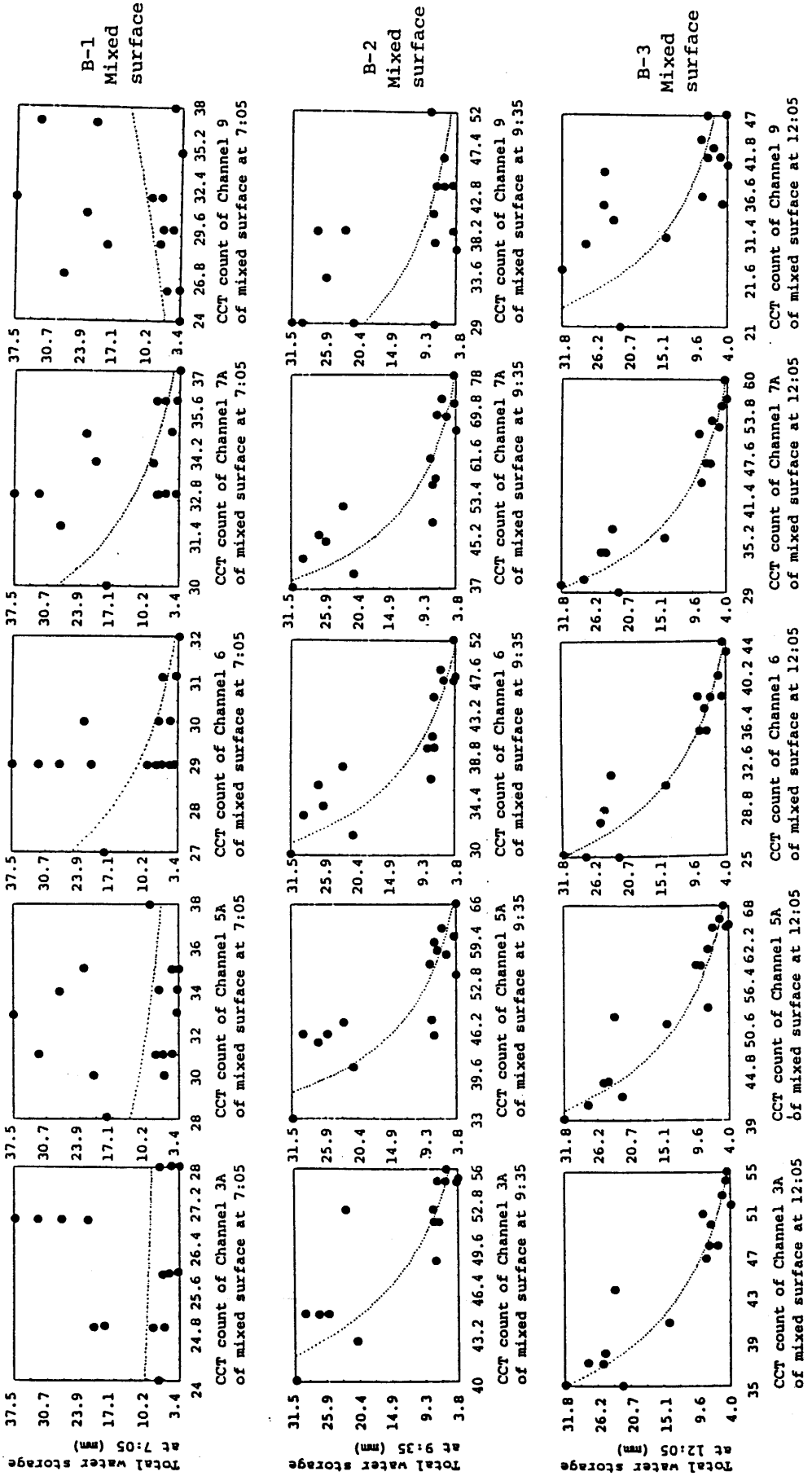

Figure 19 - continued -

Table 9 Regression results of total water storage and airborne MSS visible and near IR data for bare soil (n=10).

	Equation	r	R^2	Standard error of residuals
at 7:05	LnSW7 = 19.910 - 5.415 x LnCh 1	-0.275	8 %	0.877
	LnSW7 = 4.886 - 0.788 x LnCh 2	-0.067	0.4	0.911
	LnSW7 = 39.758 - 11.076 x LnCh 3	-0.468	22	0.806
	LnSW7 = 41.128 - 10.980 x LnCh 4	-0.502	25	0.789
	LnSW7 = -9.281 + 3.333 x LnCh 5	0.494	24	0.793
at 9:35	LnSW9 = 28.412 - 6.651** x LnCh 1	-0.797	64	0.489
	LnSW9 = 18.795 - 4.179** x LnCh 2	-0.835	70	0.446
	LnSW9 = 18.564 - 4.378*** x LnCh 3	-0.918	84	0.322
	LnSW9 = 14.664 - 3.064*** x LnCh 4	-0.903	82	0.348
	LnSW9 = 14.736 - 3.461* x LnCh 5	-0.706	50	0.574
at 12:05	LnSW12= 18.431 - 4.209*** x LnCh 1	-0.911	83	0.322
	LnSW12= 17.076 - 3.674*** x LnCh 2	-0.923	85	0.301
	LnSW12= 14.032 - 3.314*** x LnCh 3	-0.930	87	0.286
	LnSW12= 12.523 - 2.703*** x LnCh 4	-0.948	90	0.248
	LnSW12= 9.965 - 2.149* x LnCh 5	-0.711	51	0.548

SW 7, 9, 12 is total water storage (mm) at 7, 9:35, 12:05, Ch 1, Ch 2, Ch 3, CCT count of each channel of airborne MSS data, and ***, **, *, significance of t-value at 0.001, 0.01, 0.05 level, respectively. Ln is the log transformation (natural). Number of samples is 10.

Table 10 Regression results of total water storage and airborne MSS visible and near IR data for mixed surfaces (n=16).

	Equation	r	R^2	Standard error of residuals
	LnSW7 = 5.750 - 1.061 x LnCh 1	-0.060	0.4%	0.866
	LnSW7 = 9.734 - 2.139 x LnCh 2	-0.199	4	0.850
at 7:05	LnSW7 = 38.735 - 10.773* x LnCh 3	-0.502	25	0.750
	LnSW7 = 32.472 - 8.560 x LnCh 4	-0.549	30	0.725
	LnSW7 = -3.644 + 1.731 x LnCh 5	0.281	8	0.832
	LnSW9 = 26.570 - 6.188*** x LnCh 1	-0.858	74	0.413
	LnSW9 = 15.912 - 3.450*** x LnCh 2	-0.882	68	0.458
at 9:35	LnSW9 = 17.921 - 4.205*** x LnCh 3	-0.899	81	0.351
	LnSW9 = 14.276 - 2.964*** x LnCh 4	-0.896	80	0.357
	LnSW9 = 10.962 - 2.376* x LnCh 5	-0.570	33	0.661
	LnSW12= 18.678 - 4.282*** x LnCh 1	-0.942	89	0.258
	LnSW12= 16.688 - 3.581*** x LnCh 2	-0.941	89	0.261
at 12:05	LnSW12= 14.889 - 3.549*** x LnCh 3	-0.950	90	0.240
	LnSW12= 13.115 - 2.849*** x LnCh 4	-0.958	92	0.219
	LnSW12= 10.803 - 2.330 x LnCh 5	-0.667	45	0.572

SW 7, 9, 12 is total water storage (mm) at 7, 9:35, 12:05, Ch 1, Ch 2, Ch 3, CCT count of each channel of airborne MSS data, and ***, *, significance of t-value at 0.001, 0.05 level, respectively. Mixed surface consists of bare and sparsely vegetated surfaces. Ln is log transformation (natural). Number of samples is 16.

flight (7:05) was the lowest among results obtained during the period before noon. The intensive solar radiation shows that the soil moisture in daytime (e.g. 9:35 and 12:05) is well correlated with soil surface reflectance compared with that in the early morning (7:05). Tables 9 and 10 show that the intercept of the regression lines changed considerably among MSS channels. The following equations were derived from the lowest estimation error and significance of t-value:

$$\text{LnSW EXP} = 12.523 - 2.703 \times \text{LnCh 4} \quad \ldots\ldots\ldots (34)$$

($R^2 = 0.90$, standard error of the residuals = 0.248)

$$\text{LnSW COM} = 13.115 - 2.849 \times \text{LnCh 4} \quad \ldots\ldots\ldots (35)$$

($R^2 = 0.92$, standard error of the residuals = 0.219)

3.3.3 Estimation of soil moisture with Landsat MSS data

The relationship between soil moisture (total water storage) and Landsat MSS visible and near IR data obtained at 9:35 are shown in Fig. 20. Figure 20 (A) shows the relationship in bare soil, and Fig. 20 (B) in mixed surface. This figure shows the inverse relationships between MSS data and total water storage (SW).

Table 11 shows regression results of soil moisture and Landsat MSS data. The correlation coefficients between MSS data and soil moisture (SW) for the bare soil varied from -0.77 to 0.89, and for the mixed surface, from -0.69 to -0.82.

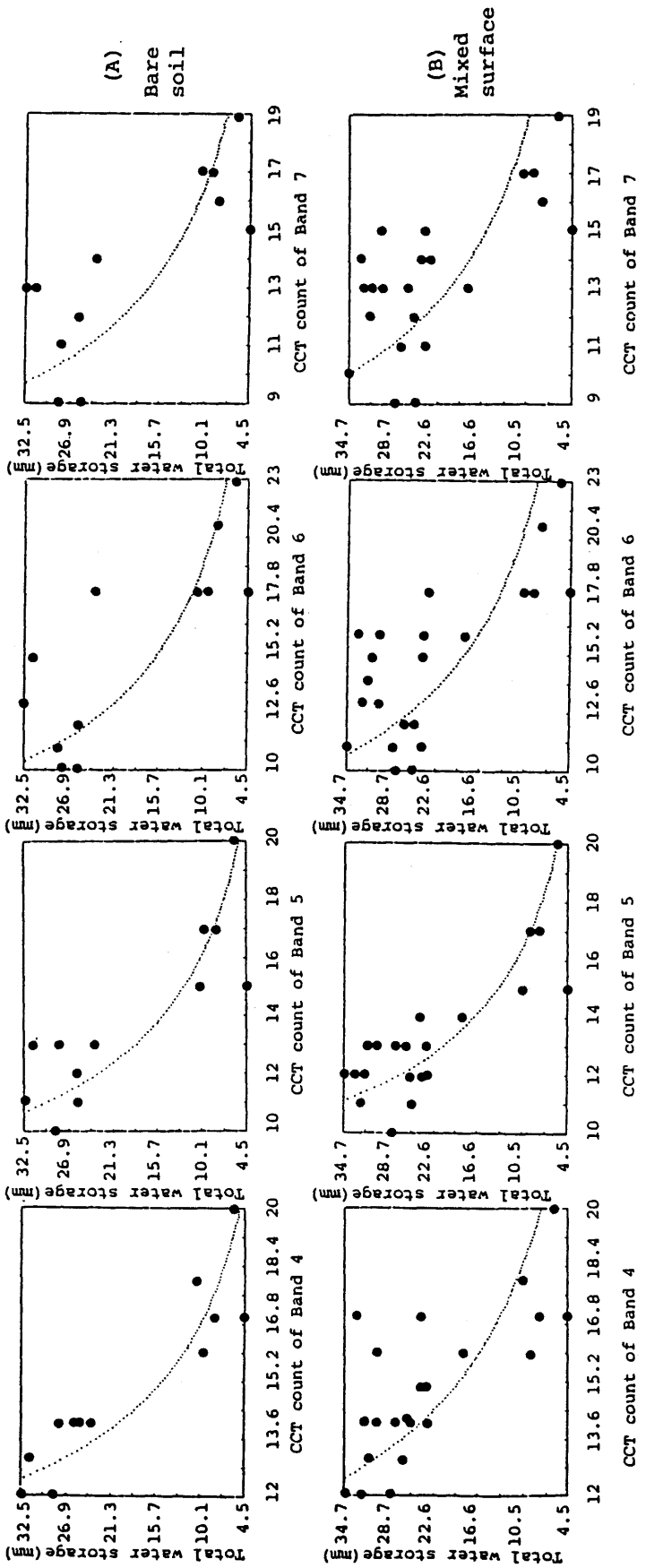

Figure 20 Landsat MSS CCT count versus total water storage in the Kujukuri coastal plain.

Table 11 Regression results of total water storage and Landsat MSS visible and near IR data in the Kujukuri coastal plain.

Equation	r	R^2	Standard error of residuals
A) Equation applied to sample of Bare soil (n=12)			
LnSW = 6.600 - 0.254*** x Band 4	-0.891	79%	0.339
LnSW = 5.546 - 0.199*** x Band 5	-0.829	69	0.417
LnSW = 4.790 - 0.129** x Band 6	-0.795	63	0.453
LnSW = 5.145 - 0.172** x Band 7	-0.773	60	0.474
B) Equation applied to sample of mixed surface (n=22)			
LnSW = 6.062 - 0.203*** x Band 4	-0.719	52%	0.424
LnSW = 5.868 - 0.213*** x Band 5	-0.822	68	0.348
LnSW = 4.863 - 0.124*** x Band 6	-0.738	55	0.412
LnSW = 5.146 - 0.159*** x Band 7	-0.685	47	0.445

SW is total water storage (mm) and ***, **, *, significance of t-value at 0.001, 0.01 level, respectively. n is the number of samples. Mixed surface consists of bare and sparsely vegetated surfaces. Ln is the log transformation (natural).

For these statistical analyses, predicting variables with smallest prediction sum of squares (PSS) (Okuno et al., 1976) and standard error of estimation were alternatively examined. Table 11 shows that the correlation coefficient was somewhat higher for the bare soil than for the mixed surface. In consideration of the size of the values of Table 9, 10 and 11, correlation coefficients between soil moisture and Landsat MSS data were somewhat lower than that between soil moisture and airborne MSS data at 9:30. The following equations were derived from the lowest estimation error and significance of t-value:

$$\text{LnSW EXP} = 6.600 - 0.254 \times \text{Band 4} \quad \text{.....(36)}$$

($R^2 = 0.79$, standard error of the residuals = 0.339)

$$\text{LnSW COM} = 5.868 - 0.213 \times \text{Band 5} \quad \text{.....(37)}$$

($R^2 = 0.68$, standard error of the residuals = 0.348)

3.3.4 Estimation of soil moisture with Landsat TM data

Figure 21 shows the relationships between total water storage (SW) and TM visible and near IR data obtained at about 9:30. Figure 21 (A) shows the inverse relationship between SW and spectral reflectance in bare soil, and Fig. 21 (B) for mixed surface. Table 12 shows that the correlation coefficient between them varied from -0.43 to -0.95 for bare soil, and from -0.54 to 0.87 for mixed surface. In both cases, the correlation coefficient was somewhat higher for bare soil fields than that for

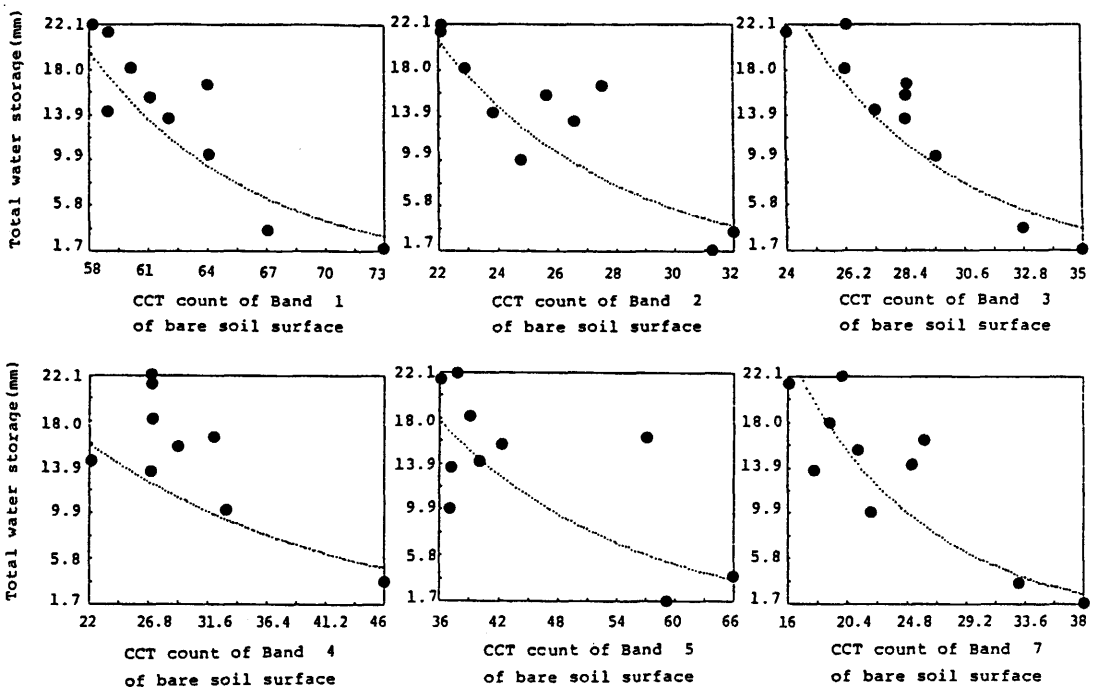

(A) Bare soil surface

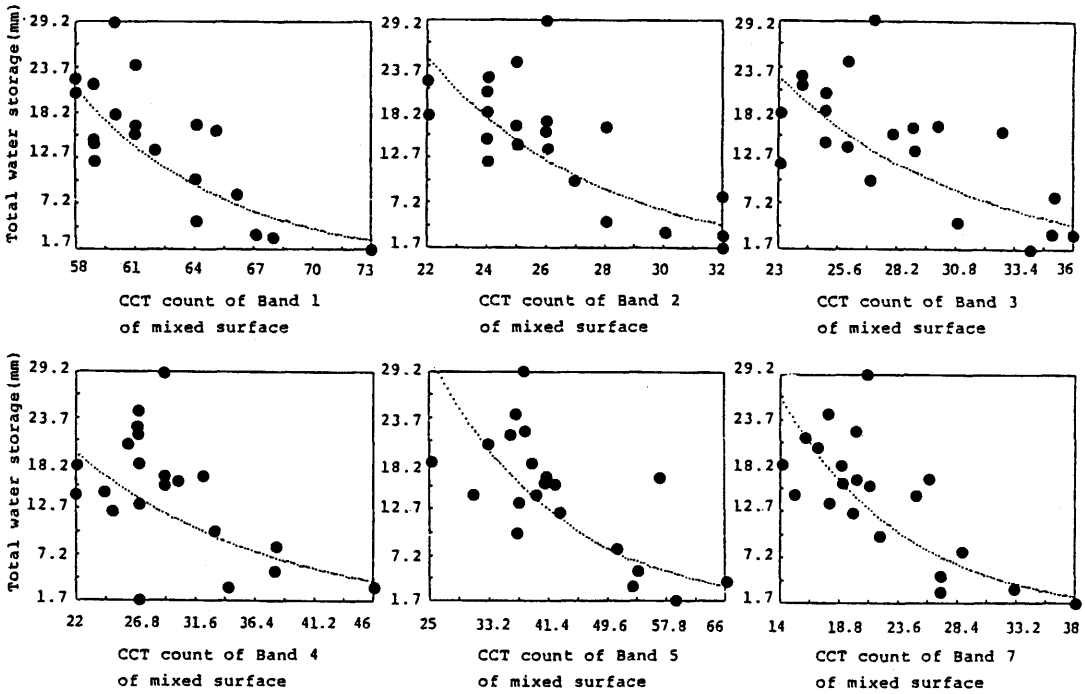

(B) Mixed surface

Figure 21 Landsat TM CCT count versus total water storage in the Kujukuri coastal plain.

Table 12 Regression results of total water storage and Landsat TM visible and near IR data in the Kujukuri coastal plain.

Equation	r	R^2	Standard error of residuals
A) Equation for bare surface (n=10)			
LnSW = 13.266 - 0.173*** x Band 1	-0.940	88%	0.306
LnSW = 9.570 - 0.274*** x Band 2	-0.953	91	0.270
LnSW = 7.724 - 0.189** x Band 3	-0.870	78	0.442
LnSW = 4.039 - 0.055 x Band 4	-0.425	18	0.809
LnSW = 4.936 - 0.056* x Band 5	-0.741	55	0.601
LnSW = 5.027 - 0.111*** x Band 7	-0.912	83	0.367
B) Equation for mixed surface (n=21)			
LnSW = 12.939 - 0.168*** x Band 1	-0.866	75%	0.386
LnSW = 7.762 - 0.201*** x Band 2	-0.816	67	0.446
LnSW = 6.249 - 0.133*** x Band 3	-0.746	56	0.514
LnSW = 4.531 - 0.069* x Band 4	-0.537	29	0.651
LnSW = 4.869 - 0.056*** x Band 5	-0.759	58	0.503
LnSW = 4.766 - 0.104*** x Band 7	-0.836	70	0.423

SW is total water storage (mm), Band 1-5, 7, band number of Landsat TM data, r, correlation coefficient, R, coefficient of determination. ***, **, * is significance of t-value at 0.001, 0.01, 0.05 level, respectively. n is the number of samples. Mixed surface consists of bare and sparsely vegetated surfaces. Ln is the log transformation (natural).

mixed surfaces. The prediction errors in the regression equations based on the spaceborne TM data are very similar to those of the airborne MSS data. This was due to the relatively smaller pixel size of TM data. The following equations were derived from the lowest estimation error and significance of t-value:

$$\text{LnSW EXP} = 9.570 - 0.274 \text{ Band 2} \quad \text{.....(38)}$$

($R^2 = 0.91$, standard error of the residuals = 0.270)

$$\text{LnSW COM} = 12.939 - 0.168 \text{ Band 1} \quad \text{.....(39)}$$

($R^2 = 0.75$, standard error of the residuals = 0.386)

4. Soil moisture map and its application

The soil moisture maps were produced for several areas such as the Kujukuri coastal plain, Tsuchiura, and the old Joban coal mining area, using airborne and spaceborne remote sensing data. The procedure for mapping consists of 1) discriminant analysis, 2) computer mapping and 3) overlay operation methods. These soil moisture maps have also been applied to mapping geomorphological characteristics and potential wind erosion.

4.1 Soil moisture distribution mapping

4.1.1 Data analysis for computer mapping

(1) Land cover discrimination

Land cover types were obtained from a broad area in the Kujukuri coastal plain. Samples of these MSS-data and codes for identifying land cover were stored on computer. Using these code numbers, samples of MSS data were grouped. Samples of spectral reflectance of 16 land cover categories and CCT count in each pixel were used in discriminant analyses. With this discriminant analysis, one pixel of CCT data was classified into one of the land cover categories based on the properties of the surface spectral reflectance. Each sample of land cover type had the shortest Mahalanobis's generalized distance (D^2) (Okuno et al,

1976). Mahalanobis's D^2 statistic can be used to group objects or to discriminate between groups (Clark and Hosking, 1986).

The distance D^2 is defined as follows:

$$D_\alpha^{2(k)} = \sum_{i=1}^{p} \sum_{j=1}^{p} V^{ij} (X_{\alpha i} - \bar{X}i^{(k)}) (X_{\alpha j} - \bar{X}j^{(k)}) \quad \ldots(40)$$

where D^2 is Mahalanobis's D statistic. V^{ij}, within - group variance-covariance matrix inverse. $X_{\alpha i} - \bar{X}_i^{(k)}$, the deviation from sample means for the group, αi on the i-th variable, and $X_{\alpha j} - \bar{X}_j^{(k)}$, the same for the j-th variable. If $D_\alpha^{2(k)}\min$ has the shortest distance, one pixel data can be clustered into group k. Each $D_\alpha^{2(k)}\min$ has α probability of deviation from the group mean. This probability is used for the restriction of the clustering. If $D_\alpha^{2(k)}\min \leqq \chi^2(p,\alpha)$, we classify the pixel into group k. If $D_\alpha^{2(k)}\min > \chi^2(p,\alpha)$, the pixel is classified as an unclassified group. The probability value (α) was assumed to be 5 % in this study.

Land cover was automatically mapped using an electronic digital computer through these discriminant analyses. The code of classified land cover and MSS data in each pixel were fed onto another magnetic tape and a hard disk.

Such land covers as pasture, pine trees, Japanese cedar trees, dry sand and open water could be precisely classified using airborne MSS data. Conversely, such land covers as truck farms, weeds, farm houses, sand, inland and sea water were successfully classified by the Landsat MSS and TM data.

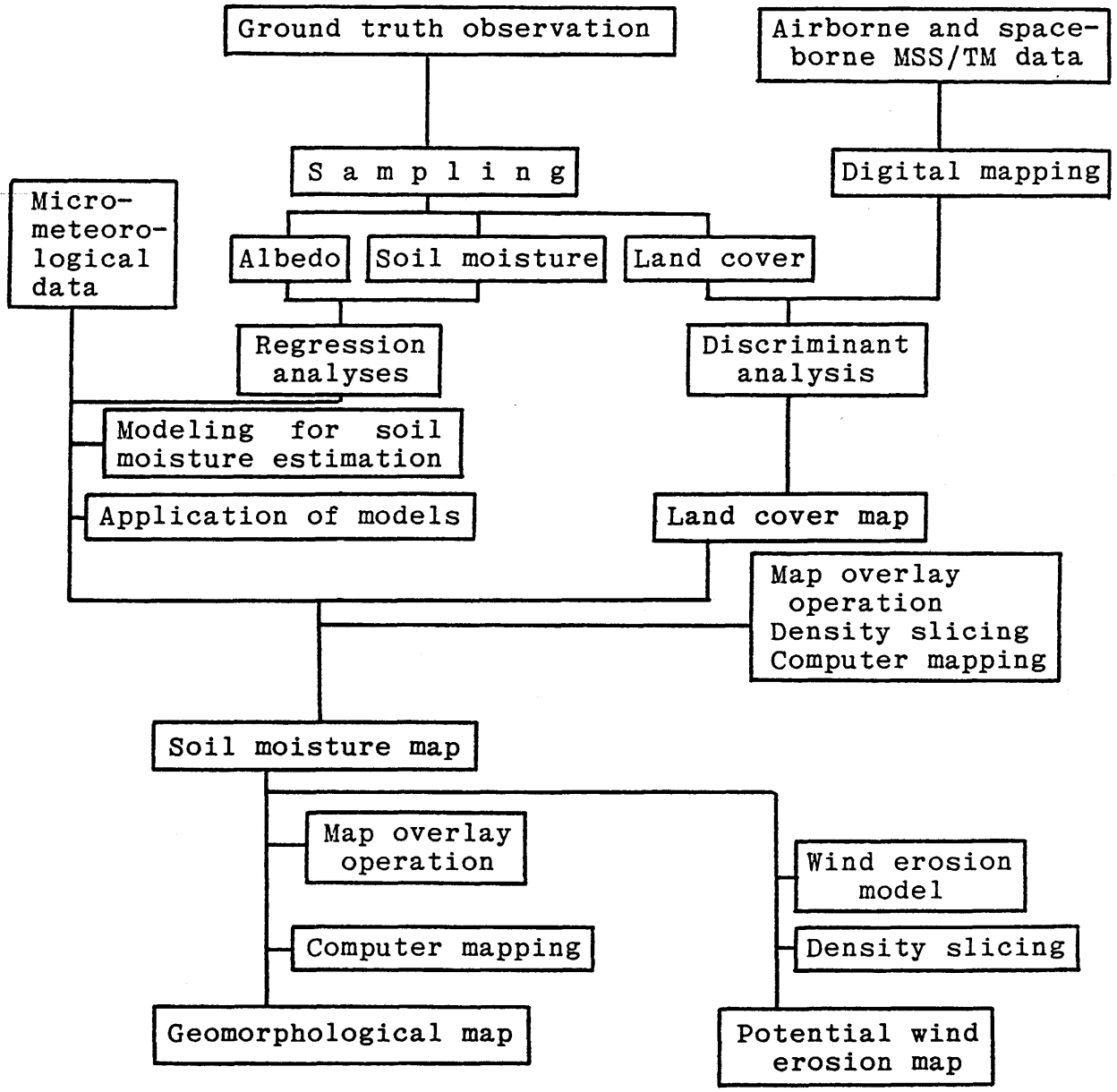

Figure 22 Flow chart of soil moisture and other thematic mapping.

(2) Soil moisture mapping

The soil moisture of the area covered by the flight course was mapped applying Eqs.(29) and (30) to the MSS data obtained at 12:05 on Jan. 23, 1981. The thermal inertia model given by Eq. (33) was applied to MSS data obtained at 6:20 and 12:58 on Nov. 15, 1985 for mapping soil moisture in and around Iyobo village in the Kujukuri coastal plain.

Equations (36) and (37) were applied to Landsat-3 MSS data to map soil moisture distribution over a wider area, and Eqs.(38) and (39) were applied to Landsat-5 TM data in the southern Kujukuri coastal plain.

The sensor (MSS) cannot detect energy radiated from the soil surface beneath vegetation and other land cover such as buildings and asphalt surfaced roads. Therefore, land surfaces overlaid with vegetation, residential areas and roads were excluded in the soil moisture(SM) mapping.

Land areas with extremely low moisture (close to 0 mm) were assumed to be 1 mm for the computer mapping. Conversely, flooded or water surfaced areas were assumed to be 100 mm of soil moisture. The flow chart of this mapping system for soil moisture is presented in Fig. 22.

4.1.2 Kujukuri coastal plain

(1) Mapping with airborne MSS data

Equations (29) and (30) were applied to thermal IR data to estimate soil moisture of the bare soil and mixed surface, respectively. Photograph 5 shows the distribution of soil moisture in the area covered by the airborne MSS flight measurement in 1981.

The Rivers Kido, Sakuta, Makame, and Nabaki cross the flight path and flow from left (west) to right (east) in the photographs. Unclassified and excluded land covers were colored white. Flooded area and water were colored red in this imagery. Other colors show the values of soil moisture (total water storage) ranging from 1 to 60 mm. In most of this area, soil moisture values were less than 42 mm. Since the ground resolution of the airborne MSS imagery is 5 m x 5 m, fine spatial difference in soil moisture can be distinguished. The soil moisture of the area between the Rivers Kido and Sakuta varied from 13 to 24 mm. The areas with soil moisture below 18 mm were widely distributed. The soil moisture of the area between Rivers Sakuta and Makame varied from 1 to 30 mm. The northern area around the River Makame showed higher moisture and some parts of the trough-like lowland between beach ridges were partly flooded.

The soil moisture of the area between the Rivers Makame and Nabaki varied from 6 to 42 mm. Flooded fields were frequently observed, especially in and around Ichiba village. On both sides of the River Nabaki, flooded paddy fields were observed.

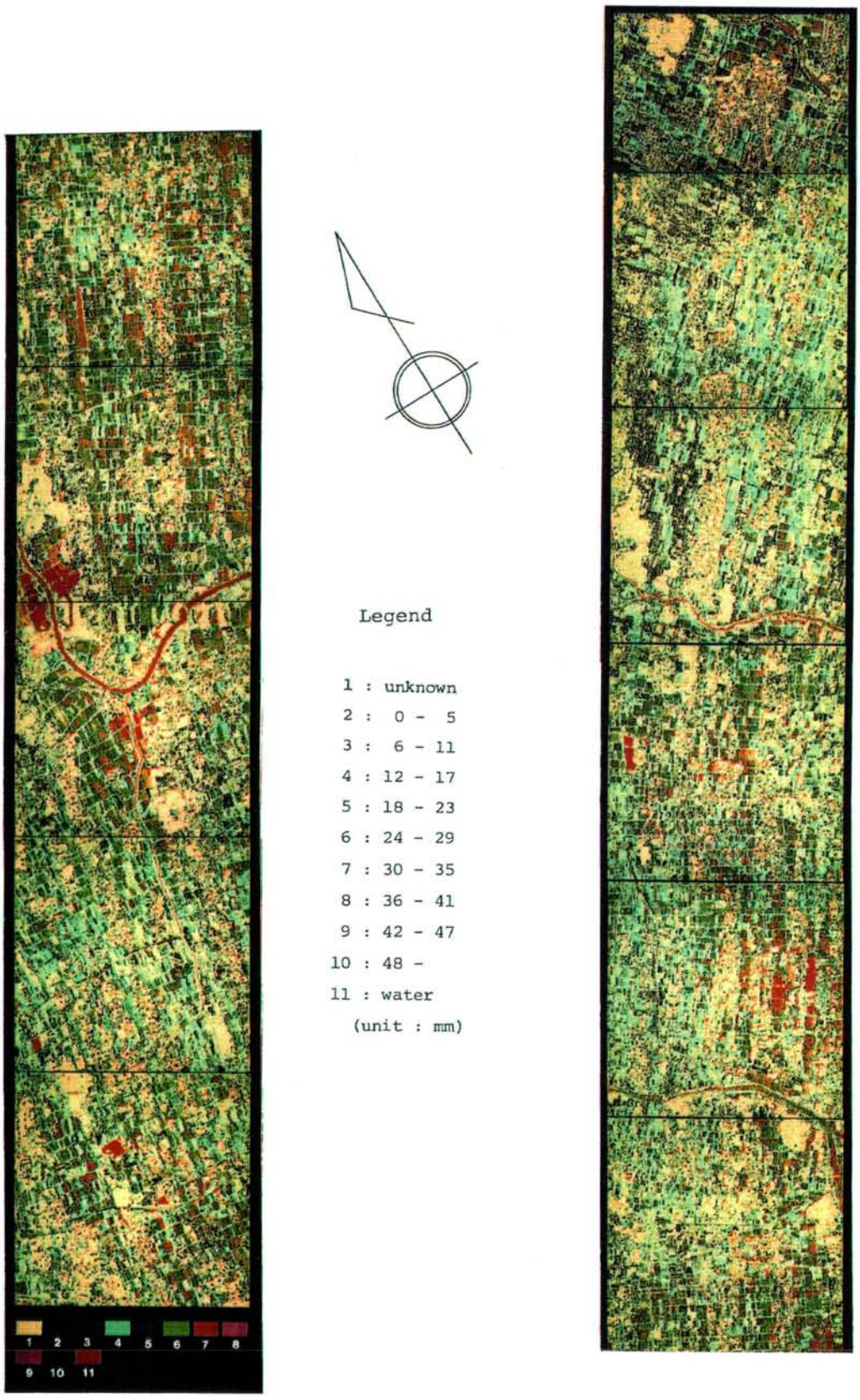

Photograph 5 Distribution of total water storage in the Kujukuri coastal plain (Jan. 23, 1981).

The soil moisture south of the River Nabaki was 1 to 30 mm. Near the Muttsuno village, high soil moisture was recognized. In the middle part between River Nabaki and Muttsuno village, the soil moisture was relatively lower. The spatial distribution of soil moisture in this area was strongly affected by topographic conditions. Areas with higher soil moisture and flooded fields extended between the Rivers Sakuta and Nabaki. Wider flooded areas existed on both sides of the River Nabaki. This area has heavy subsidence due to gas mining known as Mobara gas.

Higher soil moisture was also observed in shaded areas of northwestern parts of forests and buildings and on north-west-facing slopes. Narrow canals covered with weeds were not distinguished as a high moisture area, because the pixel-data with its spectral reference was classified into the other land cover categories.

Photograph 6 shows the moisture distribution using the thermal inertia model, Eq.(33), established by the airborne MSS experiments in 1985. This narrow area has relatively low soil moisture in the Kujukuri coastal area as shown in Photo. 5. The area with low moisture was recognized in the center and right side of the frame of Photo. 6. The area with high moisture developed in the shallow trough between beach ridges located on the left side of the frame. The soil moisture on the top of the beach ridge is very low and in contrast with the trough between the beach ridges, which has very high soil moisture. In this area the moisture distribution is affected by topography.

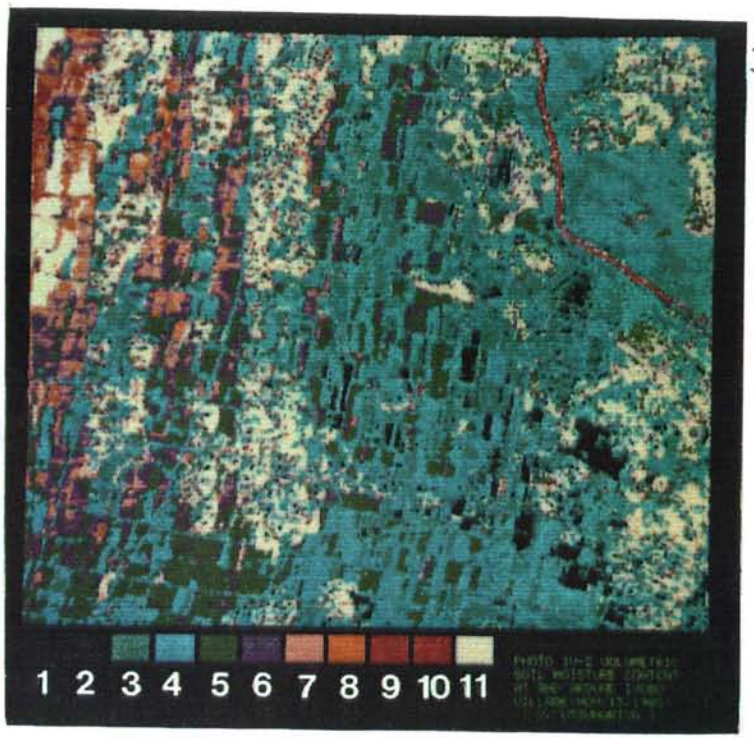

Legend

1: 0 - 2
2: 3 - 5
3: 6 - 8
4: 9 - 11
5: 12 - 14
6: 15 - 17
7: 18 - 20
8: 21 - 23
9: 24 - 26
10: 27 -
11: unknown

(unit: mm)

Photograph 6

Distribution of total water storage in and around Iyobo village in the Kujukuri coastal plain (Nov. 15, 1985).

(2) Mapping with satellite MSS data

The distribution of total water storage in the Kujukuri coastal plain is shown in Photo. 8. For mapping the distribution of soil moisture, models, Eqs.(36) and (37), were applied to Landsat MSS data.

In Photo. 7, higher moisture areas were also distributed in shaded areas and inland parts of the coastal plain. The shaded area was recognized on both sides of valleys and dells and on north-facing slopes of hills. Soil moisture below 6 mm was observed mainly in the sandy areas of beach ridges (Photo. 7).

The development of the NNE-SSW linear patterns shown in Photos. 7 and 8 were due to the distribution of micro-topographies such as emerged bars, sand spits and dunes in this plain. Areas of Hasunuma, Naruto, Oamishirasato and Shirako villages had higher soil moisture than other areas. The soil moisture decreased from Shirako and its vicinity to Kujukuri village. General characteristics of soil moisture distribution can be well explained by considering the regional distribution of ground subsidence shown in Fig. 23. This map, compiled from data by the Environmental Department of Chiba Prefecture, reveals annual subsidence data from Jan. 1, 1979 - Jan. 1, 1980 accumulated subsidence data from Feb. 1, 1963 - Jan. 1, 1980.

For example, area with higher soil moisture and flooded areas are found in the Ichiba and Aono villages, and the city of Mobara. In these areas, the accumulated ground subsidence for 17 years exceeds 400 mm.

Photograph 7

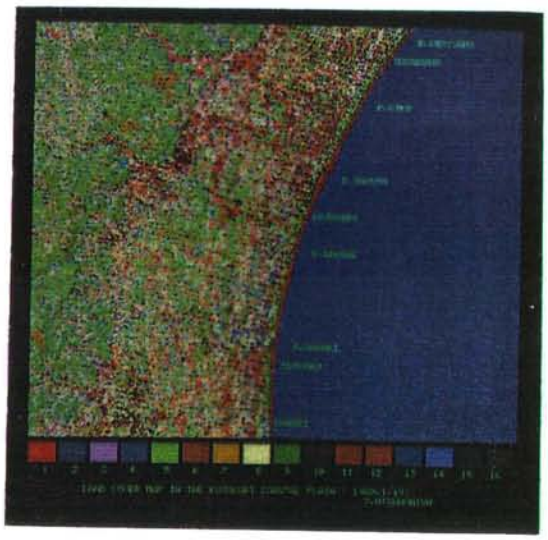

Land cover in the Kujukuri coastal plain(Jan. 19, 1980).

1: Bare soil
2: Flooded fields
3: Paddy fields
4: Flooded paddy fields
5: Truck farms
6: Weeds
7: Lawn
8: Reeds
9: Evergreen forests
10: Farm houses
11: Dry sand
12: Wet sand
13: Sea water
14: Inland water(pond, river)
15: Concrete roofs
16: Slate roofs

Photograph 8

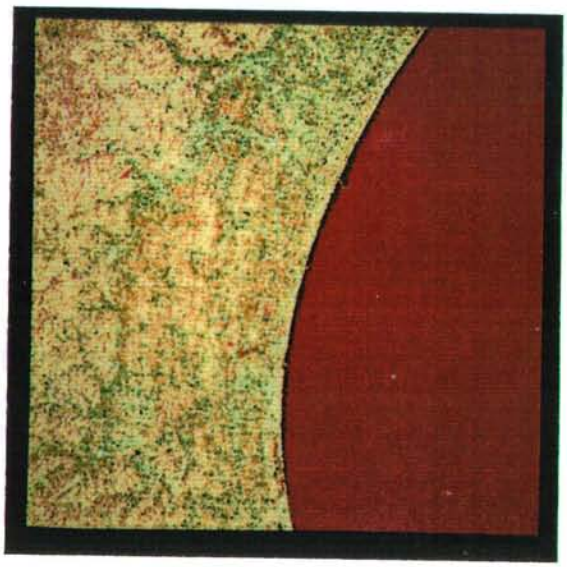

Distribution of total water storage in the Kujukuri coastal plain(Jan. 19, 1980).

unknown
0 - 5
6 - 11
12 - 17
18 - 23
24 - 29
30 - 35
36 - 41
42 - 47
48 -
water

(unit : mm)

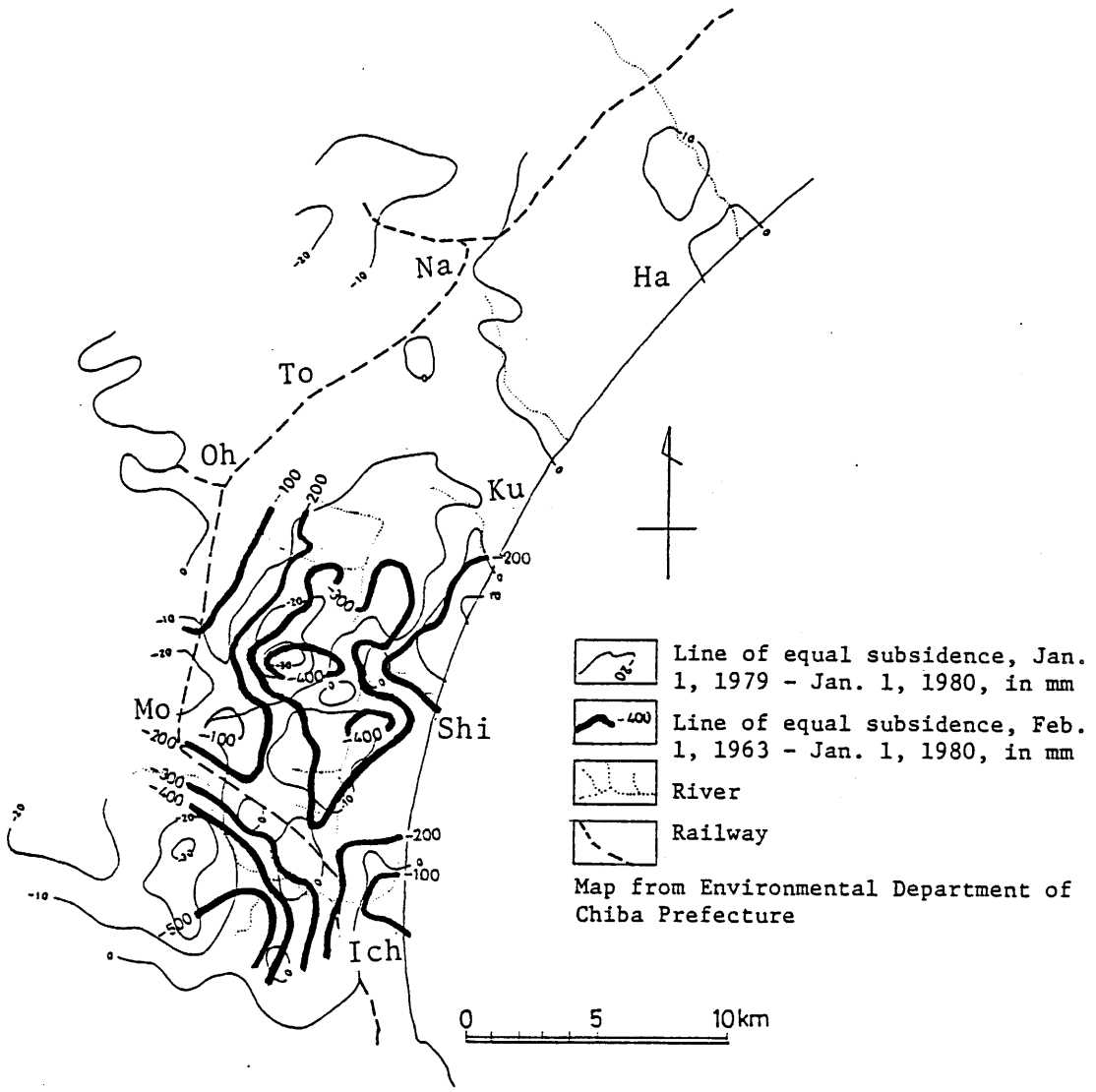

Ha: Hasunuma, Ich: Ichinomiya, Ku: Kujukuri,
Mo: Mobara, Na: Naruto, Oh: Oamishirasato,
Shi: Shirako, To: Togane

Figure 23 Land subsidence in the Kujukuri coastal plain measured by Environmental Department of Chiba Prefecture.

Flooded areas are more widespread than areas previously indicated by Yada et al. (1975, 1976) due to the continuing subsidence. Furthermore, the soil moisture maps can be used to estimate the spreading of areas that will be flooded after heavy rain.

(3) Mapping with satellite TM data

Photograph 10 shows the distribution of soil moisture in the area covered by the Landsat TM measurement in 1987. Models, Eqs. (38) and (39), were applied to Landsat TM visible and near IR data and the land cover map (Photo. 9) obtained from the experiment in the Kujukuri coastal plain to estimate total water storage.

The soil moisture map using the Landsat TM data covers a somewhat narrower area than that obtained from the Landsat MSS data. Therefore, the array of 1536 pixels x 1536 pixels of TM data were used to show the distribution of the soil moisture in the southern Kujukuri coastal plain.

The Rivers Kuriyama, Kido, Sakuta, Makame, Nabaki, Ichinomiya and Isumi flow from left (west) to right (east) on this map. Color coding in the unclassified group and flooded area was expressed the same way as that of the MSS data. Other colors characterize soil moisture (total water storage) ranging from 1 to 60 mm. In general, soil moisture less than 42 mm was widely observed as shown in Photo. 10.

Since the ground resolution of the imagery of spaceborne TM is 28.5 m x 28.5 m, relatively fine spatial difference of soil

Photograph 9

Land cover in the Kujukuri coastal plain (Feb. 14, 1987).

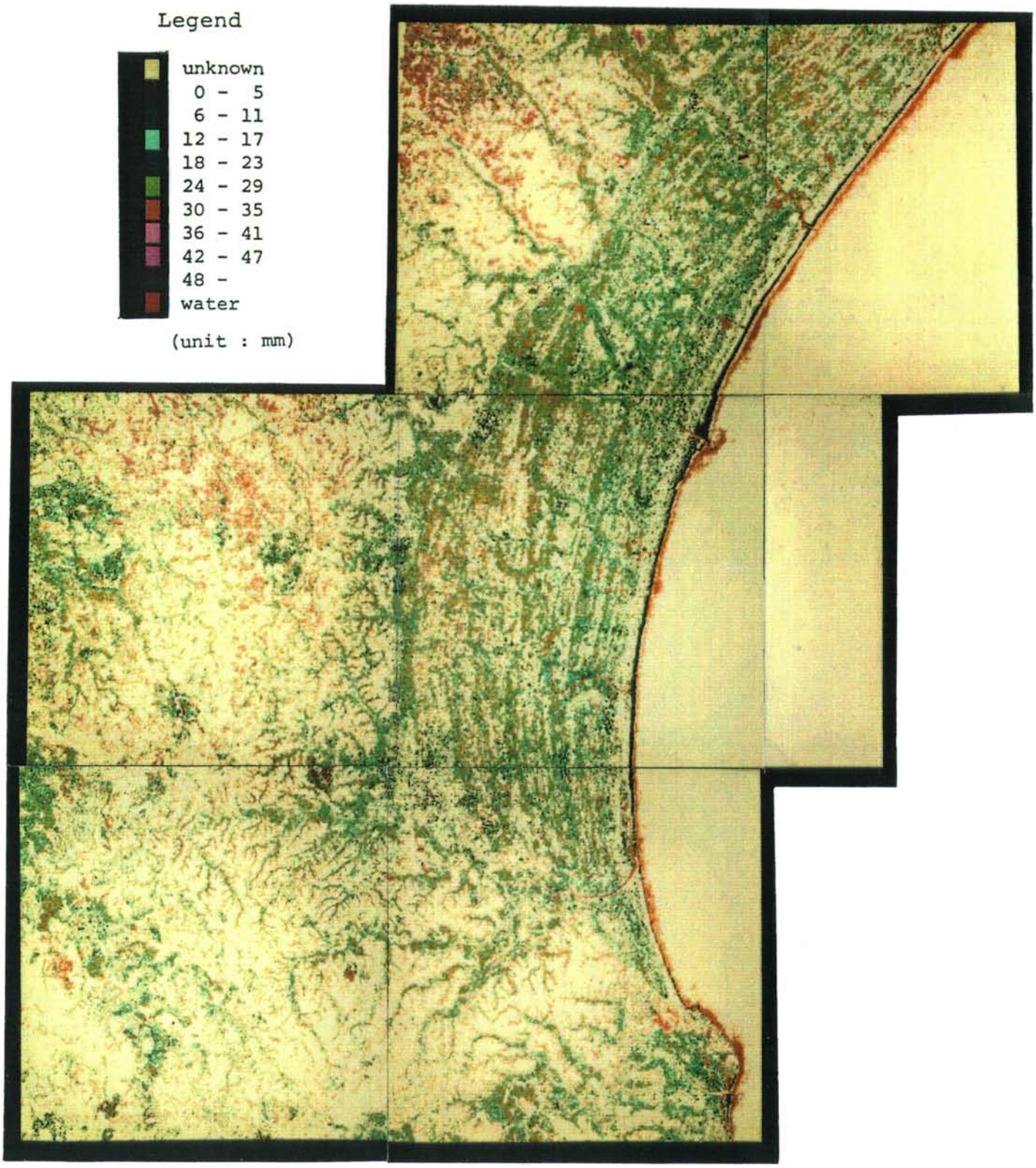

Photograph 10

Distribution of total water storage in the Kujukuri coastal plain (Feb. 14, 1987).

moisture can be observed. The soil moisture north of the River Kuriyama usually varied from 1 to 32 mm. Flooded areas were recognized in the uppermost part of the frame of Photo. 10. The area between Rivers Kuriyama and Kido had soil moisture ranging from 1 to 30 mm. Flooded areas also developed south of River Kuriyama. The soil moisture varied from 1 to 30 mm in the area between Rivers Kido and Sakuta. Soil moisture below 24 mm was widely distributed. The soil moisture varied from 1 to 24 mm between Rivers Sakuta and Makame. Both sides of the water channel of the lower basin of the River Makame showed higher moisture and some parts were flooded.

Soil moisture between the Rivers Makame and Nabaki varied from 6 to 42 mm. Flooded fields were observed in the lower basin of River Nabaki. The inner part of this alluvial plain also showed high moisture. The soil moisture between Rivers Nabaki and Ichinomiya ranged from 6 to 30 mm. South of the River Ichinomiya the moisture varied from 1 to 30 mm. The density slicing on the false color imagery excluded the shaded areas and the water surface clustered into sea water. Therefore, water surface clustered into sea water was not distinguished as a high moisture area.

Areas with higher soil moisture extended between the Rivers Nabaki and Ichinomiya. This photograph does not show the wider flooded areas on both sides of River Nabaki, and the lower soil moisture areas that were observed on the sandy beaches of this plain on field surveys or other maps. Soil moisture below 12 mm was observed mainly on the surface of swells, and it shows the

development of NNE-SSW linear patterns due to the strike of micro topographies as observed in Landsat imagery. Thus, the spatial distribution of soil moisture in this area was strongly affected by topographic conditions. Photograph 10 shows that the soil moisture distribution is concordant with that of ground subsidence. As stated above, areas with higher soil moisture and small flooded paddy fields are found in the western part of Ichiba village. Nevertheless, these regional characteristics do not appear clearly in the eastern part of Mobara and the northern part of Ichinomiya on the imagery obtained from the measurements on Feb. 14, 1987. This is mainly due to the land reclamation and housing.

4.1.3 Tsuchiura and its vicinity

Photograph 11 shows the land cover in and around Tsuchiura. Bare soils were dominantly distributed on the alluvial lowland of the River Sakura and on its surrounding diluvial upland area. Relatively wider areas of bare soil were observed in Tsukuba, 8 km west of Lake Kasumigaura. This was due to intensive spreading in the area of urbanization in the beginning of the 1980s.

Photograph 12 shows the distribution of soil moisture in and around Tsuchiura. Distribution of soil moisture was mapped using Eqs. (36) and (37) which were developed for the Kujukuri coastal plain. Photograph 12 shows that total water storage higher than 30 mm was mainly observed along shallow valleys in upland areas. The soil moisture of those upland areas varied from 6 to 24 mm

Photograph 11

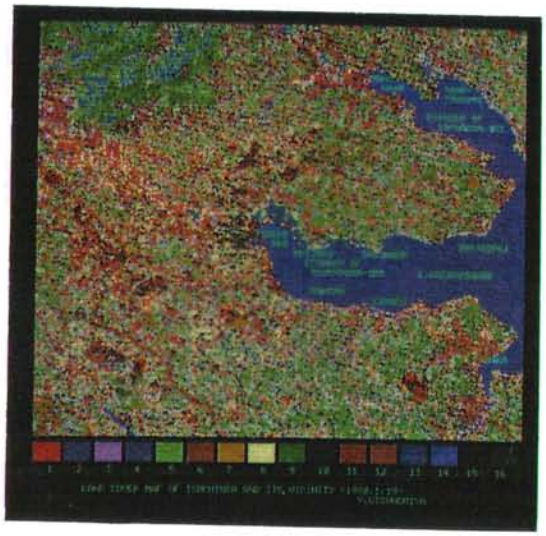

Land cover at Tsuchiura and its vicinity (Jan. 19, 1980).

1: Bare soil
2: Flooded fields
3: Paddy fields
4: Flooded paddy fields
5: Truck farms
6: Weeds
7: Lawn
8: Reeds
9: Evergreen forests
10: Farm houses
11: Dry sand
12: Wet sand
13: Sea water
14: Inland water(pond, river)
15: Concrete roofs
16: Slate roofs

Photograph 12

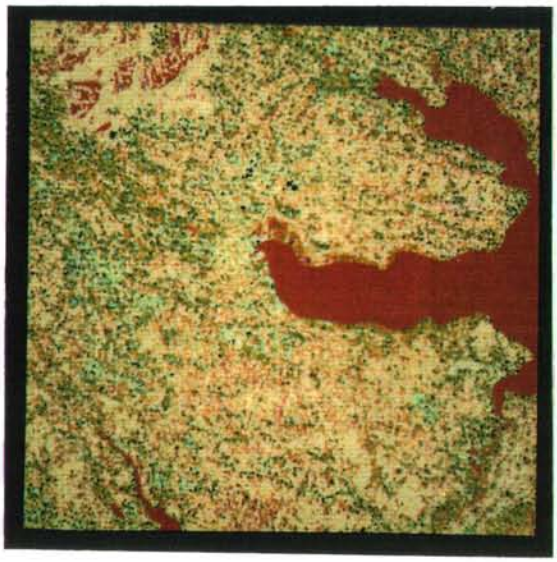

Distribution of total water storage at Tsuchiura and its vicinity (Jan. 19, 1980).

Unknown
0 - 5
6 - 11
12 - 17
18 - 23
24 - 29
30 - 35
36 - 41
42 - 47
48 -
water

(unit : mm)

excluding the shaded slopes, while soil moisture of the lowland fields varied from 24 to 42 mm.

The area surrounding the River Sakura and back marsh north west of Tsuchiura showed high soil moisture. Unreclaimed swampy parts were also shown as flooded area. Furthermore, the moisture in the lowland along the northern coast of the estuary of Tsuchiura-iri was higher than 30 mm. Particularly, areas with soil moisture over 30 - 42 mm were found mainly in swampy lowland fields after harvest of lotus roots. Areas with higher soil moisture were also found on north and west facing slopes of hills. Small ponds distributed in these areas were also recognized as higher moisture areas.

4.1.4 Old Joban coal mining area

Photograph 14 shows the distribution of total water storage in the old Joban coal mining area. Models, Eqs. (36) and (37), were applied to Landsat MSS data and the Land cover map (Photo. 13) for mapping soil moisture. Areas with higher soil moisture were observed on the west side of the mountain divide running southward parallel to the coast. This was also due to intensive shading by the mountain sides. The soil moisture in this area varied from 0 to 48 mm, while that of the alluvial lowland varied from 0 to 30 mm.

An area with higher soil moisture was also observed south of Waku village in a hilly upland area because of the existence of many north-facing slopes. The map shows that soil moisture was

Photograph 13

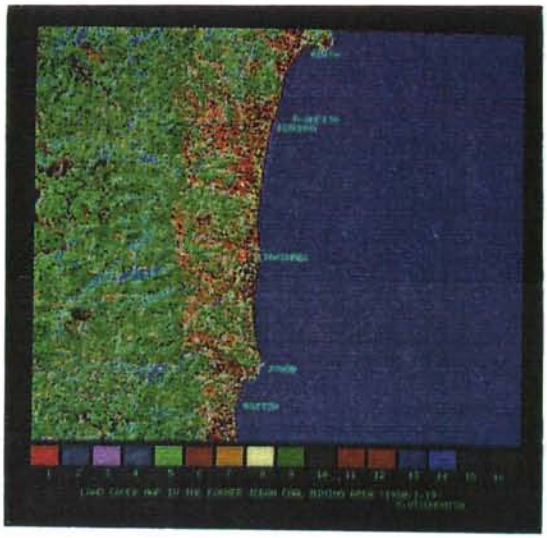

Land cover in the old Joban coal mining area (Jan. 19, 1980).

1: Bare soil
2: Flooded fields
3: Paddy fields
4: Flooded paddy fields
5: Truck farms
6: Weeds
7: Lawn
8: Reeds
9: Evergreen forests
10: Farm houses
11: Dry sand
12: Wet sand
13: Sea water
14: Inland water(pond, river)
15: Concrete roofs
16: Slate roofs

Photograph 14

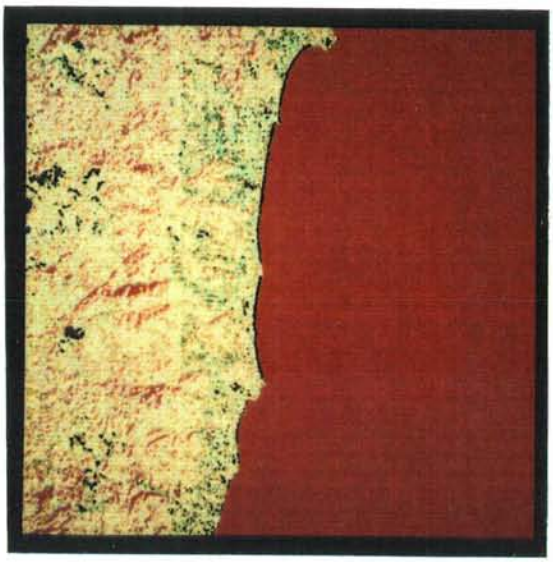

Distribution of total water storage in the old Joban coal mining area (Jan. 19, 1980).

unknown
0 - 5
6 - 11
12 - 17
18 - 23
24 - 29
30 - 35
36 - 41
42 - 47
48 -
water

(unit : mm)

higher in the village of Waku than in the area east of the village. In and around Waku, land subsidence is still continuing after severe depressions due to mining, however, swampy paddy fields with higher soil moisture were not clearly recognized in this imagery.

4.2 Application of the soil moisture map to the geomorphological mapping and potential wind erosion mapping

4.2.1 Significance of automatic geomorphological mapping

Landforms have been classified using two approaches. The first is landform division based on orogenic processes and the stages of the Davisian geographical cycle, which characterize the development of the landform. This is based on the elevation and inclination of slopes of the landforms. The other is a classification of topographical units constructed using many slopes and planes. These constructed units are then grouped systematically.

Both landform classification approaches are based on the concepts and complete knowledge of geomorphological back ground. Therefore, one who has no understanding in this area can not classify landforms and even if one has some background of geomorphology, the results of the classification may be influenced by the quality of information obtained from observations in study areas. Conversely, automatic classification

can lessen individual differences in the mapping after determination of the standard value or procedure.

Medium and large scale topographical maps are used for tracing the direction and curvature of contour lines. Inclination and area are measured by the elevation and space between two contour lines. Therefore, medium and large scale maps such as 1:25,000 and 1:50,000 topographical maps, are necessary for map reading and morphometry in the geomorphological mapping. Unfortunately, these large scale maps have been constructed only for restricted areas of the world. Therefore, efficient mapping of geomorphological classifications can be done without these medium and large scale maps.

Except the development of micro-topography, the smallest topographical unit is usually expressed by a dimension of 100 m x 100 m on a 1:50,000 topographic map. A 100 m x 100 m measurement is only 2 mm x 2 mm on the map and areas smaller than these measurements of land can not be expressed as patterns on the map. These topographical units are suitable to map on medium scale topographic maps such as 1:50,000 and 1:25,000 scale. The ground resolution of Landsat MSS is 57 m x 57 m (in the case of TM 28.5 m x 28.5 m) after the geographical correction by NASDA. These topographical units can be plotted with the scale similar to that of medium scale geomorphological sketch maps. Furthermore, these maps can be easily compiled by the automatic procedures to make maps of small scale.

Recently, photo interpretation of air photographs has been introduced into classification schemes in addition to map-reading

and field work. This procedure was widely used in the study of the classification. Even using this procedure, classification of topography is impossible without geomorphological knowledge, information of image interpretation and field work. Furthermore, relevant information must be selected for the classification because an air photograph includes complete visible information of part of the earth's surface. In detailed photo-interpretation, characteristics such as shape, pattern, structure and texture on the photograph should be recognized. The stereoscopic vision and the quantitative analyses of elevation are necessary, even though the monocular vision method enables the distinction of topographical development.

Imagery obtained using a camera system has usually been used for photo-interpretation. It should not be used to process broad areas of the earth's surface, however, because of little variation in the brightness of photographic films due to individual development procedures. Brightness variations can be observed both when comparing separate photographic films, and also, between the center and the margins within individual films. Conversely, CCT data obtained using a digital scanning system have less instrument error and fewer brightness changes in and around the nadir point. Its digital processing and automation of quantitative analysis enable efficient interpretation. Map compilation based on this automatic processing is easier than mapping by hand plotting data. Therefore, automatic mapping should be used for efficient classification of geomorphological units.

4.2.2 Automatic geomorphological classification

For evaluating the feasibility of automatic mapping, topographical units of the Kujukuri coastal plain are classified by map-reading, photo-interpretation and field observations.

(1) Geomorphological classification

Figure 24 shows twelve ridges of emerged sand bars, beach ridges and dunes parallel to the shore line. These low undulated swells are distributed in the most inland part of the plain. Swells, such as lines I to line VII, are wider and have flat top surfaces compared with lines VIII to XII. As Moriwaki (1979) reported, dune sand is distributed on the top of each ridge. In these swells (lines I to VII), paddy fields have sometimes been cultivated after the removal of dune sands.

Lines V, VII and XII formed by emerged sand bars, ridges and several spit-like landforms are mainly in the central part of the plain. Trough-like lowland between lines III and IV are parallel to beach ridges. The lowland between lines V and VI is somewhat wider than that between lines III and IV.

(2) Automatic classification of topography

Paddy fields are usually located in the trough-like lowland and back marshes. Therefore, even after harvest time, paddy fields show higher soil moisture than upland fields. Conversely, upland fields are observed on such swells as natural levees and beach ridges. Therefore, such land uses as upland fields and

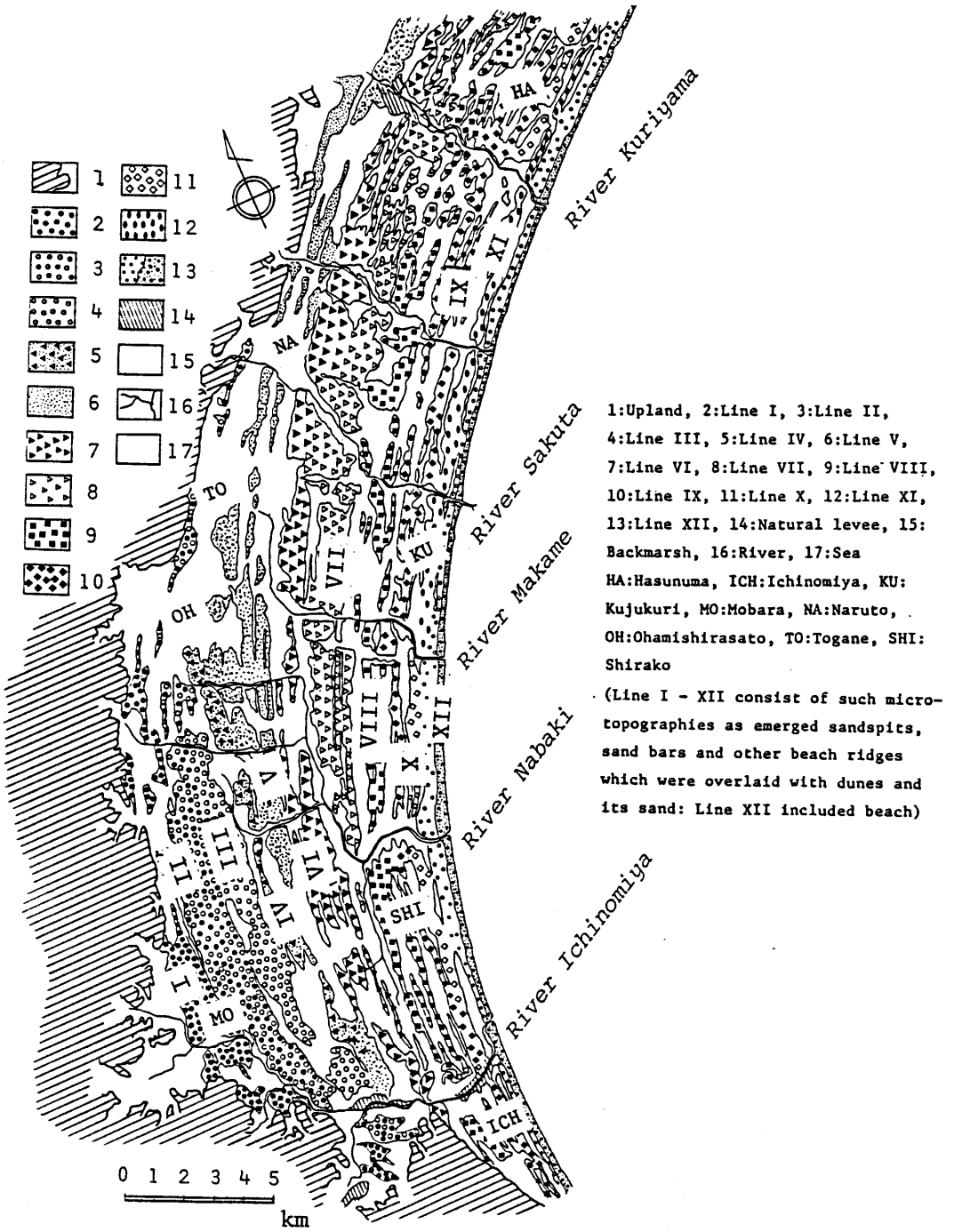

Figure 24 Geomorphological classification map in the Kujukuri coastal plain.

paddy fields are closely correlated with the development of micro-topographies in a low undulated alluvial plain.

In photo-interpretation, one can classify the surface based on the inclination and elevation of the surface with stereoscopic views of photographs. Since the area with high moisture shows dark and dry soil shows light color, the low undulated surfaces of micro-topography are empirically traced by the density in black/white film or color film. Therefore, variation in photographic density is one of the important elements in photo-interpretation. The surface reflectance in visible and near IR of MSS CCT data can be objectively analyzed by a photo-densitometer. In the case of bare soil, the variations basically depend on the relationships between micro-relief and soil moisture. Tarnocai and Kristof (1976) tried to classify automatically the topography based on and ground truth data and spectral response of Landsat MSS data.

In the alluvial plain, the soil moisture is lower for the surface of swells than for trough-like lowlands. Therefore, evergreen groves, farm houses and upland fields are usually developed on surfaces of swells. For instance, truck farms and evergreen groves are on swells such as beach ridges and elevated sand bars in the area from Kujukuri to Oamishirasato. Paddy fields are in the trough-like lowlands between beach ridges as shown in Fig. 24 and Photo. 7. At the most inner part of this plain near the cities of Mobara and Togane, residential area is mainly distributed on the low alluvial plain. Therefore, in the Kujukuri coastal plain, the spatial variations of the soil

moisture can be detected by the spectral reflectance. Topographical units, such as swells and troughs, can be classified by map overlay operations of land cover, soil moisture maps and density slicing.

Topographical development is also recognized by shapes and distribution patterns which are parallel or oblique to the direction of other units such as shore lines, river channels and cliffs. Since automatic recognition of the shape of the topography in the terrain is very difficult, the topographical units cannot always be distinguished by quantitative data processing. Therefore, the data processing by man-machine interaction is necessary for the classification. The distribution pattern and relationships of topographical units were recognized by the photographic patterns, such as direction and shapes. Our preliminary procedure of the automatic classification can reduce load and time of data processing such as hand-plotting of data and map compilation.

The automatic geomorphological mapping was constructed by similar procedures to those utilized in the previous section. The density slicing is based on reference values. In the first step, based on the above mentioned relationships between land cover and topographical development, fifteen categories of land covers were clustered into the following six groups of land cover:

1) bare soil and mixed surface or sparsely vegetated surface, such as bare soil, bare soil (with row of straw buried at one meter intervals), bare soil after radish harvest, paddy fields (with stubble), partly flooded paddy fields, frozen paddy

fields, and frost covered paddy fields, swampy surfaces after lotus root-harvest, and mossy paddy fields; 2) dry sand such as dry sand and blackish gray sand; 3) sea water; 4) inland water, such as inland water and flooded fields; 5) vegetated area, such as truck farms, and upland fields with welsh onion, barley (sprouting), weeds, lawn, reeds, and evergreen grove, 6) residential area such as farm houses, concrete buildings and slate-roofed houses.

Group 1 and 2 was divided into emerged beach ridges and swampy lowland. Sandy beaches can be easily classified by the location and direction of sand ridges. These bare and mixed surfaces consist of areas with high and low soil moisture. The humidity of the earth's surface varies with the surface topography. Therefore, it can be clustered into two classes based on the reference value of soil moisture, and one can assume that swells have low moisture and shallow troughs have high moisture. The separation value for the classification of swell and shallow troughs is assumed to be 14 mm of total water storage in this study. The precise classification does not always depend on this value, because the soil moisture changes gradually from place to place.

Group 5, vegetated area, is usually classified into emerged beach ridges because the development of truck farms and upland fields are usually found on the top of swells in the alluvial plains. Vegetation as reeds in swampy lowland and river banks.

Group 6 is classified into emerged beach ridges, because the residential areas, especially farm houses in this plain, have been

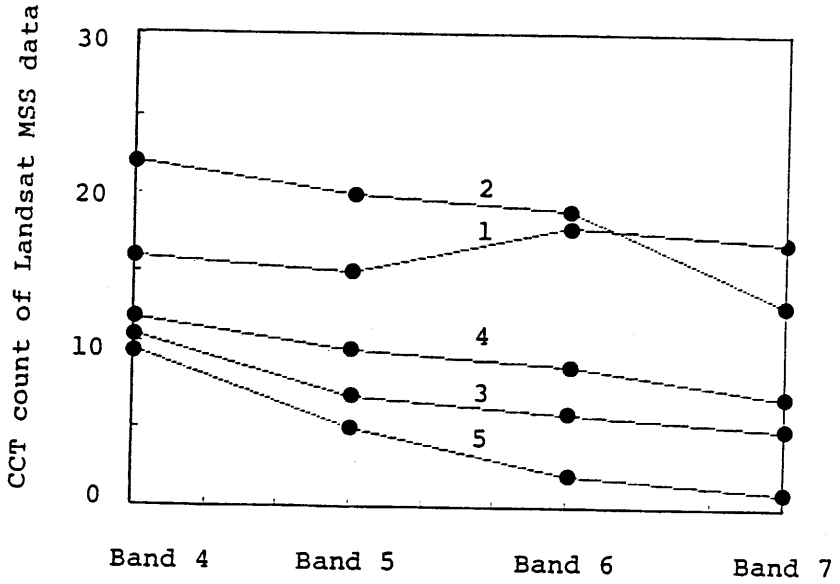

Figure 25 CCT count of each topographical category

1: Emerged beach ridge, 2: Sandy beach, 3: Swampy lowland, 4: Inland water, 5: Sea water.

constructed on the dry ground, such as the surface of swells. Therefore, the above residential areas can be clustered into dry land, such as emerged beach ridges.

Ultimately, these topographies in the Kujukuri coastal plain were clustered into the following five categories: 1) emerged beach ridge, sand bar and dune, 2) sandy beach, 3) swampy lowland and back marsh, 4) inland water and 5) sea water. Table 13 shows averaged spectral reflectance of each topographical category. These values are also shown in Fig. 25.

Table 13 Averaged spectral reflectance of each topographical category.

Topographical category	Spectral reflectance (CCT count)			
	Band 4	Band 5	Band 6	Band 7
1) Emerged beach ridge	16	15	18	17
2) Sandy beach	22	20	19	13
3) Swampy lowland	11	7	6	5
4) Inland water	12	10	9	7
5) Sea water	10	5	2	1

Photograph 15 shows the distribution of these classified topographies. Emerged beach ridges, sand bars and dunes are shown as swells between these trough-like lowlands.

Sandy beaches developed along the shore line near Mobara and in the lower reaches of the River Sakuta. Trough-like lowlands run parallel with shoreline. Particularly, they were densely distributed in the northern (upper) part of this frame. Giant cusps, cuspate delta-like topographies and offshore bar were found along the shoreline. The offshore bar near the mouth of the River

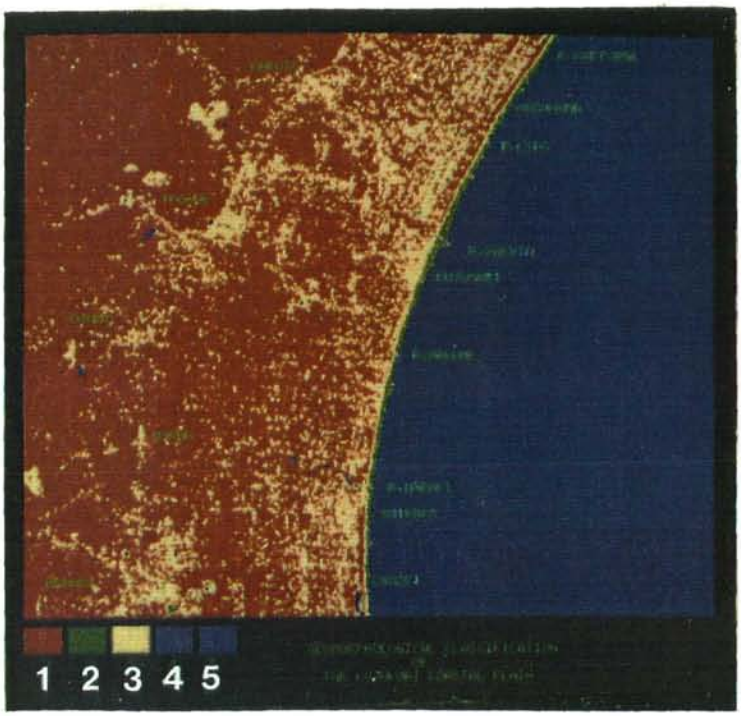

Photograph 15

Geomorphological map in the southern Kujukuri coastal plain.

1: Emerged beach ridge, sand bar and dune,
2: Sandy beach (including offshore bar),
3: Swampy lowland and back marsh,
4: Inland water; river and pond (including flooded areas),
5: Sea water.

Makame was included in this category. Air photographs in this area show that cuspate delta-like topography near the jetty of Katagai harbor at the mouth of the River Sakuta was formed after 1974. The formation is mainly due to the accumulation of sand drifted by littoral current and of sand dredged at the port entrance. According to the digital maps, the length of the intercusp spaces of giant beach cusps along the shoreline varies from 165 m to 495 m (three to nine pixels). The length of the horn of cusps ranges from 55 m to 110 m (one to two pixels).

At Shirako, Kujukuri and Hasunuma , houses with dense woods were clustered into evergreen grove in discriminant analyses. Therefore, the land cover discrimination of farm houses and other residential areas in these areas was difficult in the analyses of Landsat MSS data. Conversely, these houses were more clearly distinguished in the Landsat TM data because of smaller ground resolution.

Swampy lowlands distributed in and around Togane, Naruto and Mobara were located in the most inland part of the plain. They were also recognized in the northeastern and southeastern parts of the map. Some areas on the Shimofusa Upland were classified as swampy lowlands. This is mainly because lawn in golf courses was clustered into weed, which is usually distributed near the riversides where there is usually swampy lowland. Categories of inland and sea water showed the development of lagoons near the village of Chosei and flooded areas in Shirako.

4.2.3 Automatic mapping of potential wind erosion

The distribution of potential wind erosion is mapped using the soil moisture map and the wind erosion model. In winter, severe wind erosion has occurred in upland and lowland areas of Kanto, Tokai and Hokkaido Districts. The erosion especially is severe in the Kujukuri coastal plain.

Since the beginning of cultivation by the agrimotor around 1965, paddy straw have been buried in bare upland fields to reduce wind erosion and to fertilize with organic matter in this area. In addition to these agricultural techniques, after the mid 1970's, water sprinkling has been applied to fields to increase soil moisture and to reduce sand drifting by wind erosion. The higher moisture effectively reduces soil erosion. Thus, water sprinkling is a useful method for reducing soil erosion in winter.

Under a constant wind speed of 10 m/sec, the relationship between moisture and wind erosion was examined by J. Strendansky (1981) using a wind tunnel. One of Strendansky's models was applied to the soil moisture map for evaluating potential wind erosion. The soil erosion map was drawn automatically by the same method of computer mapping described in Section 4.1.2. The following equation for estimating volume of soil loss was obtained by Strendansky (1981).

$$\text{Soil loss} = 0.747 \exp^{-0.236\,SV} \quad \text{.....(41)}$$

(wind speed is assumed to be 10m/sec)

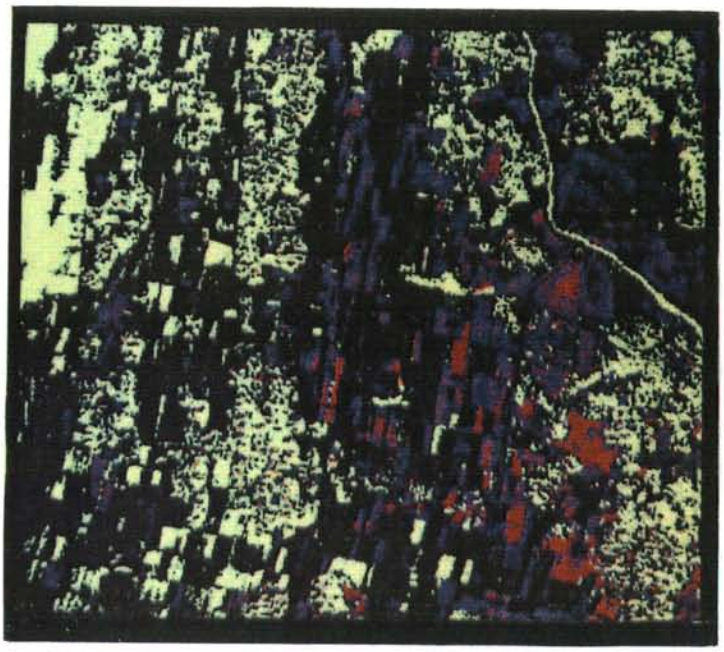

Photograph 16

Potential wind erosion map in and around Iyobo village in the Kujukuri coastal plain (Nov.15, 1985).

where SV is mass wetness (%) and wind speed is assumed as 10 m/sec. Soil loss is volume of the potential wind erosion ($kg/m^2/hour$).

The volume of potential wind erosion can be easily evaluated by a soil moisture map based on the model. Photograph 16 shows the potential wind erosion map in and around the village of Iyobo in the Kujukuri coastal plain (same scene as Photo. 6). Wind erosion can be estimated in each pixel on this map. Furthermore, the volume of wind-eroded sand can be calculated for all or part of the imagery.

Wind tunnel experiments of wind erosion usually oversimplify surrounding conditions. For example, wind blowing over fields is fluctuating in speed and direction, while wind in the tunnel is artificially controlled. Hence, the results of such experiments may not be directly applicable to field conditions. Nevertheless, as the preliminary examination, the author attempts to apply the Strendansky's model to the soil moisture map for estimating potential wind erosion. If the wind speed is fixed at 10 m/sec, the volume of the potential wind erosion can be easily evaluated by the application of the model to the soil moisture map.

The difference in wind properties between fields and the wind tunnel has important effects on wind erosion of soil. In spite of imprecise aspects, the model derived from the wind tunnel experiments can be applied to estimate the potential wind erosion of soils in the first step of the estimation of wind erosion.

5. Discussion

(1) Variations in soil moisture

Soil moisture decreases curvilinearly during a dry spell. Small periodic changes in soil moisture were superimposed on such curves in drying conditions. The daily depression of soil moisture at 5 and 10 cm depths decreased for many days after rainfall. Based on the experiment at the air monitoring station, it was found that three to seven days after rainfall, soil moisture in the surface layer approximated an equilibrium regime in which soil water loss is offset by water supply from a deeper soil layer.

(2) Soil moisture estimation with thermal parameter

The estimation parameters such as surface temperature (Ts), diurnal amplitude of Ts, daily difference between air temperature and Ts, dS/dTs and thermal inertia have been proposed for the soil moisture estimation. In the early stages of the examination, these relationships were sometimes evaluated by using advantageous data i.e., high temperature data with low SM and low temperature data with high SM in order to try to obtain a good correlation. Before the 1970's, real surface temperature could not be used because there were no thermal IR radiometers, therefore, the soil temperature immediately below the soil surface was used as surface temperature.

Therefore, the author examined precise relationships between SM and Ts using data obtained from the experimental field of the National Institute for Environmental Studies (NIES).

An appropriate time period for the soil moisture estimation was also examined because time periods in previous studies were not considered.

The estimation error of the regression model obtained from airborne MSS experiments during the period from 9:35 to 12:05 on Jan. 23, 1981 was somewhat larger than that for the other periods (7:05-9:35, 7:05-12:05). The soil surface layer was very moist during the period from 7:05 to 9:35, because of the increase of soil moisture caused by the thaw of ice needles formed in soil at night, and drying occurred throughout the period from 9:35 to 12:05. Under these conditions, the model has larger prediction errors. Thus the parameter dS/dTs during the periods 7:05-9:35 and 7:05-12:05 can be clearly used to estimate soil moisture.

Soil moisture and evapotranspiration have also been investigated using both visible and thermal IR data, the difference between Ts and air temperature, and parameters using the minimum and the maximum surface temperature. Since these parameters change with time and seasons, these models are less applicable. Though the improvement for the inadequate parts of these models have been attempted by introducing the normalized rising rate of Ts by net radiation, the model was also influenced by seasonal changes.

(3) Soil moisture estimation with thermal inertia model

As mentioned before, for the evaluation of the thermal inertia (TI), there have been two different approaches. One is the iterative calculation method. The other is an analytical approach. In the iterative calculation, heat balance and heat transfer equations were solved repeatedly for various sets of albedo, surface roughness, surface humidity, thermal conductivity, and surface temperature. In this approach, relationships between albedo, thermal inertia and soil moisture were examined to create charts in order to avoid enormous individual calculation time. Watson's theoretical examination still included some iterative solution methods for the determination of some parameters (Watson, 1971,1975,1982). In some approaches based on one dimensional heat transfer and a heat balance model, some heat balance terms were excluded. For example, the latent heat flux and the soil heat flux over a 24-hour period were ignored (Kahle et al., 1984; Price, 1980). Price's apparent thermal inertia (ATI) was not based on the physical and mathematical solution, but on the iteration method (Price, 1985).

Ho(1987) obtained the TI using the first harmonic of the variation of the surface temperature curve. Some estimation parameters of heat balance terms for bases of his soil thermal model were derived from regression analyses.

As above, regression analyses were sometimes applied to evaluate latent heat flux or sensible heat flux in some models based on both of the iterative calculation and analytical approaches. Thus, previous investigators have not successfully

obtained a mathematical solution for the evaluation of thermal inertia based on one-dimensional heat transfer and heat balance models on the earth's surface. Previous models included too many complicated input parameters such as atmospheric correction and other subjective parameters, and the least square method was easily applied to the data for the evaluation of the parameter. Furthermore, essential parameters of the heat balance model were sometimes excluded in their models. As a result of the omission of these parameters, thermal inertia (TI) was used simultaneously with albedo.

The author obtained the mathematical solution for the evaluation of TI as shown in Eqs.(15), (20) and (28) (Utsunomiya and Yamaguchi, 1986,1987 and Utunomiya, 1988). Therefore, the albedo was logically and physically adopted as one of the parameters in the thermal inertia (TI) model in this study. Naturally, the albedo and TI should not be combined and used simultaneously. Though good relationships between thermal terms such as albedo, TI and SM were obtained, these non-physical procedures should not be used for the evaluation of the value of the thermal inertia.

Though Kahle (1977) adopted a ground moisture factor for the evaluation of the latent heat flux, the estimation procedure for this parameter was not described. Most investigators have ignored relative humidity of soil surface or used it inappropriately. Sometimes, the relative humidity was assumed to be saturated (1.0) and uniform throughout the study area. This assumption for the relative humidity of the soil surface overestimates the volume of

the evaporation from soil surface. In order to avoid this overestimation, the parameter of relative humidity (μ) of the earth's surface must be included in these calculations. Relative humidity of soil surface (μ) based on the heat balance method could not be evaluated in airborne and other spaceborne remote sensing, because there was no apriori value for latent heat flux. Thus, it must be estimated using multispectral reflectance which depends on the moisture of soil surface. This parameter is introduced into the author's thermal inertia model by the normalization of the albedo of soil surface as shown in Eqs. (15) and (28). The author's advantage of this procedure is normalization of the albedo, which avoids the variations of the relationships of albedo and soil moisture with time.

As shown in Fig. 17, the total water storage was linearly correlated with thermal inertia. This is due to the normalization using both net radiation and Ts, whose intensities change with time. The variations of each intensity are canceled as shown in the first term of Eq.15.

As explained above, some ambiguities in the previous methods of the evaluation of the thermal inertia have been eliminated. Then, a model based on thermal inertia for the moisture estimation in a shallow soil layer, at least 0 to 5 cm depths, was developed in this study.

Since the quantitative relationship between TI and SM had not been clarified, a regression analysis was applied to the soil moisture evaluation only after the establishment of a mathematical solution for the thermal inertia model in this study.

In these regression analyses, the values of coefficient and constant terms of regression equations obtained from the experimental field were different from those for the equation obtained by airborne MSS measurements. This was due to differences in the porosity and mineral components of the two kinds of soil. In spite of these discrepancies, both of these equations had similar coefficients and constants in the regression equations. Therefore, the thermal inertia model for estimating soil moisture can be applied to the remote sensing data for soil moisture measurements.

For this remote sensing, soil components such as porosity and mineral/organic matter of soil in the Kujukuri coastal plain were assumed to be constant. Realistically, these soil physical elements vary with the location. For example, swampy lowland between beach ridges generally consists of somewhat peaty soil, and the apparent dry bulk density varies with the kind of soil. Furthermore, even in the same place, the porosity can vary with time.

The value of albedo was not physically examined in previous remote sensing studies except by Gillespie and Kahle (1977). True albedo could not yet be evaluated, because of the lack of ground truth data. Pratt and Ellyett (1979) used only the reflectance derived from panchromatic imagery for the value of albedo. Pohn et al.(1974) and Gillespie and Kahle (1977) used only the reflectance of visible and near IR data from MSS data.

Gillespie and Kahle (1977) obtained the albedo by weight function using a narrow range of the airborne MSS visible and near

IR data (0.33-1.07 μm). They used no global radiation and surface reflectance less than 3 μm. Instead, they used the spectral reflectance obtained by a reflective spectrometer.

Pohn et al.(1974) obtained reflectivity map from Nimbus III High Resolution Infrared Radiometer (HRIR) daytime data on Nov. 11, 1969. Day and night temperature maps was obtained from Nimbus IV Temperature Humidity Infrared Radiometer (THIR) data from May 15 and May 7, 1970. Eight days elapsed between two thermal data acquisition times. Thus, the day and night temperature differences could not be validly used in their analysis even though no major weather front moved through the study area during this time. Furthermore, the reflective map was based on the data obtained from a different year. Thus, the data had over a 7 month time gap between the reflectivity map and the temperature map. The reflectivity map was used in place of albedo. But the relationship between spectral reflectance in such wavelenghts as 0.7-1.3, 2.3-3.0 and 2.4-4.2 μm used in the Nimbus IV HRIR and the method of constructing the reflectivity map were not described. Also, thermal inertia was practically determined by the empirical curve. The albedo is indispensable for the evaluating net solar radiation and relative humidity of soil surface in the thermal inertia model.

One problem in the determination of albedo with the remote sensing is caused by the MSS hardware. Since the incident energy from the air such as global solar radiation or spectral energy cannot be observed by the MSS, there is no value to use as the denominator for calculation of albedo. Therefore, the albedo

could not help being estimated by the regression equation based on the relationships between albedo from the ground truth observation and MSS visible and near IR data.

Another problem is narrower spectral regions (0.4-1.06 μm) of MSS for the albedo estimation. The exact value of albedo cannot be obtained because of the decrease of reflectance in near IR spectral regions caused by the absorption of chlorophyll of plants. Fortunately, this problem did not influence our results, because the vegetated areas were excluded in the estimation of SM.

One ambiguous problem is in the diffusion coefficient. Some previous studies ignored this parameter or assumed it to be a constant. The other used wind speed and other parameters for the determination of the diffusion coefficient. These methods required wind velocity and roughness parameters of soil surface, such as zero displacement, Von Karman's constant, roughness length, and Monin-Obkhov length.

The diffusion coefficient varies from place to place according to the regional difference of roughness of soil surface and wind speed of the boundary layer. Therefore, the diffusion coefficient must be observed in each pixel of MSS data. Direct measurement of this diffusion coefficient (K) in each pixel is not yet possible because of the lack of such data as surface roughness and wind speed in each pixel.

The diffusion velocity based on the energy budget equation is an appropriate parameter rather than the diffusion coefficient for the evaluation of latent and sensible heat flux (Uchijima, 1974). Therefore, the diffusion velocity (D) at the ground truth center

was used in place of the diffusion coefficient and it was assumed to be uniform in the study area (512 pixels x 512 lines).

The above approaches to evaluate the turbulent diffusion resistance for heat transport were largely influenced by the stable or unstable conditions of the atmosphere. Many parameters are required to obtain the diffusion coefficient, and the approach is rather complicated in remote sensing. Wind velocity and turbulent diffusion resistance can only be solved by iteration techniques for unstable conditions (Soer, 1980).

Some problems in soil physics mentioned above can be solved by physical and in vitro experimental methods in the laboratory under constant conditions, and not by remote sensing. Though several problems are included in the thermal inertia model for determining moisture, it compares favorably with the climatological and water balance methods. The remote sensing which can instantaneously observe phenomena becomes less effective in determining the accumulated value of soil moisture. Therefore, this surveillance system is restricted to shorter time periods. But this weakness of the remote sensing method will be compensated for by the repeated surveillance of the surface.

(4) Soil moisture estimation with visible and near IR data

Reflectance of soil surface in visible and near IR wavelength regions decreases with an increase in soil moisture. The adequate relationships between SM and the surface reflectance depend on the observation time. Namely, the correlation in the early morning

(7:05 AM) was weak, while MSS-data obtained from 9:35 to 12:05 showed relatively good correlation with the soil moisture. The value of the correlation coefficient at 12:05 was higher than that obtained at 9:35. The value varied with circumstances from very weak solar radiation with low intensity from the earth's surface at dawn to strong solar radiation with high intensity of reflectance at noon.

The relationship between reflectance and moisture in a shallow soil layer (0-5 cm) was relatively higher for the airborne MSS data than for Landsat MSS data. Such weaker relationships from Landsat MSS data are related to the band-widths, because the width of the radiation band is wider than that of airborne MSS. The weak correlation is also due to the gap in size between ground truth plots and instantaneous field of view (IFOV) of MSS. The result was influenced by the variation of soil moisture within a same pixel of Landsat MSS. These problems will be solved gradually by improvement of acquisition and handling systems of spaceborne multispectral data. Some of the problems such as IFOV and the band width of the scanner have been improved in Thematic Mapper (TM) of Landsat-4 and 5.

The prediction error in soil moisture estimation is lower for the thermal IR data than for the visible and near IR data. Therefore, the thermal IR data is preferable for the soil moisture determination. From the water balance method, Heilman et. al., (1977) evaluated evapotranspiration and soil moisture through the crop cover. Their estimation equations were not based on the spectral reflectance of MSS but on the water balance in a semi-

arid region with somewhat sparse vegetations. Therefore, the model based on the water balance model must be examined on experimental data in humid regions, such as Japan and other monsoon areas. Furthermore, the estimation modeling should be developed with visible and near IR data, and this is expected to be examined in future analyses.

Among the regression models using data from visible /near IR, thermal IR data and TI for evaluating moisture, the TI is preferable over the other models. The TI model is based on the physical bases such as heat balance and a one-dimensional heat transfer model. The model with less prediction error is less influenced by the environment.

The TI model can be applied in arid and semi-arid regions and other tropical and cool climatic regions. Its applicability should be ascertained in future analyses. These models for the estimation of soil moisture were examined by using the satellite data from the Heat Capacity Mapping Mission (HCMM), and more recently by using NOAA data. In previous works using many complicated parameters in the initial stage, the model's physical examination and mathematical solution were still used with little success. Therefore, most of the investigators had failed to obtain an analytical TI model, and they used the least square method and iterative calculation by changing the parameter of the heat balance terms.

The advantage of the TI model established by the author is that the model is based on physics, such as heat balance, a transfer model and mathematical solutions.

(5) Soil moisture mapping

A few moisture maps were made in previous studies. Most of these maps were constructed by hand-plotting data, not by computer mapping. Furthermore, some of them showed the distribution of the soil moisture beneath the canopy of crops and other structures, such as roads, and buildings. There was no exclusion of the soil moisture beneath these features for land cover. For mapping of soil moisture in this study, SM estimation models were applied to bare soil and areas with sparse vegetation such as bare soil with paddy straw and paddy fields with stubble. These models were applied after the exclusion of the areas covered with vegetation and structures such as roads and buildings. Whole coverage areas of single map are 2.5 km x 25 km with an IFOV of 5 m for airborne MSS, and 35 km x 35 km with an IFOV of 57 m for Landsat MSS observations. Therefore, the satellite imagery enables mapping of wider geographical and hydrological phenomena compared to that of the airborne MSS data, because of the wider coverage and few instrument errors.

The accuracy of discrimination was not always accomplished by the airborne and spaceborne MSS/TM data because shaded areas were classified into flooded areas or water surface. The land cover discrimination is the first step in the SM mapping. For higher accuracy, the exclusion of shaded areas has been carried out in previous works on land cover classification. But the spectral reflectance in shaded areas never has the same reflectance value as in sunny places. Therefore, it is quite reasonable to exclude shaded areas based on the land cover discrimination.

On the moisture map shown in Photos. 6 and 14, the shaded area was empirically excluded by a color composite technique from the visible and near IR spectral data. Furthermore, the density slicing procedure was applied to the image by trial and error. This method was effective in excluding shaded areas in this moisture mapping. However, the water surface was excessively eliminated in this imagery. The separation value in this technique is not easily obtained, because it depends upon the intensity of surface reflectance in each scene of MSS imagery. Each pixel of Landsat MSS and TM data consists of many land covers with different optical properties. For example, one pixel located in lowland sometimes includes small canals and footpaths. The ground cover of each plot was still assumed to be homogeneous in the remote sensing study.

In the modeling for soil moisture estimation using Landsat data, al least, two samples of soil moisture obtained from the area corresponding to the IFOV of Landsat MSS or TM CCT data were averaged. Land use observations and soil sampling for Landsat MSS data were made during four days. Therefore, daily change in soil moisture influenced the accuracy of ground truth data of soil moisture, while in airborne MSS measurement, the soil sampling was carried out immediately after the airplane flight. The soil moisture variation with time were negligibly small in the airborne MSS experiments.

In the Kujukuri coastal plain with somewhat simple topographic units, the distribution of soil moisture is mainly affected by micro-topographies. Nevertheless, the map obtained

from Landsat MSS shows that soil moisture gradually decreases toward the north of the lower basin of the River Nabaki. The distribution of soil moisture is similar to that of the land subsidence areas. The lower basin of the River Nabaki has flooded paddy fields and swampy areas and has subsidence exceeding 400 mm from 1963 to 1980.

The comparison of air photographs obtained from two different years (1974 and 1985) shows that these flooded areas in the lower basin of the River Nabaki are still gradually spreading year by year. The lagoon area located in the bottom of Fig. 23 and Photo. 8 has also spread, while a part of the lagoon has been recently reclaimed for housing. This fact was also confirmed by our field survey.

At Tsuchiura and its vicinity, lotus fields have been developed in the alluvial lowland along the northern coast of the Tsuchiura-iri estuary. Back marsh is observed behind the emerged bar on which Tsuchiura is located. Swampy lowland was also recognized on the northern shore of the River Sakura. Soils with higher moisture are distributed in the alluvial lowland along the northern coast of Tsuchiura-iri and on the northern shore of the lower reaches of the River Sakura. The distribution of high moisture in the area is similar to that of the back marsh on the river plain.

As observed in the lowland field of Tsuchiura and its vicinity, lotus fields show high moisture in winter. Therefore, accurate and detailed land use development can be evaluated from the relationships between soil moisture and land cover

distribution of study areas. Though it is not always possible to indicate land use development by soil moisture mapping, soil moisture maps can serve as base maps for understanding the land use as shown in the relationships between the lotus root planting area and high soil moisture distribution.

(6) Automatic geomorphological mapping

The soil moisture map can also be utilized for the geomorphological classification. This study attempted automatic mapping of geomorphological units based on the soil moisture map and land cover map. Since this procedure has never been accomplished in previous studies, automatic topographic classification based on a map overlay technique was attempted. It can be difficult to avoid classification error in the automatic recognition of shaded areas. Therefore, shaded areas in mountains, hilly land and upland areas must be excluded before the soil moisture and topographic classification mapping. Such topographical units as swells and shallow troughs observed in the alluvial lowland of the Kujukuri coastal plain can be partly classified automatically by the overlay operation method of land cover and soil moisture map. Swell and trough-like lowland consist of partially dry ground and wet ground, respectively. These topographic units in bare soil and paddy fields were classified using the separation value of 14 mm of soil moisture.

Though this land classification gave successful results in the classification of the topographic units in such low undulating areas of alluvial lowland, further studies are needed for the

determination of more refined values in the classification. If further detailed evaluation of the areas could be conducted, it would help to eliminate the rough estimation of the soil moisture which was 14 mm as standard value in this study.

As Verstappen (1977) pointed out, spatial changes of topographical units are more gradual than abrupt in nature. After the examination on a grid mesh of 10 km in the Netherlands, he concluded that Landsat MSS data were not suitable for the geomorphological classification of the study areas.

The author examined the development of terrain features in the Netherlands on some large and medium-scale topographical maps(1:50,000 and 1:250,000). He has found that the terrain features consist of broad lowland (polder), plain, dune and somewhat narrow hilly land. Thus, the terrain in the Netherlands is somewhat monotonous, and the land use varies from place to place. It was recognized that the quantitative digital approach to the discrimination of the topographic features based on the spectral response is less effective in such areas.

Verstappen's conclusion is due to the use of a large grid mesh (10 km). A large grid mesh inevitably includes many land units with different reflectance properties. Thus, such a large grid mesh decreases the correlation coefficient between MSS data and topographic units. Discrimination of topographic units is usually more difficult than classification of superficial deposit and material. Therefore, Verstappen's conclusion on classification, regardless of the relationship between land use and topographical development, is quite reasonable in the

Netherlands. Furthermore, choice of the appropriate size for the grid mesh is important for automatic classification. One pixel (57 m x 57 m) of Landsat MSS data used as a fundamental grid mesh in this study means a small grid size compared to the grid size used by Verstappen. It is an improvement in the accuracy of land classification . The reflectance energy from the surface is a composite of beams radiated from each land unit with different physical properties. Therefore, lithological and mineralogical characteristics and their composite ratio are very important in the analysis of spectral reflectance from the earth's surface and topographical classification (Townshend and Hancock, 1981).

In this approach, the respective spectral reflectance of surface materials and the ratio of their composition should be clarified by laborious field and laboratory experiments. Conversely, the topographical classification based on overlay operation using soil moisture and land cover maps is a useful approach to reduce this laborious work and time for data processing. The author's procedure for the geomorphological mapping can be applied for the classification of the micro-topographies such as emerged beach ridges and back marsh. Furthermore, changes in the micro-topographies can be clarified using repeated surveillance.

(7) Potential wind erosion map

The soil loss model, derived from the experiment using a wind tunnel, was applied to the soil moisture map for potential wind erosion mapping. The potential erosion in this map was somewhat

overestimated, because the accumulation process in the fields was simplified or neglected in the model.

Some hazard maps, for such disasters as flooding, erosion, earthquakes and landslides, have been made by hand plotting data obtained by laborious field work. The erodibility in Denmark was mapped using a computer mapping procedure (Madsen et al.,1986). The map indicated that the erosion was mainly caused by rain showers and melting snow and not by wind erosion.

The soil moisture map can also be used as a base map for other thematic mapping. We can examine the potential wind erosion indicated by the soil moisture. The mapping of potential wind erosion based on the soil moisture map has not been carried out in previous studies. This is due to the lack of soil-loss models except Strendansky's model. Some wind erosion maps have been constructed using weather data instead of soil moisture in Tokachi and Kanto district in Japan. These mapping procedures were somewhat analogous to that of the wind erosion mapping. The volume of estimated soil loss was integrated in somewhat longer periods rather than those used in our procedure. These maps could not be used to estimate the soil volume loss in real time. This mapping procedure can evaluate the volume of soil loss in a short time. Therefore, the procedure will enable creation of a real time system for evaluation of wind erosion. The estimation of the volume in a long period is not easy, and will require wind speed data and soil moisture maps for specific study areas.

In the low undulated alluvial lowland of the Kujukuri coastal plain, soil erosion is mainly caused by wind in dry conditions.

The estimation of potential wind erosion can be made available for soil conservation and irrigation management of plowland of this area. The mapping method using such parameters as soil moisture and wind speed data is effective for future hazard mapping.

Potential wind erosion increases with increasing wind speed. Therefore, a multi-variate regression model for the erosion should be developed by using the relationships among soil loss, wind speed and soil moisture. These parameters can be obtained from wind tunnel experiments for precise evaluation of soil volume loss.

6. Conclusion

This study was concerned with modeling for determining soil moisture and its application for soil moisture and other thematic mapping using airborne multispectral scanner (MSS) and space-borne MSS and Thematic Mapper(TM) data. Conclusions can be summarized as follows.

1. The relationships between visible, near IR ,thermal IR data and soil moisture were examined using regression analyses. The regression result showed a better line fitness in thermal IR data than for visible and near IR data.

In spite of the poor relationships between soil moisture and visible/ near IR data, thermal IR-data and soil moisture showed a good correlation even in the early morning. The thermal model with low prediction error is applicable to the MSS thermal data obtained from the sparsely distributed vegetation area.

2. The author examined analytically and mathematically the thermal model on the earth surface and established a concise thermal inertia model for determining soil moisture. The model was also evolved by introducing relative humidity of soil surface obtained from the ground based measurement at the field of the National Institute for Environmental Studies (NIES) and airborne MSS measurements in the Kujukuri coastal plain.

In this experiment, the relative humidity of soil surface was substituted by estimated relative humidity of soil surface derived from the normalized albedo. The model, thus obtained in the Kujukuri coastal plain, was very similar to that obtained from the experiment at the field. By comparing this physical model with the other models based on the visible and near IR data, the thermal inertia model is the most appropriate for soil moisture estimation. Therefore, the model is applicable to a wide range of fields.

3. Empirical models with visible and near IR data for estimating soil moisture were also developed. These models based on the airborne MSS data showed smaller prediction error than that based on Landsat Thematic Mapper (TM) and MSS data. This may be due to a narrower wavelength band, small size of its instantaneous field of view (IFOV) and low influence of path radiance between target area and platform.

4. The soil moisture maps in the Kujukuri coastal plain, Tsuchiura and its vicinity, and the old Joban coal mining area were constructed using the airborne and spaceborne MSS and TM data. In the Kujukuri coastal plain, soil moisture was highest in the lower reaches of the River Nabaki and gradually decreased to the northeast of the area. A comparison of photographs from different years shows an increase in the flooded areas in the lower basin of the River Nabaki. The soil moisture map of Tsuchiura and its vicinity showed the swampy lowland being used as

lotus and paddy fields on the inner part of emerged spits. Swampy lowland also developed along the northern coast of the Tsuchiura-iri (estuary) of Lake Kasumigaura.

5. Spaceborne multispectral data is useful for the evaluation of soil moisture distribution in a broad area. Therefore, these data topographic units were automatically classified by an overlay operation of land cover maps on soil moisture maps. The geomorphological map was useful to distinguish micro configurations of terrain such as swells, shallow troughs, sandy beaches, and sea and inland water.

6. Potential wind erosion maps derived from the soil moisture maps, show regional characteristics of wind erosion. Thus, the maps can be applied to the effective management against wind erosion.

ACKNOWLEDGMENTS

The author would first like to express his sincere appreciation to Dr. Masatoshi Yoshino, Dr. Takeshi Kawamura and Dr. Kazuo Kotoda, Professors of the Institute of Geoscience, and Dr. Masamu Aniya, associate Professor of the same Institute at the University of Tsukuba for their kind supervising the present study. Also, sincere thanks are to go to Dr. Tadakazu Okuno, Professor of the Science University of Tokyo (former Division Head of the National Institute for Environmental Studies). Without their guidance and help, this study would not have been possible.

Special thanks should go to Dr. Zenbei Uchijima, Professor at Ochanomizu University, who advised this study and English wording of this manuscript. The author was also certainly indebted to Mr. Rich Wittrup for editing of this manuscript.

Thanks are due to Dr. Takenori Yamaguchi, Mr. Kimio Ichijyo, Dr. Tatsuya Yokota and Mr. Ryoichi Tsukada, all of who helped in data transfer and equipment operation. Also, thanks are due to Dr. Shota Hirosaki, former Division Head of the National Institute for Environmental Studies, and Dr. Yoshiro Haga, Professor of the Science University of Tokyo, for their help on feasibility of multivariate statistical analysis and programming computer input/output in this study.

REFERENCES

Abdellaoui, A., Becker, F., and Olory-Hechinger, E. Use of Meteosat for mapping thermal inertia and evapotranspiration over a limited region of Mali. Journal of climate and Applied Meteorology, 25, 1986, pp. 1489-1506.

Asami, S. Some attempts on landform divisions. Geographical Review of Japan, 24, 1951, pp.436-446. (J,E)

Bernard, R., Martin, P. H., Thony, J. L., Vauclin, M., and Vidal-Madjar, D. C-band radar for determining surface soil moisture. Remote Sensing of Environment, 12, 1982, pp.189-200.

Bernard, R., Soares, J. V. and Vidal-Madjar, D. Differential bare field drainage properties from airborne microwave observations. Water Resources Research, 22, 1986, pp. 869-875.

Bowers,S. A. and Hanks, R. J. Reflection of radiant energy from soils. Soil Science, 100, 1965, pp.130-138.

Bruckler, L., Witono, H. and Stengel, P. Near surface soil moisture estimation from microwave measurements. Remote Sensing of Environment, 26, 1988, pp.101-121.

Budyko, M. I. The heat balance of the earth surface. Translated by Z. Uchijima.from the Russian edition (1956), Tokyo: Kasen Suion Chosakai, 1957, p.181. (J)

Burke, H., and Schmugge, T. J. Effects of varying soil moisture contents and vegetation canopies on microwave emissions. IEEE Transactions on Geoscience and Remote Sensing, GE-20, 1982, 268-274.

Camillo, P. J., O'Neill, P. E., and Gurney, R. J. Estimating soil hydraulic parameters using passive microwave data. IEEE Transactions on Geoscience and Remote Sensing, GE-24, 1986, 930-936.

Carlson,T. N., Dodd, J. K.,Benjamin,S. G. and Cooper, J. N. Satellite estimation of the surface energy balance , moisture availability and thermal inertia. Journal of Applied Meteorology, 20, 1981, pp.67-87.

Adscript to references: J, Japanese, J, E, Japanese with English abstract, J,G, Japanese with German abstract, R,Russian, S, E, Slovakian with English abstract.

Chang, A. T. C., Atwater, S. G., Salomonson, V. V., Estes, J. E., Simonett, D. S., and Bryan, M. L. L-band radar sensing of soil moisture. IEEE Transactions on Geoscience and Remote Sensing, GE-18, 1980, pp. 303-310.

Chepil, W. S. Dynamics of wind erosion. Soil Science, 60, 1945,pp.305-320, 397-411, 475-480., 61, 1946, pp.167-177, 257-263, 331-340.

Chepil, W. S. Properties of soil which influence wind erosion. Soil Science, 69, 1950, pp.149-162.

Chepil, W. S. and Milne, R. A. Wind erosion of soil in relation to roughness of surface. Soil Science, 52, 1941, pp.417- 433.

Chudnovsky, A. F. Fundamental of agrophysics. edited by Ioffe & Revuta, Moscow, Press of physics & mathematics, 1959,pp.446, p.903. (R)

Clark,W. A. V. and Hosking,P. L. Statistical methods for geographer.New York,John Wiley & Sons,1986,p.518.,pp. 479-484.

Condit, H. R. The spectral reflectance of American soils. Photogrammetric Engineering, 36, 1970, pp.955-966.

Connors, K. F., Gardner, T. W. and Petersen, G. W. Classification of geomorphic features and landscape stability in Northwestern New Mexico using simulated Spot imagery. Remote Sensing of Environment, 22, 1987, pp. 187-207.

Curran, P. J. A photographic method for the recording of polarized visible light for soil surface moisture indications. Remote Sensing of Environment, 7, 1978, pp.305-322.

Curran, P. J. The use of polarized panchromatic and false color infrared film in the monitoring of soil surface moisture. Remote Sensing of Environment, 8, 1979, pp.249-266.

Dajace, J., Megier, J., Kahl, M., Maracci, G., Reiniger, P.,Tassone, G. and Huygen, J. Mapping thermal inertia, soil moisture and evaporation from aircraft day and night thermal data.Proceeding of the 13th International Symposium on Remote Sensing of Environment, Ann Arbor, Michigan, 23-27, April, 1979, pp.1015-1024.

Darch, J. P. A study of moisture conditions in the Pantanal of Brazil using satellite imagery. Remote Sensing of Environment, 8, 1979, pp. 331-348.

de Vries, D. A. Thermal properties of soil. Physics of Plant Environment, Edited by W. R. van Wijk, Amsterdum, North-Holland Publishing Company, 1963, p.382, p.210-235.

Dobson, M. C., and Ulaby Microwave backscatter dependence on surface roughness, soil moisture, and soil texture: part III, soil tension. IEEE Transactions on Geoscience and Remote Sensing, GE-19, 1981, pp. 51-61.

Dobson, M. C., Ulaby, F. T., Hallikainen, M. T., and El-Rayes, M. A. Microwave dielectric behavior of wet soil- part II: dielectric mixing models. IEEE Transactions on Geoscience and Remote Sensing, GE-23, 1985, pp. 35-46.

Dobson, M. C. and Ulaby, F. T. Active microwave soil moisture research. IEEE Transactions on Geoscience and Remote Sensing, GE-24, 1986a, pp. 23-36.

Dobson, M. C. and Ulaby, F. T. Preliminary evaluation of the SIR-B response to soil moisture, surface roughness, and crop canopy cover. IEEE Transactions on Geoscience and Remote Sensing, GE-24, 1986b, pp. 517-526.

Eagleman, J. R. and Lin, W. C. Remote sensing of soil moisture by a 21 cm passive radiometer. Journal of Geophysical Research, 81, 1976, pp. 3660-3666.

Editorial Committee for Handbook of Soil physics Measurement Handbook of physical properties of soils. 5th ed. Tokyo, Yokendo Co., 1980, p.505. (J)

Estes, J. E., Mel, M. R.and Hooper, J. O. Measuring soil moisture with an airborne imaging passive microwave radiometer. Photogrammetric Engineering and Remote Sensing , 43, 1977, pp.1273-1281.

Fenneman, N. M. Physiographic boundaries within the United States. Annals of the Association of American Geographers, 4, 1914, pp.84-134.

Fenneman, N. M. Physiographic provinces of the United States. Annals of the Association of American Geographers, 18, 1928, pp.251-353.

Flores, A. L. and Carlson, T. N. Estimation of surface moisture availability from remote temperature

measurements. Journal of Geophysical Research, 92, D8, 1987, pp. 9581-9585.

Franklin, S. E. Terrain analysis from digital patterns in geomorphometry and Landsat MSS spectral response. Photo-grammetric Engineering and Remote Sensing, 53, 1987, pp.59-65.

Fujiwara, T. and Oneda, N. Soil temperature and physical properties of soil, depend on different methods of irrigation at the field. Journal of Agricultural Meteorology, 15, 1959, pp. 25-28. (J,E)

Fukuhara, M. Remote sensing of soil. Remote Sensing, 1st ed. Edited by Cannon Image Editorial staff, 1974, p. 481., pp.165-178. (J,E)

Fung, A. K., and Eom, H. J. A comparison between active and passive sensing of soil moisture from vegetated terrains. IEEE Transactions on Geoscience and Remote Sensing, GE-23, 1985, pp. 768-775.

Gillespie, A. R. and Kahle, A. B. Construction and interpretation of a digital thermal inertia image. Photogrammetric Engineering and Remote Sensing, 43, 1977, pp. 983-1000.

Hallikainen, M. T., Ulaby, F. T., Dobson, M. C., El-Rayes, M. A., and Wu, L. Microwave dielectric behavior of wet soil- part I: empirical models and experimental observations. IEEE Transactions on Geoscience and Remote Sensing, GE-23, 1985, pp. 25-34.

Hall, R. B.and Watanabe, A. Landforms of Japan. Michigan Academy of Science Art and Literature, 18, 1932, pp.157- 207.

Heilman, J. L., Kanemasu, E. T., Bagley, J. O. and Rasmussen, V. P. Evaluating soil moisture and yield of winter wheat in the Great Plains using Landsat data. Remote Sensing of Environment, 6, 1977, pp. 315-326.

Heilman, J. L. and Moore, D. G. Evaluating near-surface soil moisture using Heat Capacity Mapping Mission data. Remote Sensing of Environment, 12, 1982, pp. 117-121.

Hirosawa, H., Komiyama, S. and Matsuzaka, Y. Cross-polarized radar backscatter from moist soil. Remote Sensing of Environment, 7, 1978, pp.211-217.

Ho, D. A soil thermal model for remote sensing. IEEE Transactions on Geoscience and Remote Sensing, GE-25, 1987, pp. 221-229.

Huntley, D. On the detection of shallow aquifers using thermal infrared imagery. Water Resources Research, 14, 1978, pp. 1075-1083.

Idso, S. B. and Reginato, R. J. Assessing soil water status via albedo measurement. Hydrological Water Research of Arizona Southwest, 4, 1974, pp.41-55.

Idso, S. B., Jackson, R. D., Reginato, R. J., Kimball, B. A. and Nakayama, F. S. The dependence of bare soil albedo on soil water content. Journal of Applied Meteorology, 14,1975a, pp.109-113.

Idso, S. B., Schmugge, T. J., Jackson, R. D. and Reginato, R. J. The Utility of surface temperature measurements for the remote sensing of surface soil water status. Journal of Geophysical Research, 1975b, pp. 3044-3049.

Idso, S. B., Jackson, R. D. and Reginato, R. J. Compensating for environmental variability in the thermal inertia approach to remote sensing of soil moisture. Journal of Applied Meteorology, 15, 1976, pp.811-817.

Imamura, R., Hashimoto, T. and Shimada, N. Moisture condition ranking of cultivated fields on an alluvial plain using aerial photographs. Journal of Japan Society of Photogrammetry and Remote Sensing, 19, 1980, pp. 14- 21.(J,E)

Jackson, R. D. and Idso, S. B. Surface albedo and desertification. Science, 189, 1975, pp. 1012-1013.

Jackson, T. J., Chang, A. and Schmugge, T. J. Aircraft active microwave measurements for estimating soil moisture. Photogrammetric Engineering and Remote Sensing, 47, 1981, pp. 801-805.

Jackson, R. D. Soil moisture inferences from thermal-infrared measurements of vegetation temperatures. IEEE Transactions on Geoscience and Remote Sensing, GE-20, 1982, pp. 282-286.

Jackson, T. J., Schmugge, T. J., and Wang, J. R. Passive microwave sensing of soil moisture under vegetation canopies. Water Resources Research, 18, 1982, pp. 1137-1142.

Jackson, T. J., Schmugge, T. J. and P. E. O'Neill Passive microwave remote sensing of soil moisture from an aircraft platform. Remote Sensing of Environment, 14, 1984, pp. 135-151.

Jackson, T. J., and P. E. O'Neill Microwave dielectric model for aggregated soils. IEEE Transactions on Geoscience and Remote Sensing, GE-24, 1986, pp. 920-929.

Jackson, T. J. Soil water modeling and remote sensing. IEEE Transactions on Geoscience and Remote Sensing, GE-24, 1986, pp. 37-46.

Jackson, T. J., Hawley, M. E., and P. E. O'Neill Preplanting soil moisture using passive microwave sensors. Water Resources Bulletin, 23, 1987a, pp. 11-19.

Jackson, T. J., and P. E. O'Neill Temporal observations of surface soil moisture using a passive microwave sensor. Remote Sensing of Environment, 21, 1987b, pp. 281-296.

Kanemasu, E. T., Heilman, J. L., Bagley, J. O. and Powers, W. L. Using Landsat data to estimate evapotranspiration of winter wheat. Environmental Management, 1, 1977, pp. 515-520.

Kahle, A. B., Gillespie, A. R., and Goetz, A. F. H. Thermal inertia imaging: A new geologic mapping tool. Geophysical Research Letters, 82, 1976, pp.26-28.

Kahle, A. B. A simple thermal model of the earth's surface for geologic mapping by remote sensing. Journal of Geophysical Research , 82, 1977, pp. 1673-1680.

Kahle, A. B., Schieldge, J. P. and Alley, R. E. Sensitivity of thermal inertia calculations to variations in environmental factors. Remote Sensing of Environment, 16, 1984, pp. 211-232.

Kahle, A. B. and Alley, R. E. Calculation of thermal inertia from Day-Night measurements separated by days or weeks. Photogrammetric Engineering and Remote Sensing, 51, 1985, pp. 73-75.

Kasubuchi, T. Problems of the mechanism of heat conduction in soil. Journal of Agricultural Meteorology, 29, 1973, pp.201-207.(J)

Kasubuchi, T. Water and heat balance of soil under the condition of constant ground water table - comparison between Kuronoppo soil (volcanic ash soil) and Iwatahara soil (diluvial soil) packed in lysimeter.

Transactions of the Japanese Society of Irrigation, Drainage and Reclamation Engineering, 75, 1978, pp. 20-25.

Kusakabe, M. Wind damage in Spring over Tokachi District, Hokkaido from the viewpoint of soil water. Journal of Agricultural Meteorology, 20, 1964, pp.93-95.(J,E)

Laiktman, D. L. Physics of atmospheric boundary layer. Gidrometeorology, Leningrad, 1961, p.253, pp.92-97.(R)

Linton, D. L. The delimitation of morphological regions. London essay in geography, edited by Stamp, L. D. and Wooldridge, S.W. London, Longmans, 1951, pp.199-217.

Madsen, H. B., Hasholt, B. and Platou, S. W. The development of a computerized erodibility map covering Denmark.Soil erosion in the European community -Impact of changing agriculture, Edited by Chisci, G. and Morgan, R. P. C., Rotterdam, A. A. Balkema, 1986, p.233, pp.143-154.

Marui, H. The expansion of coal production in the Joban coal field. Geographical Review of Japan, 34, 1961, pp. 22-36. (J,E)

Maruyama, E. Study on the everporation from the bare soil. Journal of Agricultural Meteorology, 23, 1967, pp.35-37. (J)

Maruyama, E. Effects of moisture on the heat conductivity, diffusivity, specific heat and apparent specific volume of the loam and the mixture of loam and clay (preliminary report). Journal of Agricultural Meteorology, 12, 1957, pp. 125 - 127. (J,E)

Matthias, A. D., Yates, S. R. Zhang, R. and Warrick, A. W. Radiant temperatures of sparse plant canopies and soil using IR thermometry. IEEE Transactions on Geoscience and Remote Sensing, GE-25, 1987, 517-520.

McCumber, M. C. and Pielke, R. A. Simulation of the effects of surface fluxes of heat and moisture in a mesoscale numerical model. Journal of Geophysical Research, 86, 1981, C10, pp. 9929-9938.

Mino, Y. Landform division based on several morphological elements in Shikoku Island. Chirigaku, 3, 1935, pp.627-634, pp.851-860. (J)

Monteith, J. L. Principles of environmental physics. London, Edward Arnold, 1973, p.242.

Morgan, R. P. C. Wind erosion.Soil erosion and conservation, Edited by D. A.Davidson, Longman Scientific & Technical Co., 1986, p.298, pp.47-56.

Moriwaki, H. The landform evolution of Kujukuri coastal plain, Central Japan. The Quaternary Research, 18, 1979, pp.1- 16. (J,E)

Musick, H. B. and Pelletier, R. E. Response to soil moisture of spectral indexes derived from bidirectional reflectance in thematic mapper wavebands. Remote Sensing of Environment, 25, 1988, pp.167-184.

Myers, V.I. and Heilman, M.D. Thermal infrared for soil temperature studies. Photogrammetric Engineering, 35, 1969, pp. 1024-1032.

Nakano,T. Landform type-an example of Kochi plain. Geographical Review of Japan, 25, 1952, pp.127-133. (J,E)

Nakano, T., Kadomura, H. and Matsuda, I. Buried landforms and ground subsidence in the Tokyo lowland. Geographical Review of Japan, 41, 1968, pp.427-449. (J,E)

Nappo, Jr. C. J. Parameterization of surface moisture and evaporation rate in a planetary boundary layer model. Journal of Applied Meteorology, 14, 1975, pp. 289-296.

Newton, R. W., Black, Q. R., Makanvand, S., Blanchard, A. J., and Jean, B. R. Soil moisture information and thermal microwave emission. IEEE Transactions on Geoscience and Remote Sensing, GS-20, 1982, pp.275-281.

Njoku, E. G. and Kong, J. Theory for passive microwave remote sensing of near-surface soil moisture. Journal of Geophysical Research, 82, 1977, pp. 3108-3118.

Njoku, E. G. and O'Neill, P. E. Multifrequency microwave radiometer measurements of soil moisture. IEEE Transactions on Geoscience and Remote Sensing, GE-20, 1982, pp. 468-475.

Oga, T. Heat transfer theories and its application. Tokyo, Iwanami Co., 1931, p.372.(J)

Okabe, F. Tone-densitometric analysis of soil properties. Geographical Review of Japan, 41, 1968, pp.48-52.(J,E)

Oke, T. R. Boundary Layer Climates. London, Methuen & Co., 1978, p.372., pp.3-60.

Okuno, T., Haga, T., Yajima, K., Okuno, C., Hashimoto, S. and Koga, Y. Multivariable statistical analysis. Second series. Tokyo: Nikka Giken Co., 1976, p.299. (J)

O'Neill, P. E., Jackson, T. J., Blanchard, B. J., Wang, J. R. and Gould, W. I. Effects of corn stalk orientation and water content of passive microwave sensing of soil moisture. Remote Sensing of Environment, 16, 1984, pp. 55-67.

Oya, M., Umitsu, M., Maruyama, Y., Omori, H., Akagiri, T., Wakamatu, K., Ida, S., Hirai, Y., and Uchida, K. Technique and development of geomorphologic land classification. edited by Oya, Tokyo, Kokon-Shoin, 1987, p.218. (J)

Owe, M., Chang, A., and Golus, R. E. Estimating surface soil moisture from satellite microwave measurements and a satellite derived vegetation index. Remote Sensing of Environment, 24, 1988, pp. 331-345.

Parry, J. T. and Beswick, J. A. The application of two morphometric terrain classification systems using air-photo interpretation methods. Photogrammetria, 29, 1973, pp.153-186.

Pohn, H. A.,Offield, T. W.and Watson, K. Thermal inertia mapping from satellite- discrimination of geologic units in Oman. Journal of Research of U.S. Geological Survey, 2, 1974, p.147-158.

Pratt, D. A., Ellyett, C. D., McLauchlan, E. C., and McNabb, P. Recent advances in the application of thermal infrared scanning to geological and hydrological studies.Remote Sensing of Environment, 7, 1978, pp.177-184.

Pratt, D. A.and Ellyett, C. D. The thermal Inertia approach to mapping of soil moisture and geology. Remote Sensing of Environment, 8, 1979, pp.151-168.

Price, J. C. Thermal inertia mapping: a new view of the earth. Journal of Geophysical Research, 82, 1977, pp.2582-2590.

Price, J. C. The potential of remotely sensed thermal infrared data to infer surface soil moisture and evaporation. Water Resources Research, 16, 1980, pp.787- 795.

Price, J. C. Estimation of regional scale evapotranspiration through analysis of satellite thermal-infrared data. IEEE Transactions on Geoscience and Remote Sensing, GE-20, 1982, 286-292.

Price, J. C. On the analysis of thermal infrared imagery: the limited utility of apparent thermal inertia. Remote Sensing of Environment, 18, 1985, pp.59-73.

Rao, K. S., Sowmya, A., Mohan, B. K., Venkatachalam, P.,and Ahmed, N., Karale, R. L. and Narula, K. K. Computer-aided brightness temperature map of Indian subcontinent - inference on soil moisture variations. Remote Sensing of Environment, 20, 1986, pp. 195-207.

Reginato, R. J., Idso, S. B., Vedder, J. F., Jackson, R. D., Blanchard, M. B.and Goettelman, R. Soil water content and evaporation determined by thermal parameters obtained from ground-based and remote measurements. Journal of Geophysical Research, 81, 1976, pp.1617-1620.

Rosema, A. Heat capacity mapping, is it feasible ?. Proceeding of the 10th International Symposium on Remote Sensing of Environment, Ann Arbor, Michigan, 6-10 October, 1975, pp.571-582.

Schmugge, T., Gloersen, P., Wilheit, T. and Geiger, F. Remote sensing of soil moisture with microwave radiometers. Journal of Geophysical Research, 79, 1974, pp.317-323.

Schmugge, T., Blanchard, B., Anderson, A. and Wang, J. Soil moisture sensing with aircraft observations of the diurnal range of surface temperature. Water Resources Research, Bulletin, 14, 1978, pp. 169-178.

Schmugge, T. J. and O'Neill, P. E., and Wang, J. R. Passive microwave soil moisture research. IEEE Transactions on Geoscience and Remote Sensing, GE-24, 1986, pp. 12-22.

Shimomura, H. Landform divisions of Japanese Island (1), (2), (3). Geographical Review of Japan, 2, 1926, pp.1027-1039, pp.327-336, pp.863-873. (J)

Shimomura, H., Hanai, J., Watanabe, H., Okayama, T. and Makiyama, M. Landform divisions. Tokyo, Iwanami Co., 1934, p.98. (J)

Shinjo, A. Movement of vapor in a soil under thermal gradient. Transactions of the Japanese Society of

Irrigation, Drainage and Reclamation Engineering, 69, 1977, pp.8-12. (J,E)

Shiyatyy, Y. I., Lavrovskiy, A. B. and Khmolenko, M. I. Effect on texture on the cohesion and wind resistance of soil clods. Soviet Soil Science, 4, 1972, pp.105-112.

Snedecor,G. W, and Cochran, W. G. Statistical methods, 6th ed. Translated to Japanese by Hatamura, M., Okuno, T., Tsujimura, Y., Tokyo, Iwanami Co., 1967, p.546. (J)

Soer, G. J. R.Estimation of regional evapotranspiration and soil moisture conditions using remotely sensed crop surface temperatures. Remote Sensing of Environment, 9, 1980, pp.27-45.

Stancioff, A. and Hill, P. A. Satellite image analysis in mineral exploration in complicated structure terrains, Great Northern Peninsula, Newfoundland. The American Association of Petroleum Geologists Bulletin, 63, 1979, pp.951-966.

Stroosnijder, L., Lascano, R. J., Van Bavel, C. H. M. and Newton, R. W. Relation between L-band soil emittance and soil water content. Remote Sensing of Environment, 19, 1986, pp. 117-125.

Stredansky, I. J. Dependence of soil run off on the wind speed and soil moisture. Acta Fytotechnica Universitatis Agriculturae-NITRA-, 37, 1981, pp.249-255.(S,E)

Tanaka, S., Sano, H. and Kakinuma, S. Study on the control of wind erosion (1) Relation of soil moisture to the wind velocity required to initiate soil movement. Journal of Agricultural Meteorology, 10, 1954, pp.57-60.(J,E)

Tanaka, S., Tanizawa, T., Sano, S. and Kakinuma, S. Actual condition of the wind erosion. Journal of Agricultural Meteorology, 14, 1959, pp.101-104. (J,E)

Tarnocai, C. and Kristof, S. J. Computer-aided classification of land and water bodies using LANDSAT data, Mackenzie delta area,N. W. T., Canada. Arctic and alpine Research, 8, 1976, pp.151-159.

Theis, S. W., Blanchard, B. J. and Newton, R. W. Utilization of vegetation indices to improve microwave soil moisture estimates over agricultural lands. IEEE

Transactions on Geoscience and Remote Sensing, GE-22, 1984, pp. 490-496.

Townshend, J. R. G. and Hancock, P. J. The role of remote sensing in mapping surficical deposits. Terrain Analysis and Remote Sensing, edited by J. R. G. Townshend, London: George Allen & Unwin, 1981, p.232., pp.204-217.

Uchijima, Z. Agricultural meteorology for technologist. Nogyo-gijyutsu, 19, 1964, pp.139-145, 238-243, 290-295, 334-341, 582-587.(J)

Uchijima, Z. Handbook of Agricultural Meteorology. edited by Y. Tsuboi et al., Tokyo: Yokendo Co., 1974, p.854., pp.82-84. (J)

Ulaby, F. T., Cihlar, J. and Moore, R. K. Active microwave measurement of soil water content. Remote Sensing of Environment, 3, 1974, pp.185-203.

Ulaby, F. T., Batlivala, P. P. and Dobson, M. C. Microwave backscatter dependence on surface roughness, soil moisture, and soil texture: part I- bare soil. IEEE Transactions on Geoscience Electronics, GE-16, 1978, pp.286-295.

Ulaby, F. T., Bradley, G. A. and Dobson, M. C. Microwave backscatter dependence on surface roughness, soil moisture, and soil texture, part II- vegetation-covered soil. IEEE Transactions on Geoscience Electronics, GE-17, 1979, pp. 33-40.

Ulaby, F. T., Aslam, A., and Dobson, M. C. Effects of vegetation cover on the radar sensitivity to soil moisture. IEEE Transactions on Geoscience and Remote Sensing, GE-20, 1982, pp. 476-481.

Ulaby, F. T., Razani, M., and Dobson, M. C. Effects of vegetation cover on the microwave radiometric sensitivity to soil moisture. IEEE Transactions on Geoscience and Remote Sensing, GE-21, 1983a, pp. 51-61.

Ulaby, F. T., Dobson, M. C., and Brunfeldt, D. R. Improvement of moisture estimation accuracy of vegetation-covered soil by combined active/ passive microwave remote sensing. IEEE Transactions on Geoscience and Remote Sensing, GE-21, 1983b, pp. 300-307.

Umetani, H. On the estimate of the soil moisture contents during the non-precipitation periods. Journal of Agricultural Meteorology, 7, 1951, pp.9-10. (J,E)

Utsunomiya, Y. Diurnal variation of surface radiant temperature associated with landuse in the Tokyo Metropolitan area. Journal of the Japan Society of Photogrammetry and Remote Sensing, 19, 1980, pp.20-30. (J,E)

Utsunomiya, Y. Preliminary interpretation of mapping of soil moisture contents with satellite remote sensing data in the Kujukuri land subsiding area, Eastern Part of Boso peninsula, Central Japan. Geographical Review of Japan, 54, 1981, pp.740-750. (J,E)

Utsunomiya, Y. Experimental studies on measurement systems of soil moisture with thermal infrared data. Journal of the Japan Society of Photogrammetry and Remote Sensing, 21, 1982, pp.15-25. (J,E)

Utsunomiya, Y. Infrared remote sensing for soil moisture measurement with airborne multispectral scanner. Annals of the Tohoku Geographical Association, 36, 1984, pp.39-45.(J,E)

Utsunomiya, Y. and Yamaguchi, T. Soil moisture measurement using remotely sensed soil surface temperature. Proceeding of the 12th Remote Sensing Symposium, Tokyo, 27-28, October, 1986, pp.113-114. (J)

Utsunomiya, Y. and Yamaguchi, T. Soil moisture measurement using airborne MSS thermal IR data. Proceeding of the 13th Remote Sensing Symposium, Tokyo, 26-27, October, 1987, pp.31-32. (J)

Utsunomiya, Y. Soil moisture estimation based on thermal inertia from airborne MSS measurement. Proceeding of the 16th Congress of International Society for Photogrammetry and Remote Sensing., Kyoto, 1-10, July, 1988

Verstappen,H. Th. Remote Sensing in Geomorphology. Amsterdum Elsevier Scientific Publishing Co., 1977, p.214, pp.148-153.

Vieillefosse, M. and Favard, J. C. CITHARE: Thermal inertia and humidity cartography over Africa by geostationary satellite. Proceeding of the 13th International Symposium on Remote Sensing of Environment, Ann Arbor, Michigan, 23-27, April, 1979, pp.1025-1033.

Vlcek, J. and King, D. Detection of subsurface soil moisture by thermal sensing: results of laboratory, close-range, and aerial studies. Photogrammetric Engineering and Remote Sensing, 49, 1983, pp. 1593-1597.

Wang, J. R. and Schmugge, T. J. An empirical model for the complex dielectric permittivity of soils as a function of water content. IEEE Transactions on Geoscience and Remote Sensing, GE-18, 1980a, pp. 288-295.

Wang, J. R., Newton, R. W., and Rouse, J. W. Passive microwave remote sensing of soil moisture: the effect of tilled row structure. IEEE Transactions on Geoscience and Remote Sensing, GE-18, 1980b, pp. 296-302.

Wang, J. R. and Shiue, J. C., and McMurtrey, J. E. Microwave remote sensing of soil moisture content over bare and vegetated fields. Geophysical Research Letters, 7, 1980c, pp. 801-804.

Wang, J. R. and Choudhury, B. J. Remote sensing of soil moisture content over bare field at 1.4 GHz frequency. Journal of Geophysical Research, 86, C6, 5277-5282, 1981.

Wang, J. R., Schmugge, T. J., Gould, W. I., Glazar, W. S., and Fuchs, J. E. Multi-frequency radiometric measurement of soil moisture content over bare and vegetated fields. Geophysical Research Letters, 9, 1982, pp. 416-419.

Wang, J. R., O'Neill, P. E., Jackson, T. J. and Engman, E. T. Multifrequency measurements of the effects of soil moisture, soil texture, and surface roughness. IEEE Transactions on Geoscience and Remote Sensing, GE-21, 1983, pp. 44-51.

Wang, J. R. Passive microwave sensing of soil moisture content: the effects of soil bulk density and surface roughness. Remote Sensing of Environment, 13, 1983, pp. 329-344.

Wang, J. R. Effect of vegetation on soil moisture sensing observed from orbiting microwave radiometers. Remote Sensing of Environment, 17, 1985, pp. 141-151.

Wang, J. R. Microwave emission from smooth bare fields and soil moisture sampling depth. IEEE Transactions on Geoscience and Remote Sensing, GE-25, 1987, 616-622.

Watanabe, A. Landform division. Physical Geography, Edited by Inoue, S., Hanai, J., Okayama, T., Watanabe, A., Tada, F., Tokyo, Chizin shokan Co., 1940, p.327, pp.302 -310. (J)

Watanabe, A. Landform divisions of Japan. Journal of Geography, 61, 1952, pp.1-7. (J,E)

Watson, K. A computer program of thermal modeling for interpretation of infrared images. National Technical Information Service, PB-203-578, 1971, p.33.

Watson, K. Geologic applications of thermal infrared images. Proceedings of the IEEE, 1, 1975, pp. 128-137.

Watson, K. Regional thermal inertia mapping from an experimental satellite. Geophysics, 47, 1982, pp. 1681-1687.

Wetzel, P. J., Atlas, D. and Woodward, R. H. Determining soil moisture from geosynchronous satellite infrared data: a feasibility study. Journal of climate and applied meteorology, 23, 1984, pp. 375-391.

Wetzel, P. J., and Woodward, R. H. Soil moisture estimation using GOES-VISSR infrared data: a case study with a simple statistical method. Journal of climate and applied Meteorology, 26,

Wilson, S. J.and Cooke, R. U. Wind erosion. Soil Erosion, Edited by M. J. Kirkby and R. P. C. Morgan, Chichester: John Wiley & Sons, Ltd., 1980, p.312, pp.217-251.

Yada,T.,Shirai, T., Ishii, H. and Akagiri, K. Environmental development of natural gas mining area in the Kujukuri plain, Chiba Prefecture. Proceeding of the Annual Meeting of Japanese Geographical Society, No.8, Tokyo, 29, April - 4 May, 1975, p.226. (J)

Yada, T., Ishii,H. and Akagiri, K. Land subsidence and environmental development in the Kujukuri plain, Chiba Prefecture. Proceeding of the annual meeting of Japanese geographical society, No.11, Hirosaki, 10-13 October, 1976, pp.98-99.(J)

Yamamoto, Y. Visual observation of soil moisture. Journal of Agricultural Meteorology, 17, 1962, pp. 119-121. (J,E)

Yamanaka, K. Soil moisture decrease at Ohwada observation station. Journal of Agricultural Meteorology, 5, 1949, pp. 27-28. (J)

Yamazaki, H. Study of the depression in the coal mining area from the viewpoint of geography. Geographical Review of Japan, 36, 1963, pp.553-558. (J,D)

Zhang, R. H. Investigation of remote sensing of the soil moisture. Proceedings of the 14th International Symposium on Remote Sensing, San Jose, 23-30 April, 1980, pp.121-133.